THE OPTICAL SYSTEM OF A BALLOON TELESCOPE FOR HIGH RESOLUTION FOURIER SPECTROSCOPY IN THE INFRARED SPECTRAL REGION

Reiner Hofmann

Translation of: "Das optische System eines Ballonteleskops für hochauflösende Fourier Spektroskopie im infraroten Spektralbereich," Max-Planck Institute for Physics and Astro-Physics, Institute for Extraterrestrial Physics, MPI-PAE/Extraterr. 103, September, 1974, 150 pages.

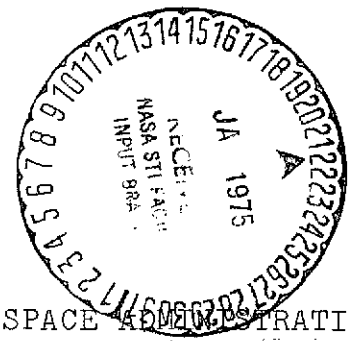

NATIONAL AERONAUTICS AND SPACE ADMINISTRATION
WASHINGTON, D. C. 20546 JANUARY 1975

STANDARD TITLE PAGE

1. Report No. NASA TT F 16,071	2. Government Accession No.	3. Recipient's Catalog No.
4. Title and Subtitle: The Optical System of a Balloon Telescope for High Resolution Fourier Spectroscopy in the Infrared Spectral Region		5. Report Date: 6 January 1975 6. Performing Organization Code
7. Author(s): Reiner Hofmann		8. Performing Organization Report No. 10. Work Unit No.
9. Performing Organization Name and Address: SCITRAN, Box 5456, Santa Barbara, CA 93108		11. Contract or Grant No. NASw-2483 13. Type of Report and Period Covered: Translation
12. Sponsoring Agency Name and Address: National Aeronautics and Space Administration, Washington, D.C. 20546		14. Sponsoring Agency Code

15. Supplementary Notes

Translation of: Das optische System eines Ballonteleskops für hochauflösende Fourier Spektroskopie im infraroten Spectralbereich," Max-Planck Institute for Physics and Astrophysics, Institute for Extraterrestrial Physics, MPI-PAE/Exterterr. 103, September, 1974, 150 pages.

16. Abstract

The selection and optimization of a dispersion element for a balloon-based high resolution infrared spectroscopy project are described. The signal/noise ratio for observations of interstellar sources, dust, and other sources is given. It is demonstrated that a lamella grid is superior to the Michelson interferometer. An analysis of the entire optical systems is carried out. Expressions are derived for normalized noise power of the detector and perturbation radiation, and for the optimum modulation frequency. A rocking mirror configuration is adapted for the instrument.

17. Key Words (Selected by Author(s))	18. Distribution Statement: Unclassified - Unlimited		
19. Security Classif. (of this report): Unclassified	20. Security Classif. (of this page): Unclassified	21. No. of Pages: 201	22. Price

PRECEDING PAGE BLANK NOT FILMED

TABLE OF CONTENTS

Translated for National Aeronautics and Space Administration under Contract No. NASw-2483 by SCITRAN, P. O. Box 5456, Santa Barbara, California, 93108.

THE OPTICAL SYSTEM OF A BALLOON TELESCOPE FOR HIGH RESOLUTION FOURIER SPECTROSCOPY IN THE INFRARED SPECTRAL REGION*

Reiner Hofmann**

1. Introduction

1.1. Problem Formulation

The chemical composition and temperature of interstellar /1*** infrared sources, for example, clouds and collapsing gas clouds, will be investigated in order to obtain new information on the production of stars, interstellar material, and cosmological problems, for example, the H/D ratio. Such information is contained in the line radiation of various molecules, and these lines are distributed over the entire infrared spectral range. Some examples for wavelengths and intensities of the most important lines are given in Table 1. The absorption by dust, which usually surrounds the sources, is not considered [1].

We wish to investigate the largest possible spectral range with a high resolution, in order to observe these lines. We wish to investigate the spectral range between 5 and 200 μ, and probably several dispersion elements will be required. First of all, we will only consider one single dispersion element in the

*MPI-PAE/Extraterr. 103, September, 1974.

**Max-Planck Institute for Physics and Astrophysics, Institute for Extraterrestrial Physics.

***Numbers in the margin indicate pagination of original foreign text.

TABLE 1*

/2

Radiation	Source	Wavelength	Intensity: $Wcm^{-2}sr^{-1}$	Wcm^{-2}
H_2 S(0)	Sgr B2	28,22		$4,5\ 10^{-16}$
S(1)	"	17,0		$20,0\ 10^{-16}$
S(2)	"	12,3		$0,7\ 10^{-16}$
HD R(0)	"	112		$1,2\ 10^{-16}$
R(1)	"	56,2		$6,3\ 10^{-16}$
R(2)	"	37,7		$3,7\ 10^{-16}$
R(3)	"	28,5		$0,6\ 10^{-16}$
H_2 S(0)	near interstellar clouds	28,22	$5\ 10^{-11}$	
CII	shock front between clouds	156	10^{-13}	
OI	"	63	10^{-14}	
OIV	planetary clouds (NGC 7027)	26		$4,0\ 10^{-15}$
NeII	planetary clouds (IC 418)	12,8		$2,0\ 10^{-17}$
CH_4	interstellar clouds**	3,39		$0,6\ 10^{-15}$
OH	"	119,5/79,2		10^{-17}
CO	"	5,4		10^{-18}
CH	"	352/176		10^{-17}
OI	"	63		10^{-18}
NeII	HII, Orion	12,8	10^{-5}	
CII	" "	156,2	10^{-8}	
FeII	HII, gal. center	25,99		10^{-14}
NII	" "	121,6		10^{-14}

*Commas in numbers indicate decimal points.

**We assume the following for the interstellar cloud: central temperature 1000° K, diameter 100 · $R_\odot$, distance from Earth 500 pc.

range up to 200 μ, and we are considering the lower limit of 20 μ as a target.

The atmosphere in this spectral range is partially optically dense, which will mean that the experiment has to be carried out at the highest possible altitude. Because of the low intensity of the interstellar sources, long measurement times are desirable because, in the case where the detector is the dominating noise source, which corresponds to the present state of the art in the far infrared for optimum design of all components, the signal-to-noise ratio is proportional to the square root of the measurement time. Therefore, the measurements can only be carried out with an instrument carried on a balloon, considering the present state of the art. The maximum possible altitude is about 50 km. Even there, the radiation power reaching the detector per line from the residual atmosphere (primarily CO_2, N_2O, H_2O, and O_3 here) /3 can still amount to between 2 and 3 powers of 10 times the detectable power per line from the investigated interstellar sources.

In order to be able to detect the radiation of these weak sources, nevertheless, their signal must be very accurately separated from the signal of the atmospheric radiation. In practice, this is done by forming the difference from two measured values, and one of these values is only determined by the radiation flux of the atmosphere. The other also contains additional information about the flux from the interstellar source. In this paper, we will discuss how this difference is formed and we will discuss the selection of the suitable detector.

The main emphasis is on the selection and optimization of a suitable dispersion element and its adaptation to the telescope and the detector, considering the special features of the balloon flight. In the first chapter, we will only discuss this problem.

1.2. Boundary Conditions, the Influence on the Dispersion Element Concept

One important point is the compatibility of the dispersion element and the optical components of the telescope. Here we have no restrictions on the selection of the dispersion element because, for the time being, only the diameter of the main mirror is specified at 1 m. In addition, we require that the main mirror should have a short focal length, in order to have a small length of the telescope. The secondary mirror should not be too large, so that the vignetting of the main mirror will remain small. In addition, it should also possibly be used as a rocking mirror, which alternately will image the source and an area of the sky as close to the source as possible without the infrared source onto the detector. This can easily be done for /4 a small mirror diameter.

Additional points, which must be considered when selecting the dispersion element, are the following:

i) the dispersion element and the detector should be designed so that in one measurement period it is possible to process the spectral range between 20 and 200 μ.

ii) we want to have a resolution of $R = \frac{\lambda}{\Delta\lambda} = \frac{\sigma}{\Delta\sigma} \geq 10^3$ over the entire spectral range.

iii) because of the small source intensity, we must have optimum light yield and minimum eigen radiation of the instruments.

iv) a maximum of two hours are available for recording a spectrum because of the motion of the sources in the sky. If possible, no more than 30 minutes should be used for one measurement because of the limited balloon flight time.

The boundary conditions refer to the last stage of the experiment. It is therefore possible that various requirements will have to be modified or reduced for practical reasons. Therefore, we will always consider the final version of the dispersion element and we will try to use it, if possible.

1.3. Consequences of the Boundary Conditions

The requirements and boundary conditions specified above lead to the following conclusions for selecting the dispersion element:

i) the use of normal dispersion grids:

If electromagnetic radiation from the wavelength range λ_1 to λ_2 falls on a grid with a grid constant d, then an n^{th} spectrum is obtained with an angular separation between $\varphi_1 = n\lambda_1/d$ to $\varphi_2 = n\lambda_2/d$ of zero order. If $\lambda_2 > 2\lambda_1$, then the spectra of the first and second order will partially overlap. /5 For λ_1 = 20 μ, the first and second order spectra overlap already for $\lambda \geq$ 40 μ. Therefore, the given wavelength range can only be observed if exchangeable filters are placed in front of the grid, which each let a maximum of one octave pass through. In

order to record the spectrum between 20 and 200 μ, it would be necessary to have four filters, which would have to be exchanged during the measurements.

Another disadvantage of the dispersion grid is the low light yield. If the required resolution is to be achieved, then the ray divergence at the dispersion element and, therefore, the energy flux would have to be reduced. The multiplex technology* [2] could help here, but it requires complex techniques and can only be used to a limited extent.

ii) Use of prisms:

Prisms are not very well suited for wideband infrared spectroscopy, because no materials exist which have sufficient transmissivity and dispersion capacity over the entire spectral range. In addition, because they do not have ideal transmissivity, prisms have a high emissivity, which contradicts the requirement for minimum eigen radiation. Their light yield is just as low as that of the dispersion grid.

iii) Since not much more than $2 \cdot 10^3$ s is to be used for recording of spectra and, for the required resolution of $R \gtrsim 10^3$, at least $5 \cdot 10^3$ measurement points are to be determined (see below), the grid or prism scan methods will allow a maximum measurement time of 0.4 seconds per spectral element. This integration time produces such a small signal-to-noise ratio that it is not usable for observing weak sources.

The number of measurement points per spectrum is found from the following: for a grid spectrometer, we have

*Hadamard spectroscopy.

$\lambda/\Delta\lambda = R = \text{const}$; with $R = 10^3$ we then have for $\lambda = 20\ \mu$: $\Delta\lambda =$ /6
0.02 μ and for $\lambda = 200\ \mu$: $\Delta\lambda = 0.2\ \mu$. For 20 μ, therefore, 50 measurement points are required for μ and for 200 μ, 5 measurement points are required in order to have the desired resolution. On the other hand, we have $\Delta\lambda \sim \lambda$, so that, on the average, $(50 + 5)/2 = 27.5$ measurement points per μ must be recorded. If this number is multiplied with the width of the spectral range of interest of $(200 - 20)\mu = 180\ \mu$, we obtain the number of measurement points given above.

iv) Another instrument which can be used for astronomical measurements is the Fabry-Perot tipping filter (see 2.4.2), which provides good light yield because the ray divergence at the instrument can be just as large as in an interferometer. However, its useful spectral range is very narrow (less than one tenth of the central wavelength). Therefore, it is not suited for recording spectra with a large width.

v) The points (i — v) show that conventional spectroscopy is not suited for the problem formulated here. Fourier spectroscopy is a solution. Its essential advantages are the following:

a) all spectral elements can be recorded at the same time and, therefore, over the entire measurement time, and

b) for a high resolution, it is possible to have a relatively large ray divergence at the dispersion element and, therefore, a high light yield, which can also improve the signal-noise ratio.

The Fourier spectroscopy is especially well suited for wideband recording of spectra of extended sources, with a low radiation intensity.

Therefore, only an interferometer can be used as a dispersion element. Various types of instruments should be compared. First of all, we will discuss the Fourier spectroscopy theory as far as it is important for our problem.

2. Theoretical Foundations of Fourier Spectroscopy /7

2.1. Various Methods of Spectroscopy

High resolution spectroscopy from the ultraviolet to the infrared spectral range is performed almost exclusively by producing phase differences between interfering ray bundles. The purpose of spectroscopy is always to determine the radiation intensity of the source as a function of wave number or wave length. In other words, a Fourier decomposition of intensity is made for a given source.

If we consider the operational principle of various dispersion elements, it can be seen that, as one progresses from the prism to the grid and then to the interferometer, this goal becomes more and more simple physically, but the goal is not realized completely [2].

In the prism, the incident parallel light bundle is divided into an infinite number of rays, which pass through various layer thicknesses of the prism material and thus obtain corresponding phase differences, compared with a reference beam. These rays interfere in the image plane of a collimator system so as to produce a unique spectrum for finite spectral regions.

In the case of the grid, the number of ray bundles equals the number of grid lines, which is a finite number. Therefore, the spectrum produced in the image plane repeats periodically and various orders are produced. For a spectral range of a given width, the spectra overlap, starting with a certain order and they are no longer uniquely determined.

If we now consider the Michelson interferometer, then the number of interfering rays is reduced to two. It is then no longer possible to determine the spectral distribution of intensity from the interference pattern. This information is contained in the dependence of the interference pattern on the phase difference, which can be changed using a movable interferometer mirror. For example, if the intensity of the central /8 spot (see 2.3.1) of the interference pattern is recorded as a function of mirror position and, therefore, of phase difference of the interfering rays, then this function, the "interferogram," contains the total spectral information. Later on, we will show that the interferogram is the same as the Fourier transform of the spectrum.

The best way to represent the spectrum is to use a prism. The spectrum is not as well represented if a grid is used. The interferogram produced by the interferometer cannot be used to directly determine the spectrum. The reason for this spectrum representation is the different numbers of interfering ray bundles. The interference of an infinite number of bundles in the case of the prism is an analog representation of the Fourier transformation. The prism produces not only phase differences between rays, but also it provides a good presentation of the spectral information.

In a similar way, the grid produces not only phase differences, but also produces a representation of the spectrum, even though it is not unique. It contains a type of analog computer for the Fourier series.

The interferometer no longer produces such a representation; it only produces the phase differences. However, the instrument is so simple that it is easy to analyze the production of the phase difference between the two rays. In addition, the shift of the movable mirror is correlated with the phase difference in a simple manner. By measuring the mirror shift and the intensity of the central spot, we obtain enough information to carry out the Fourier transformation. The interferometer therefore has one function less than the grid and the prism. This leads to the fact that the limitations placed on the ray path are not as limiting as in conventional dispersion elements, which means that a greater ray divergence can be used than in the case of the interferometer. This results in a better light yield than /9 would be possible for a prism and grid for the same resolution. The diagram of the information flux for conventional and Fourier spectroscopy is shown in Figure 1.

One disadvantage of the interferometer is the fact that a very complex auxiliary instrument is required to obtain a spectrum, which is the computer. It can be either analog or digital, but for the required resolutions and the large number of interferogram points, only digital computers can be used. For these computers, special programs are available today which make it possible to calculate a spectrum in an acceptable amount of time, even if a large number of points are being processed. (P. Connes has recorded planetary spectra with 10^6 points using this method [3, 4].) One big advantage is that the computer can be used in a universal way, which makes it possible to transfer many problems from the experiment to the calculation. For example, it is possible to reduce the resolution of the spectrum at a later time in favor of the more favorable signal-noise ratio.

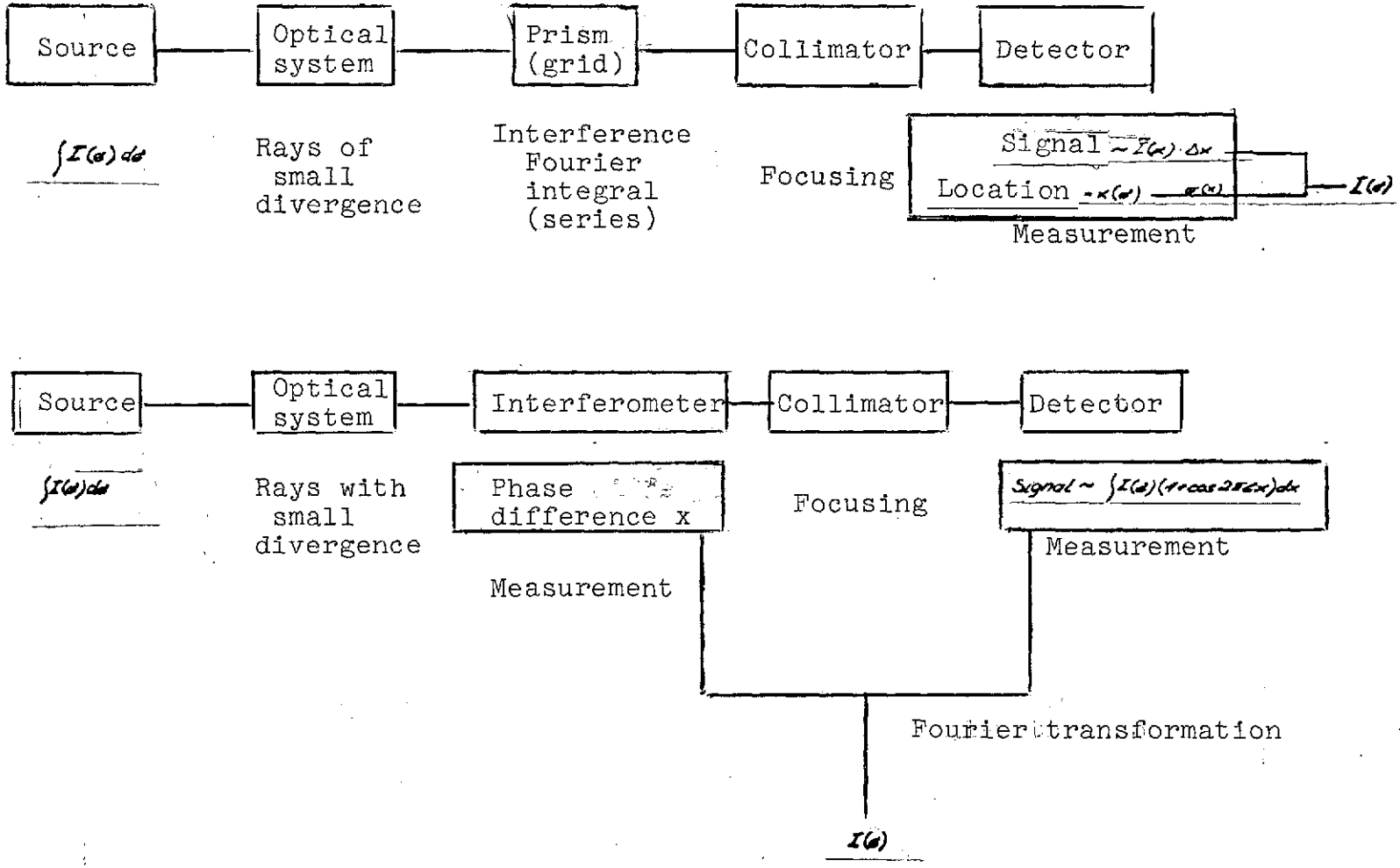

Figure 1. Information flow for the determination of spectra.

2.2. Mathematical Foundations of Fourier Spectroscopy /10

2.2.1. The Fourier transformation

Let it be assumed that a quasi-monochromatic radiation bundle is given, the flux of which is concentrated around the wave number σ in the interval $d\sigma$ and that it amounts to $B(\sigma)d\sigma$ there. It impinges on the interferometer and is then divided into two ray bundles, between which the phase difference x is produced. After superposition of these bundles, the resulting flux equals $\frac{1}{2} B(\sigma)d\sigma (1 + \cos 2\pi\sigma x)$ (see 2.3.1).

By changing x, the radiation flux is modulated. The non-constant part of the flux, plotted against x, is called the interferogram. The constant term does not furnish any information and is automatically suppressed after the detector, when using an alternating voltage amplifier.

For a non-monochromatic spectrum, the idealized interferogram is given by the integral of the modulation term over the spectral range:

$$F(x) = \int_0^\infty B(\sigma) \cdot \cos 2\pi\sigma x \, d\sigma = Re \int_0^\infty B(\sigma) e^{i2\pi\sigma x} d\sigma \qquad (2.1)$$

$B(\sigma)$ only has physical meaning for $\sigma \geq 0$. For the mathematical operations, it is advantageous to extend the range of definition of B to the negative real numbers, and to divide B into an even and uneven part:

$$B(\sigma) = B_e(\sigma) + B_o(\sigma) \qquad (2.2)$$

with

$$B_e(\sigma) = \begin{cases} 1/2\ B(\sigma) & \text{for } \sigma \geq 0 \\ 1/2\ B(-\sigma) & \text{for } \sigma < 0 \end{cases}$$

and

$$B_o(\sigma) = \begin{cases} 1/2\ B(\sigma) & \text{for } \sigma \geq 0 \\ -1/2\ B(-\sigma) & \text{for } \sigma < 0 \end{cases}$$

Using this definition, the Fourier transform of the spectrum can be written as /11

$$\bar{B}(x) = \int_0^\infty B(\sigma) \cdot e^{i2\pi\sigma x} d\sigma = \int_0^\infty B(\sigma) \cdot \cos 2\pi\sigma x \, d\sigma + i \int_0^\infty B(\sigma) \cdot \sin 2\pi\sigma x \, d\sigma$$

$$= \int_{-\infty}^{+\infty} B_e(\sigma) \cdot e^{i2\pi\sigma x} d\sigma + \int_{-\infty}^{+\infty} B_o(\sigma) e^{i2\pi\sigma x} d\sigma$$

and

$$Re(\bar{B}(x)) = \int_{-\infty}^{+\infty} B_e(\sigma) \cdot e^{i2\pi\sigma x} d\sigma = \int_{-\infty}^{+\infty} B_e(\sigma) \cdot \cos 2\pi\sigma x \, d\sigma = F(x) \qquad (2.3)$$

i.e., the inteferogram is a real part of the Fourier transform of the spectrum or: the interferogram equals the Fourier transform of the even part of the spectrum. Therefore, one obtains the even part of the spectrum by the reverse transformation of the interferogram:

$$B_e(\sigma) = \int_{-\infty}^{+\infty} F(x) \cdot e^{-i2\pi\sigma x} dx = \int_{-\infty}^{+\infty} F(x) \cdot \cos 2\pi\sigma x \, dx = 2 \cdot \int_0^\infty F(x) \cdot \cos 2\pi\sigma x \, dx \qquad (2.4)$$

The spectrum itself is given by $2 \cdot B_e(\sigma)$ for $\sigma \geq 0$.

2.2.2. Determination of the spectrum from the interferogram

i) The resolution.

The formulas given in the last section are mathematically correct but do not correspond to the experimental facts. A substantial change in the expressions given up to the present is produced by the fact that only a finite phase difference can be produced using interferometers. This effect is considered by introducing a weighting function A(x) in the integral (2.4):

$$B_e'(\sigma) = \int_{-\infty}^{+\infty} F(x) \cdot A(x) \cdot \cos 2\pi\sigma x \, dx = \int_{-\infty}^{+\infty} \tilde{A}(\sigma) \cdot \tilde{F}(\sigma - \sigma') \, d\sigma = \tilde{A}(\sigma) * \tilde{F}(\sigma) \qquad (2.5)$$

This means that the reverse-transformed spectrum is the convolution of the input spectrum and the function A. The spectrum is smeared and is superimposed with lines, which correspond to a side maximum of A. $\tilde{A}(\sigma)$ is an oscillating function. For example, if $B(\sigma) = \delta(\sigma - \sigma_0)$, then the transformation produces: $B'(\sigma) = \tilde{A}(\sigma - \sigma_0)$. If the interferogram is truncated at x = X and if the measured values are then transformed without further mathematical manipulations, then A equals the rectangle function R, defined by:

/12

$$R_{2X}(x) = \begin{cases} 1 & \text{for } |x| \leq X \\ 0 & \text{for } |x| > X \end{cases}$$

The Fourier transform of this function is [5]:

$$\tilde{R}(\sigma) = 2X \frac{\sin 2\pi\sigma X}{2\pi\sigma X} = 2X \cdot \operatorname{sinc}[2\sigma X] \qquad (2.6)$$

where sinc[x] = sin πx/πx. This expression also, at the same time, represents the instrument profile of the interferometer (Figure 2).

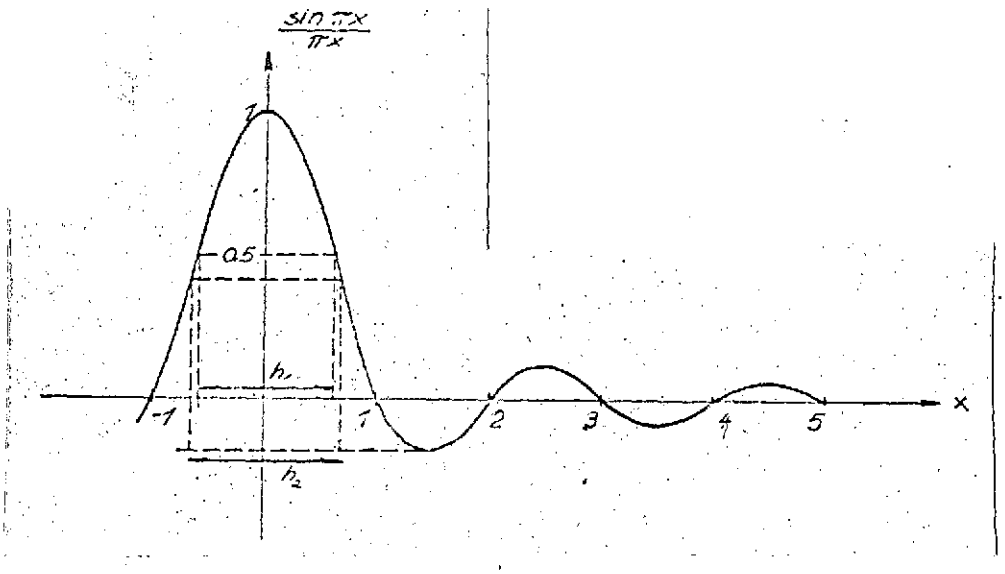

Figure 2. Instrument profile and definition of halfwidth.

In general, the spectral resolution is defined as the halfwidth of the instrument profile (h_1 in Figure 2). This is certainly meaningful for conventional spectroscopy, where the origin of intensity is uniquely specified by the measurement specification and, therefore, no negative intensities occur. In the case of Fourier spectroscopy, such an origin does not exist and, instead, it is determined by the data processing method. Usually, the constant term of the interferogram is suppressed by an alternating voltage amplification of the measurement signal. This leads to the fact that negative intensities can also occur in the calculated spectrum. One example of this is the transformation of a spectrum consisting only of a delta function, that is, of the instrument profile. For $\sigma X = 3/4$, we find $\tilde{R}(\sigma) = -2X \cdot \frac{2}{3\pi}$. /13

As we can easily see, this value equals the absolute minimum of the intensity distribution. Therefore, the usual definition of the resolution capacity can be accepted if the minimum of the calculated spectrum is considered to be the new origin. The magnitude of the maximum is then given by:

$$2X\cdot(1 + 2/3\pi) = 2X\cdot 1{,}212$$

and the half value is $2X\cdot 0{,}606$.

The resolution is defined as the wave number interval $\delta\sigma$, for which we have:

$$2X\cdot\frac{\sin(2\pi X\delta\sigma/2)}{2\pi X\cdot\delta\sigma/2} + 2X\cdot\frac{2}{3\pi} = 2X\cdot 0{,}606$$

or

$$2X\cdot\frac{\sin 2\pi X\cdot\delta\sigma/2}{2\pi X\cdot\delta\sigma/2} = 2X\cdot 0{,}398$$

The solution of this equation gives:

$$2\pi X\cdot\delta\sigma/2 = 0{,}681\pi$$

or

$$\delta\sigma = 0{,}681/X \qquad (2.7)$$

This selection of $\delta\sigma$ corresponds to h_2 in Figure 2. In the literature, this fact is not taken into account and the half width is calculated with respect to the first zero of sinc, so that the resolution is /14

$$\delta\sigma = 0{,}607/X$$

The deviation is not very large, but becomes important if we consider the fact that the interference shift is determined

from this relationship, which is required to produce this resolution $\delta\sigma$.

Here we should also mention the fact that (2.7) shows that there is a considerable difference with respect to the resolution of refraction grids. In our case, $\delta\sigma$ is determined by the maximum phase difference and is, therefore, constant. We have the following relationship for the resolution of refraction grids for spectra of $m^{\underline{th}}$ order for n effective grid lines:

$$\lambda/\Delta\lambda = \sigma/\Delta\sigma = m \cdot n = \text{const}$$

and $\Delta\lambda$ or $\Delta\sigma$ vary. On the other hand, in the case of interferometers, the resolution is proportional to the wave number:

$$R = \sigma/\delta\sigma = \sigma/\text{const.}$$

The resolution defined by (2.7) can only be achieved if the measured data are directly used for the Fourier transformation. This corresponds to the selection $A(x) = R(x)$ in (2.5). If another weighting function is selected for A, in general functions are used which decrease monotonically to zero; when one speaks of apodisation, then $\delta\sigma$ is enlarged. $\tilde{A}(\sigma)$ is always "wider" than $\tilde{R}(\sigma)$. By suitably choosing A, we can make the side maxima of the weighting function smaller than those of R, or we can make them vanish completely. In this way, under some conditions, it is possible to separate a very weak line which is at the edge of a strong line, from the strong line. If the side maxima of A are sufficiently small, then it is possible to improve the unique nature considerably when assigning lines in unknown spectra.

REMARK: In the case of conventional spectroscopy, we have /15 a similar effect. The spectrum is convoluted with the instrument

profile:

$$B'(\sigma) = B(\sigma) * S(\sigma) \ .$$

For a rectangular slit, S also has the form $(\sin x/x)^2$ here.

ii) Support points and interpolation:

A second deviation from the ideal mathematical model caused by the experiment is the fact that the interferogram F(x) is not given analytically but by M measured points. For M equidistant measurement points, F(x) can be represented as a step function with steps having the width x = X/M. The function value for each step is then given by the measurement point which lies in its x interval. The integral then becomes the following:

$$B_e'(\sigma_n) = 2\frac{x}{M} \cdot \sum_{m=0}^{M-1} F(x_m) \cdot A(x_m) \cdot \cos 2\pi \sigma_n x_m \qquad (2.8)$$

with

$$x_m = mX/M \quad \text{for} \quad \sigma_n = n\sigma_M/N \quad \text{and} \quad \begin{cases} m = 0, \ldots, M-1 \\ n = 0, \ldots, N-1 \end{cases}$$

σ_N is the maximum wave number in the spectrum. Thus, one obtains a Fourier series, where the x as well as the σ values are only used at discrete points. In order to again obtain an integral representation, the "delta comb" is defined

$$\amalg_\chi(x) = \sum_{m=-\infty}^{+\infty} \delta(x - m\chi)$$

where here we must set $\chi = X/M$. By using this symbol, (2.8) can be written as:

$$B_e'(\sigma_n) = \chi \int_{-\infty}^{+\infty} \amalg_\chi(x) \cdot A(x) \cdot F(x) \cdot \cos 2\pi \sigma_n x \, dx. \qquad (2.9)$$

Since the Fourier transform of the delta comb is again a delta comb, we can write the following in σ space [5]:

$$B_e'(\sigma_n) = \coprod_{1/\chi}(\sigma) * \tilde{A}(\sigma) * B_e(\sigma). \qquad (2.10)$$

According to this definition, the comb is periodic in σ with the period length $1/\chi$. $B_e'(\sigma)$ is explained by a convolution with the comb. Therefore, B_e has the same periodicity as the comb. /16

Now, χ must be specified so that the spectrum can be contained in a range having the bandwidth smaller than $1/2\chi$. (In the period $1/\chi$, the "physical" spectrum must be included two times, because the "mathematical" spectrum contains also the part with the negative wave numbers to $-\delta_M$.) Therefore, we have:

$$1/\chi = 2\sigma_M \quad \text{or} \quad \chi = X/M = 1/2\sigma_M \qquad (2.11)$$

which produces a relationship between spectral range, maximum phase difference, and number of interferogram points:

$$M = 2\sigma_M X \qquad (2.12)$$

The number of support points of a spectrum which extends over a spectral range from $\sigma = 0$ to $\sigma = \sigma_M$ with spectral elements having widths $\Delta\chi = 1/2x$ is given by:

$$N = \frac{\sigma_M}{\Delta\sigma} = 2\sigma_M X = M \qquad (2.13)$$

The selection $\Delta\sigma = 1/2x$ makes sense because, for this case, $\Delta\sigma < \delta\sigma$ [$\delta\sigma$ is the resolution according to Equation (2.7)]. The number of support points in the interferogram and in the spectrum can be selected the same (the expressions given here result in minimum

values and, by using a larger number of measurement points, we can bring about a simpler interpolation in the spectrum).

The following theorems are important for evaluating the interferograms [5]:

For an interferogram with a maximum phase difference of X, we have:

1.) There are exactly $N = 2 \cdot \sigma_M X$ independent points which uniquely define the spectrum between $\sigma = 0$ and $\sigma = \sigma_M$.

2.) All other points of the spectrum in this spectral range are determined by interpolation using the N independent points. /17

The statement made in 1.) is called the sampling theorem.

2.3. Physical Foundations of Fourier Spectroscopy

We will now investigate the physical processes which lead to the creation of the interferogram and the resulting relationships between resolution, maximum phase difference, and light yield.

We can consider the Michelson interferometer in its simplest form as a dispersion element. Its construction and operation are easy to understand, have a high degree of symmetry, and produce no side effects in contrast to other dispersion elements, which are disturbing in our fundamental analysis.

2.3.1. Production of the interferogram using a Michelson interferometer

As shown in Figure 3, the instrument consists of two flat mirrors perpendicular to each other, of which one is fixed and the other can be displaced in the direction of its surface normal. Between the mirrors, there is a ray divider whose surface normal is inclined by 45° with respect to the normals of the surfaces of the mirrors. In the ideal case, this ray divider reflects 50% of the incoming radiation onto one mirror and lets 50% pass through to the other mirror. Both mirrors /18
reflect the radiation back to the ray divider and half of the flux contained in the rays leaves the instrument perpendicular to the incident direction and then reaches the detector through a collimator. The other half is reflected in the incident direction. (Of course, these values are only valid on the average, because the actual values change with the position of the mirrors, with respect to each other.)

Now we will assume that a plane monochromatic wave hits the interferometer at an inclination angle of α with respect to the optical axis. In order to find the phase difference between the two reflected partial rays, Figure 4 shows one of the mirror surfaces rotated around the central point of the ray divider in such a way that it is parallel to the other one. The ray path is invariant with respect to this rotation. For the rays shown, we obtain the following expression for the phase difference (solid line in Figure 4) for a mirror separation z: /19

$$x = z/\cos\alpha + (z/\cos\alpha - 2z\tan\alpha/\sin\alpha) =$$

$$= 2z\,(1/\cos\alpha - \tan\alpha\sin\alpha) = \frac{2z}{\cos\alpha}(1 - \sin^2\alpha)$$

$$x = 2z \cdot \cos\alpha \qquad (2.14)$$

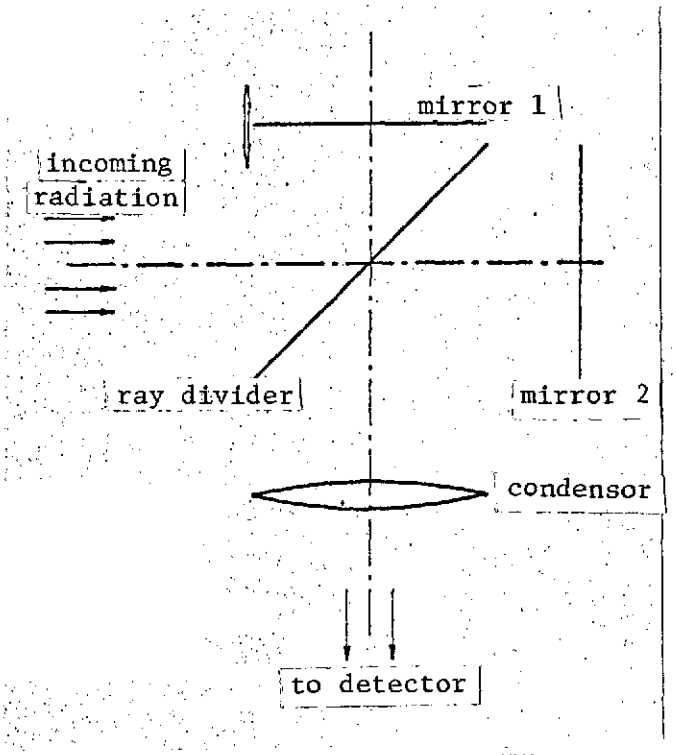

Figure 3. Michelson interferometer.

The phase difference is then:

$$\delta = 2\pi\sigma x = 2\pi\sigma 2z \cos\alpha \qquad (2.15)$$

where σ is again the wave number of the considered monochromatic radiation.

If we assign the amplitude 1 of the electromagnetic field to both rays, and if, in addition, we set the phase of one field vector in the image plane equal to zero, we obtain the following for the field of the interfering radiation:

$$E = 1 + e^{i\delta} = e^{i\delta/2} \cdot 2 \cdot \cos(\delta/2)$$

or for the energy density:

$$u \sim EE^* = 2\,(1 + \cos\delta) = 2\,(1 + \cos 2\pi\sigma x) \qquad (2.16)$$

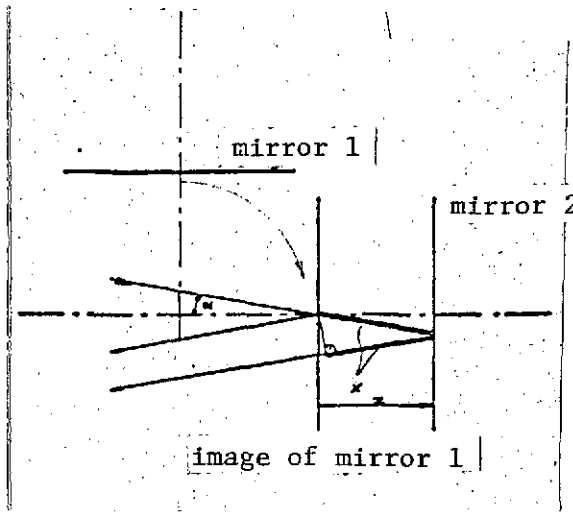

Figure 4. Production of the phase difference.

The intensity distribution in the image plane is found from (2.16) if we consider that, to each direction in the field of plane waves in front of the collimator, there is assigned one point in the focal plane in a unique way and that the entire installation is symmetric about the interferometer mirror axes. If the incident radiation does not come exactly from one direction, but instead, as is usually the case, from a cone, the axis of which coincides with the optical axis of the interferometer, and which has the aperture angle α, then a concentric brightness distribution is produced in the focal plane of the collimator, which are called the Haidinger rings.

If the interferometer is adjusted so that the rays parallel to the axis ($\alpha = 0$) interfere in a constructive way, then the flux through the central circular disc of the interference pattern is a maximum, i.e.,

$$1 + \cos 2\pi\sigma x_0 = 2$$

or

$$2\pi\sigma x_0 = 2n\pi$$

$$\sigma x_0 = n \qquad n = 0, 1, \ldots$$

The position of the flux minima in the image plane is found from the condition /20

$$1 + \cos\left(2\pi\sigma x_o \cdot \cos\alpha_m\right) = 0$$

or

$$2\pi\sigma x_o \cdot \cos\alpha_m = (2m + 1)\pi$$

$$\cos\alpha_m = \frac{2m + 1}{2n} \quad \text{with } m = 0, 1, \ldots, n - 1;$$

In a similar way, we obtain the positions of the maxima from:

$$1 + \cos\left(2\pi\sigma x_o \cdot \cos\alpha_m\right) = 2$$

or

$$2\pi\sigma x_o \cdot \cos\alpha_M = 2l\cdot\pi$$

$$\cos\alpha_M = \frac{l}{n}, \quad l = 0, 1, \ldots, n;$$

Figure 5a shows a cross section through the ring structure of the interference pattern for $\sigma x_o = n$, that is, for constructive interference. Figure 5b shows the same thing for destructive interference in the center.

If the aperture angle of the cone of the incident radiation /21 is small, i.e.,

$$\alpha_o \ll 1\,\text{rad}$$

then the solid angle enclosed by the cone can approximately be written as:

$$\Omega \approx \pi\alpha_o^2.$$

If the incoming radiation is also quasi-monochromatic and if it has the flux $B(\sigma)d\sigma$, then we obtain the following modulated

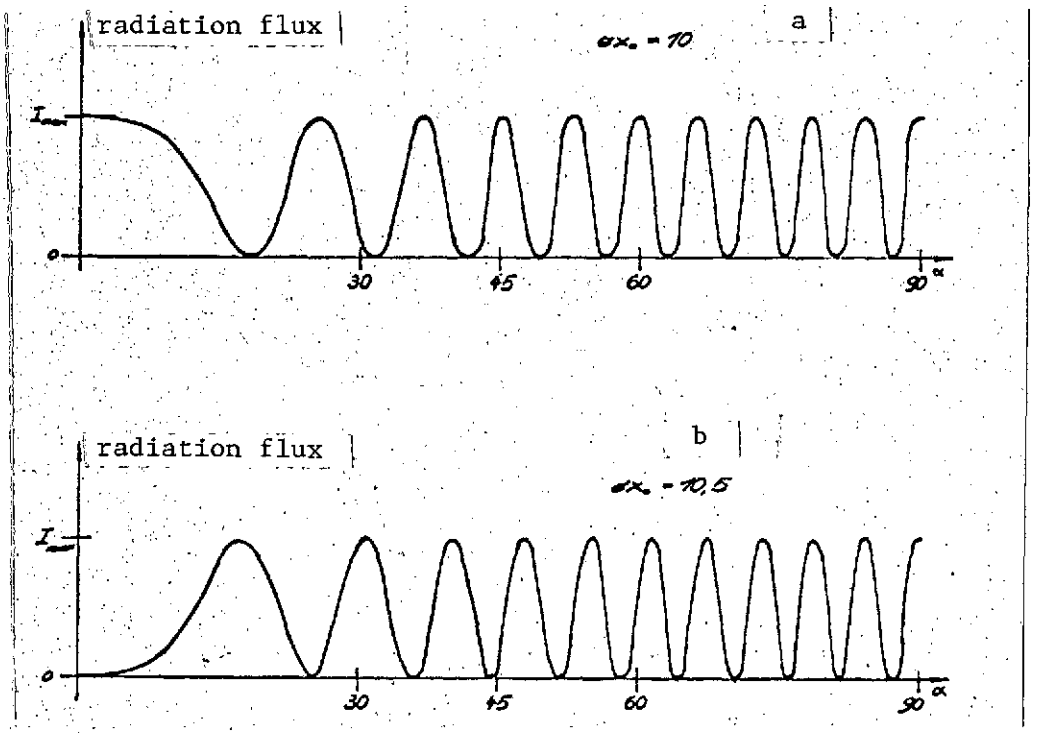

Figure 5. Angular distribution of the Haidinger rings in the interference figure of the Michelson interferometer.

radiation flux arriving in the image plane of the system:

$$dF = B(\sigma)d\sigma \cdot (1 + \cos 2\pi\sigma x)d\sigma$$

where

$$x = x_0 \cdot \cos\alpha \approx x_0 \cdot (1 - \alpha^2/2) \approx x_0 \cdot (1 - \Omega/2\pi) .$$

If we substitute this in dF and integrate over Ω, we find the following [5]:

$$F(x_0) = B(\sigma)d\sigma \cdot \left\{1 + \operatorname{sinc}\left[\frac{\sigma x_0}{2\pi}\Omega\right] \cdot \cos\left[2\pi\sigma x_0 (1 - \Omega/2\pi)\right]\right\} \qquad (2.17)$$

A discussion of this expression shows that the divergence of the incident radiation in the Michelson interferometer produces two effects:

i) The factor $\mathrm{sinc}(\frac{\sigma x_0}{2\pi}\Omega)$ means that the contrast in the interferogram is reduced and completely vanishes in the first zero of sinc. This occurs if the argument of sinc becomes 1, i.e., for

$$\sigma x_0 \Omega = 2\pi \Longrightarrow \alpha_0 = \sqrt{2/\sigma x_0} \qquad (2.18)$$

The divergence of the incident radiation must, therefore, be smaller than $2\alpha_0$ at the interferometer, or the detector can only see a part of the interference pattern in the image plane. (In this case, part of the incident power is lost.) For $\sigma_M = 500\,\mathrm{cm}^{-1}$ ($\hat{=} \lambda_m = 20\mu$) and $x_0 = 20\,\mathrm{cm}$, we have $\alpha_0 = 0{,}014\,\mathrm{rad} = 0{,}81^\circ$, and the ray divergence at the interferometer is then equal to $2\cdot\alpha_0 = 1{,}6^\circ$.

ii) In the argument of cos, there is a factor which is equivalent to a phase displacement. The phase is reduced by the factor $(1 - \Omega/2\pi)$. In this way, either a smaller wave number or a smaller phase difference than actually present is simulated: /22 either x_0 is replaced by $x_0 (1 - \Omega/2\pi)$ or σ is replaced by $\sigma (1 - \Omega/2\pi)$.

This error can easily be corrected and does not have to be discussed here.

The first effect, on the other hand, produces an important relationship between the maximum resolution and the light yield [6] for the Fourier spectroscopy. This relationship will be considered in detail in the following.

2.3.2. Resolution and light yield

If, in the wave number interval $d\sigma$, the spectral intensity I_σ is radiated from the solid angle Ω onto the interferometer, then the radiation power arriving at the detector is given by:

$$F_\sigma \cdot d\sigma = T_\sigma \cdot I_\sigma \, E_\sigma \cdot d\sigma \, . \qquad (2.19)$$

T_σ is the transmission of the system from the first optical element to the detector, and the detector properties are not considered here. It depends on the ray geometry and, in particular, on the ray divergence at the interferometer, as well as on its properties and on the adjusted phase difference. Therefore, the transmission is defined as follows for the wave number σ and the phase difference x (it determines the shading, together with the ray divergence in the case of the lamella grid, see 3.2):

$$T_\sigma(x) = \frac{F_M(x,\sigma)}{F_e(\sigma)} \leq 1 \qquad (2.20)$$

where F_M is the flux reaching the detector when the interferometer is adjusted to constructive interference. F_e is the radiation flux at the inlet aperture of the telescope. This definition only makes sense when F_e comes from one line which is quasi-monochromatic with respect to the instrument, i.e., its width must be smaller than the resolution of the interferometer.

E_σ is the solid angle range of the system, determined by: /23

$$E_\sigma = A_i \cdot \Omega_i$$

A_i here is the ray cross section for an optical element or in an image plane of the system. Ω_i is the solid angle under which this element is illuminated.

T_σ depends on the wave number, whereas E_σ is defined for large sources by the field of view of the total instrument (telescope and detector). For smaller sources, it is determined by the source diameter. It is only when the image of the source becomes smaller than the refraction disc that E_σ also becomes wave number dependent. The light yield of the system is defined as:

$$L_\sigma = \frac{E_\sigma d\sigma}{I_\sigma d\sigma} = T_\sigma E_\sigma \qquad (2.21)$$

Since E determines the ray divergence at the dispersion element and, therefore, the resolution through Ω, we find a relationship between the light yield and the resolution from this relationship.

In Section 2.2, we showed that the resolution of the interferometer is given as follows for parallel incident light:

$$\delta\sigma = 0{,}681/X$$

where X is the maximum phase difference. Therefore, $\delta\sigma$ could be made theoretically as small as possible, if X, or in the final analysis, the displacement of the movable interferometer mirror, was made large enough. Now Relationship (2.17) shows that for finite ray divergence at the interferometer, the modulation of the radiation flux becomes smaller with increasing x when the phase difference changes, until finally, the detector is illuminated with constant power, independent of the mirror shift. The contrast vanishes for the maximum wave number σ_M

of the spectrum exactly then, when the condition

$$\operatorname{sinc}\left[\frac{\sigma_M \cdot X}{2\pi}\Omega_M\right] = 0$$

is met, or

$$\frac{\sigma_M \cdot X}{2\pi}\Omega_M = 1.$$

Because of $\Omega_M \approx \pi\alpha_M^2$, we find the following for small angles

$$\alpha_M = \sqrt{2/\sigma_M X} \tag{2.22}$$

or for the ray divergence:

$$2\alpha_M = \sqrt{8/\sigma_M X} \approx \sqrt{\frac{12{,}56}{\sigma_M}}$$

$$2\alpha_M \approx \sqrt{\frac{12}{R_M}} \tag{2.23}$$

where R_M is the maximum resolution of the interferometer [see remark according to (2.17)].

In the selection of α_M, according to (2.23), the maximum resolution is only achieved with an infinitesimally weak contrast, that is, not at all in practice. Therefore, it makes more sense to use a relationship involving the ray divergence and the resolution, which will still provide a measurable contrast for $x_0 = X$. Such a relationship is obtained if the ray path is selected so that the phase difference between the rays with $\alpha = 0$ and those with $\alpha = \alpha_0$ is a maximum of π for the path difference X. Transferred to the interference pattern, this means that it consists only of the central circular disc and the ring structure is not present or is washed out. Therefore,

we require:

$$2\pi\sigma_M (X - X\cos\alpha_0) = \pi$$

$$1 - \cos\alpha_0 = 1/(2\sigma_M X)$$

and, again for small angles:

$$\alpha_0 \ll 1, \qquad 1 - \cos\alpha_0 \approx \alpha_0^2/2 = 1/2\sigma_M X$$

$$2\alpha_0 = 2\sqrt{1/\sigma_M X} \approx \sqrt{6/R_M} \qquad (2.24)$$

$$\Omega_0 \approx \frac{15\pi}{R_M} \qquad (2.25)$$

For this selection of Ω_0, the modulation of intensity at the detector still amounts to 64% of the modulation for phase difference 0 at the maximum phase difference.

If we substitute (2.25) in the defining equation (2.21) for the light yield, we find:

$$L = T_\sigma \cdot F \cdot 1{,}5\pi/R_M \quad \text{or} \quad L \cdot R_M = 1{,}5\pi T_\sigma F = \text{const} \qquad (2.26)$$

The last relationship applies if T does not depend on the wave number. If the resolution of the interferometer is increased, then the ray divergence at the dispersion element must be reduced and, for a constant surface area of the dispersion area, the light yield and, therefore, the power arriving at the detector is reduced. Therefore, we must make a compromise in order to arrive at reasonable values for the resolution and light-yield.

For the infrared experiment, we have $R_M = 10^4$ and, therefore, we find the following for the maximum ray divergence:

$$2\alpha_0 = \sqrt{\frac{6}{10^4}} = \frac{\sqrt{1,5}}{50} = 0,024\,\text{rad} \triangleq 1,4^\circ$$

This value does not represent a restriction for the experiment, according to the present state of the art. This ray divergence is not even completely exploited for extended sources (see 4).

In principle, this represents an important advantage of interferometry over normal spectroscopy. Conventional dispersion elements are illuminated by an inlet slit and they then illuminate the detector through an outlet slit. If both slits are assumed to be equally large, of length l and width b, then we have the following relationship for the solid angle under which the radiation falls on the grid:

$$\Omega \approx bl/f^2$$

where f is the focal length of the collimator. A conventional spectrometer having the dispersion $(d\theta/d\sigma)$ and resolution R has a slit width of:

$$w = f \cdot (d\theta/d\sigma) \cdot \sigma/R$$

The instrument is operated in the range where [5, 7]

$$\sigma\,(d\theta/d\sigma) \approx 1.0$$

Therefore, we find: /26

$$\Omega_G = l/fR$$

and, typically, we have $l/f \approx 1.50$. If we compare this with the solid angle for the Michelson interferometer (2.25), then we obtain

$$\Omega_0/\Omega_0 \approx 10\pi \approx 30, \qquad (R/R_M = 0,1) \tag{2.27}$$

For the same dimensions of the dispersion element, Fourier spectroscopy provides approximately 30 times as much light yield than conventional spectroscopy.

This "solid angle range advantage" was first investigated in 1954 by P. Jacquinot [8] and can be used if the radiation sources have sufficient width. Therefore, they will not be important for astronomical purposes. [In an indirect way, it is advantageous because, since the solid angle range is constant, the size of the dispersion element can be reduced (see 3.4).] On the other hand, the so-called multiplex gain can be very well exploited in these measurements. Whether it contributes to an improvement in the signal-noise ratio in the calculated spectrum depends on the type of dominating noise source. In the following, we will investigate the influence of this noise on the calculated spectrum.

2.4. Signal-Noise Ratio

In addition to the spectral resolution, the signal-noise ratio in the measured spectrum represents one factor which determines the usability of measurements. The resolution was a clear concept and could be analyzed mathematically in a simple way. The signal-noise ratio is determined by many components which are sometimes not completely known. The results of the following sections, therefore, apply only for certain cases and cannot be transferred to general conditions.

2.4.1. Basic fundamentals on signal-noise ratio

/27

The various noise sources first have a direct effect on the measured values and, therefore, on the interferogram points. For the interpretation of the spectrum, we are interested in the

Fourier transform of these measurement errors. Therefore, we will first consider the relationship between the noise and the Fourier transformation.

Not enough is known about frequency-dependent noise sources in order to make valid statements. For white noise, which is not correlated with the signal, we can determine the transformation behavior as follows [7]. First, we consider the measurement of a constant physical variable. Its value can be determined by measuring the variable N times ($N \gg 1$) where each time integration over the measurement time τ is carried out. τ is the elementary measurement time. The measured values are then given by a collection $S_1, \ldots, S_N$. The average value is defined as the measured point, as follows:

$$\langle S \rangle = \frac{1}{N} \sum_{i=1}^{N} S_i \quad . \tag{2.28}$$

The quadratic deviation of these values is:

$$(\Delta S)^2 = \frac{1}{N} \sum_i (S_i - \langle S \rangle)^2 = \langle (S_i - \langle S \rangle)^2 \rangle \quad . \tag{2.29}$$

The square root of this expression is the standard deviation:

$$\Delta S = \sqrt{\langle (S_i - \langle S \rangle)^2 \rangle} \quad . \tag{2.30}$$

ΔS is a measure for the accuracy with which S was measured.

The signal-noise ratio for a measurement series is defined as:

$$(s/n)_N = \langle S \rangle / \Delta S \quad . \tag{2.31}$$

Now a new group of N/m values G_i is produced from the measured values S_i:

$$\begin{aligned} G_1 &= S_1 + \dots + S_m \\ &\vdots \quad \vdots \\ G_{N/m} &= S_{N-m+1} + \dots + S_N \,. \end{aligned}$$

In order to be able to apply statistical methods, we specify that $N/m \gg 1$. The average value for this group is given by:

$$\langle G \rangle = \frac{1}{N/m} \sum_i G_i = \frac{m}{N} \sum_i S_i = m \langle S \rangle$$

and the quadratic deviation is:

$$\begin{aligned} (\Delta G)^2 &= \frac{m}{N} \cdot \sum_i (G_i - \langle G \rangle)^2 = \frac{m}{N} \{ (S_1 + \dots + S_m - m\langle S \rangle)^2 + \\ &\quad + \dots + (S_{N-m+1} + \dots + S_N - m\langle S \rangle)^2 \} = \\ &= \frac{m}{N} \sum_i (S_i - \langle S \rangle)^2 + \frac{m}{N} \sum_i \sum_{j \neq i} (S_i - \langle S \rangle)(S_j - \langle S \rangle) \\ (\Delta G)^2 &= \frac{m}{N} \sum_i (S_i - \langle S \rangle)^2 + \qquad \varnothing \,. \end{aligned}$$

For sufficiently large N and white noise, we find $\varnothing = 0$,* and then we have:

$$\begin{aligned} (\Delta G)^2 &= m(\Delta S)^2, \\ \Delta G &= \sqrt{m} \cdot \Delta S \,, \\ (s/n)_{N/m} &= \sqrt{m} \cdot (s/n)_N \,. \end{aligned} \qquad (2.32)$$

*$\varnothing = 0$ means that the noise components are statistically independent, that is the case for a white noise spectrum [7].

The signal-noise ratio is improved by summation of the measured values. This summation corresponds to an extension in the elementary measurement time τ by the factor m.

This calculation is valid only if the noise components are statistically independent, i.e., if $\emptyset$ vanishes and there must be a sufficient number of values G_i. Nevertheless, we can extrapolate to m = N in order to estimate the measurement accuracy, even though the usual definitions of noise and standard deviation are no longer valid. (The exact formulation is made possible by using statistical ensembles.) We then obtain:

$$\langle S \rangle_1 = N \cdot \langle S \rangle_N \quad \text{and} \quad (\Delta S)_1 = \sqrt{N}\,(\Delta S)_N \qquad /29$$

where we find

$$(s/n)_1 = \sqrt{N}\,(s/n)_N \qquad (2.33)$$

Now we again consider the N original measurement points. They are subjected to Fourier transformation according to the following equation, just like the interferogram points:

$$\tilde{x}_m = \sum_n x_n \cdot \exp\left(2i\pi \frac{nm}{N}\right) \qquad n,m = 0,1,\ldots,N-1$$

This then produces

$$\tilde{S}_m = \sum_n S_n \exp\left(2i\pi \frac{nm}{N}\right)$$

or

$$\tilde{S}_o = \sum_n S_n = N \cdot \langle S \rangle, \quad \tilde{S}_m \approx 0 \quad \text{for } m \neq 0 \qquad (2.34)$$

$\tilde{S}_m$ for $m \neq 0$ almost vanishes, because a constant signal has been transformed. The values are, in general, determined by the noise. If there is no noise, they are exactly zero. The quadratic deviation of these values from zero is given by:

$$(\Delta\tilde{S})^2 = \langle \tilde{S}_m \tilde{S}_m^* \rangle = \left\langle \sum_{n,n'} S_n S_{n'}^* \cdot \exp\left\{2\pi i \frac{m}{N}(n-n')\right\} \right\rangle$$

$$= \left\langle \sum_{n,k} S_n S_{n+k} \cdot \exp\left\{2\pi i \frac{mk}{N}\right\} \right\rangle = \left\langle \sum_k N \cdot \langle S_n S_{n+k} \rangle \cdot \exp\left\{2\pi i \frac{mk}{N}\right\} \right\rangle$$

$$= \langle (\Delta S)^2 \cdot N \rangle = N \cdot (\Delta S)^2$$

Its standard deviation is:

$$\Delta\tilde{S} = \sqrt{N} \cdot \Delta S \qquad (2.35)$$

This means that the Fourier transformation changes the s/n ratio just like the summation of all measured values. Equation (2.34) shows that this summation does indeed occur, even though there is a phase displacement in general, which is produced by the complex exponential function. This displacement leads to a filtering at the "correct" frequency of the components of the measured values. They are "corrected" at a certain S_m, as can be seen above for $m = 0$.

Here again, Ø must vanish in order for (2.35) to be correct./30 We have the following for the s/n ratio:

$$\frac{\tilde{S}}{\Delta\tilde{S}} = \sqrt{N} \cdot \frac{S}{\Delta S} \cdot$$

The physical reason for the improvement of the s/n ratio can be most simply recognized using the example of Fourier spectroscopy: a measured point of the interferogram is obtained

during the elementary measurement time τ. It contains information on all spectral elements of the spectrogram. The integration time per spectral element, therefore, effectively amounts to $N\tau$ seconds and this time is decisive for the s/n ratio in the spectrum.

2.4.2. Multiplex advantage

Up to the present, we determined that the s/n ratio is improved by a factor of $\sqrt{N}$ if the integration time for one point of the spectrum is extended from τ to $N\tau$. Therefore, it is proportional to the square root of the total measurement time:

$$s/n \sim \sqrt{t}\,.$$

Now let us assume that the spectrum is recorded with various methods [5]: using the sequential method, where the spectral elements are interrogated in a time sequence, as well as using the simultaneous method, i.e., by simultaneous recording of all spectral elements. The first method is used in conventional spectroscopy when a detector interrogates the spectrum. The second method is done using Fourier spectroscopy. (It would also be thinkable to have an arrangement which uses a narrow band filter on a detector for each spectral element, which would be a multichannel analyzer. The method becomes impractical even for small resolution.)

If the same integration time per spectral element is selected for both methods, that is, the same s/n ratio in the spectrum (for the same light yield), then the measurement time for the sequential method is N times as large as the time using the simultaneous method, when N spectral elements are to be measured. /31
On the other hand, if we assume equal total measurement time,

then the simultaneous measurement will produce a s/n ratio which is better than that of the sequential method by a factor of $\sqrt{N}$. This gain is called the multiplex advantage. It was discussed in 1951 by Fellgett [9].

In fact, the gain is reduced by the factor $\sqrt{2}$, because the flux from the spectral element occurs only during one-half of the measurement time in full force at the detector, because of the modulation caused by the change in the phase difference. On the other hand, it should be noted that the advantage over conventional spectrometers, because of the solid angle range advantage, can be substantially larger. (The solid angle range advantage cannot be exploited here because of the small source dimensions in our experiment.)

If we are to investigate an unknown spectrum, then the Fourier spectroscopy should be preferred over the scan method, using conventional technology, because of the multiplex and solid angle range advantages. However, if we want to determine the flux from a few lines with known wavelengths or if we want to investigate a few spectral elements, then the conventional method is more advantageous because it produces results with less complexity than the Fourier spectroscopy and because the multiplex gain can be ignored.

Tippable Fabry-Perot filters are especially well suited for such measurements, in which the mirror distance is fixed. By rotating the filters in the ray path, the wavelength which is passed through is varied, so that a spectral range of about 1 μ can be covered.* Since the filter operates as an

*The free spectral range is given by $\Delta\sigma = \frac{\sigma^2}{2nd}$ [30]. d: distance of reflected surfaces; n: index of refraction of material between them.

interferometer with fixed phase difference, the solid angle range advantage is maintained and can be exploited, by reducing the diameter of the filter, which increases the ray divergence [2, 10]. Therefore, these filters are to be looked upon as accessory instruments.

In general, we may state that the multiplex method should always be preferred when the number of spectral elements exceeds the order of magnitude one. /32

2.4.3. General expression for the signal/noise ratio

The s/n ratio for an arbitrary element of the calculated spectrum can be written as follows for the considered case of white noise not correlated with the signal:

$$(s/n) = \frac{\left(\int S_Q\, dt\right)_{\sigma,\Delta\sigma}}{\sqrt{\int S_{st}^2\, dt}} = \frac{i(\sigma)\cdot\Delta\sigma\cdot L\cdot\eta t}{NP\cdot\sqrt{\eta t}} = \frac{i(\sigma)\cdot\Delta\sigma\cdot L}{NEP}\cdot\sqrt{\frac{\eta t}{1s\cdot\Delta f}}\cdot \quad (2.37)$$

Here we have S — source (S_Q) and perturbation signal (S_{st}), respectively, [W]; NP — noise power [W]; $i(\sigma)$ — radiation density for the wave number [W/cm^{-1} cm^2 sr]; L — light yield of the instrument [cm^2 sr] (L was assumed to be independent of σ for simplicity here); $\Delta\sigma$ — width of considered spectral element [cm^{-1}]; $i(\delta)\cdot\Delta\delta\cdot L$ — power absorbed by detector [W]; η — effectiveness of measurement (integration time per interferogram divided by measurement duration) because two interferograms are recorded during the measurement; t — duration of the measurement [s]; NEP — normalized noise power (noise equivalent power), defined as the signal for which s/n = 1 when the integration is 1 sec and the amplifier bandwidth is 1 Hz

$[W/\sqrt{Hz}]$; $(NP = NEP \cdot \sqrt{\Delta f})$; Δf — bandwidth of amplifier [Hz].

The 1 s in the square root of (2.37) is caused by the definition of NEP.

2.4.4. Detector and photon noise

As long as the detector operates linearly, the detector noise is independent from the absorbed radiation power and is, therefore, not modulated together with the radiation flux. In addition, by directional modulation of the radiation flux and by suitably operating the interferometer, it is possible to record /33 only white noise at the detector. (By suitable selection of the modulation frequency, for example, it is possible to suppress the flicker noise.) Then it will have the same behavior with respect to the Fourier transformation as the noise considered in Section 2.4.1, and therefore (2.37) can be applied.

The normalized noise power cannot be directly calculated and it will be investigated more thoroughly when we select the detector (see 4.3).

The photon noise, on the other hand, can be determined relatively simply. The number of photons emitted by a thermally excited source per frequency interval and solid angle is given by:

$$\frac{dL}{d\nu} = \varepsilon(\nu) \cdot \frac{2\nu^2}{c^2} \cdot \frac{1}{e^{h\nu/kT} - 1} \Big/ \left[\frac{\text{Photons}}{cm^2 s\, sr\, Hz}\right]$$

where $\varepsilon(\nu)$ is the emissivity and T is the temperature of the source. From this relationship, it is possible to determine for any frequency of the photons the average square of the fluctuations in the photon number using the Bose statistics.

From this, it is possible to determine it for the flux as well. The normalized noise power is then determined by the power of the fluctuating flux from all frequencies and equals [11]:

$$NEP_{Phot} = \frac{h}{c}\left\{2L \cdot \int_0^\infty \frac{\varepsilon(\nu) \cdot \nu^4 \cdot e^{h\nu/kT}}{(e^{h\nu/kT}-1)^2}\, d\nu\right\}^{1/2}. \qquad (2.38)$$

Since the source is thermally excited, we have $0 \leq \varepsilon \leq 1$. In general, the emissivity will not be known and, therefore, $\varepsilon(\nu)$ is replaced by the average value $\bar{\varepsilon}$. In this case, the integral can be evaluated:

$$\bar{\varepsilon} \cdot \int_0^\infty \frac{\nu^4 \cdot e^{h\nu/kT}}{(e^{h\nu/kT}-1)^2}\, d\nu = \bar{\varepsilon}\left(\frac{kT}{h}\right)^5 \cdot \int_0^\infty \frac{x^4 e^x}{(e^x-1)^2}\, dx = \bar{\varepsilon}\left(\frac{kT}{h}\right)^5 \cdot \frac{4\pi^4}{15}.$$

and, therefore, we have:

$$NEP_{Phot} = \left\{4L\bar{\varepsilon} \cdot b \cdot kT\right\}^{1/2} \qquad (2.39)$$

$$NEP_{Phot} = \left\{\varepsilon L \cdot T^5 \cdot 9{,}96 \cdot 10^{-35}\, W^2 s^3/cm^2 deg^5\right\}^{1/2} \qquad (2.40)$$

where $b = (\tilde{\sigma}/\pi)\, T^4\ W/cm^2 sr$ is the flux density of a black body at temperature T and $\tilde{\sigma}$ is the Stefan-Boltzmann constant. /34

The photon noise per spectral element is proportional to the square root of the radiation power in this element and is, therefore, correlated with the signal. In the frequency range of interest, it can be assumed to be white. Therefore, not all the requirements for the validity of (2.38) are satisfied. Nevertheless, this relationship applies for astronomical measurements, as will now be discussed:

If the spectrum to be measured consists of a single line which is narrower than the resolution which can be achieved, then the interferogram points have a noise superimposed on them. Its amplitude is proportional to the square root of the amplitude of the ideal interferogram points. In particular, the noise vanishes when the flux vanishes in the case of destructive interference. In the calculated spectrum, the noise is concentrated in the spectral element of the line.

In the IR experiment, conditions are different because the spectrum of the rays arriving at the detector contains the lines of the source and of the atmosphere, as well as the continuum radiation of the dust surrounding the source as well as the radiation of the telescope optics. Therefore, the interferogram will no longer have any points for which the radiation flux vanishes at the detector. Therefore, the correlation between the signal and the noise will become much smaller or will completely vanish. In addition, the photon noise is determined by the radiation from the atmosphere and from the telescope optics and not by the interstellar source, which again reduces the correlation with the signal. Therefore, the noise is distributed over the entire calculated spectrum when the Fourier transformation is carried out.

Therefore, the conditions for using (2.38) are satisfied in the case of astronomical measurements. It follows from this that, in contrast to the opinion of many authors, the multiplex /35
advantage also is maintained when the photon noise is the dominating noise source. However, this only applies for the signal/noise ratio of those spectral elements which contain a line. When we average over the recorded spectral range, the multiplex advantage does not appear [12], which has no meaning for the evaluation of the data. Therefore. in the case where

the photon noise dominates, we have the following relationship for the s/n ratio in a spectral element:

$$(s/n)_{Phot} = \frac{i(\sigma)\cdot\Delta\sigma\cdot L}{\sqrt{4L\cdot\varepsilon b\cdot kT}}\cdot\sqrt{\frac{\varrho t}{1s\cdot\Delta f}} = \frac{i(\sigma)\cdot\Delta\sigma}{\sqrt{4L\varepsilon bkT}}\cdot\sqrt{\frac{L\varrho t}{1s\cdot\Delta f}} \quad (2.41)$$

The s/n ratio is given by the following for dominating detector noise:*

$$(s/n)_{Det} = \frac{i(\sigma)\cdot\Delta\sigma\cdot L}{NEP_{Det}}\sqrt{\frac{\varrho t}{1s\cdot\Delta f}} \quad (2.42)$$

These two relationships apply for the signal-noise ratio when the width of the spectral element is fixed, that is, after the measurement is over. In order to perform a functional check of the instrument, it is important to calculate a spectrum during the measurement, even though it will have a reduced resolution. Therefore, we are interested in the time variation of the s/n ratio when there is time-dependent resolution. This can be calculated if we consider that the width of a spectral element is given by:

$$\Delta\sigma = 1/2x = 1/(4v\cdot t') \quad (2.43)$$

where v is the velocity with which the movable interferometer part is displaced. If this relationship for $\Delta\sigma$ is substituted in (2.41/42), then we obtain the following for the s/n ratio per resolved spectral element:

$$(s/n)'_{Phot} = \frac{i(\sigma)}{4v\cdot\sqrt{4b\varepsilon kT}}\cdot\sqrt{\frac{L\varrho}{1s\cdot\Delta f\cdot t'}} \quad (2.44)$$

$$(s/n)'_{Det} = \frac{i(\sigma)\cdot L}{4v\cdot NEP_{Det}}\cdot\sqrt{\frac{\varrho}{1s\cdot\Delta f\cdot t'}} \quad (2.45)$$

*P. F. Parshin [22] arrives at the same result.

The s/n ratio, therefore, decreases in the spectral elements. This behavior is understandable because, for an element with fixed width, it will only increase in proportion to $\sqrt{t}$, whereas here the width is decreasing with $1/t$, which together results in a decrease according to $1/\sqrt{t}$. /36

The last two relationships are only correct when the source radiates continuously. On the other hand, if it only emits line radiation, then the time variation of the s/n ratio is more complex. If a certain spectral element contains exactly one line, for example, and if this element is continuously being divided further, then s/n = 0 holds in the elements which do not contain the line. In those elements which contain the line, the relationship (2.41) applies, where $\Delta\sigma$ is the line width. It is only when the line width becomes greater than the resolution, that is, when the line consists of several spectral elements, that the s/n ratio again decreases.

The amplification bandwidth Δf is one unknown in the relationships given above. Let τ_i be the time which is required for determining a point of the source interferogram. It can be shown that, independent of the measurement technique used, the following relationship is valid: $|\Delta f \geq 1/\tau_i|$. If the interferogram consists of N points, then we also have $t = N\tau_i$. A spectrum is then calculated after a time t' from the interferogram points previously measured. It will then consist of $N' = t' \cdot N/t$ points. If this relationship is substituted in (2.41/42) or (2.44/45), and if we also assume $\Delta f = 1/\tau_i$, then we find:

$$\left|(s/n)_{Phot} = \frac{i(\sigma)\cdot\Delta\sigma}{\sqrt{4bkT}}\cdot\sqrt{\frac{\eta_0 N}{\eta_s}}\cdot\tau_i\right| \qquad (2.41a)$$

$$(s/n)_{Det} = \frac{i(\sigma)\cdot\Delta\sigma\cdot L}{NEP_{Det}}\cdot\sqrt{\frac{2N}{15}}\cdot\tau_i \qquad (2.42a)$$

$$(s/n)'_{Phot} = \frac{i(\sigma)}{4V\cdot\sqrt{4bkT}}\cdot\sqrt{\frac{L_0}{15\cdot N}} \qquad (2.44a)$$

$$(s/n)'_{Det} = \frac{i(\sigma)}{4V\cdot NEP_{Det}}\cdot\sqrt{\frac{2}{15\cdot N}} \qquad (2.45a)$$

The last two expressions again give the s/n ratio per /37
resolved spectral element. This somewhat unusual point of view makes sense for the IR experiment, because the spectrum is to be calculated during the measurement using the already available interferogram points, in order to obtain a check on the functioning of the instrument. Equations (2.44a/45a) show that the s/n ratio in the spectrum is independent of the number of transformed interferogram points and of the measurement time. Therefore, already shortly after the measurement, we can decide whether the spectrum of the interstellar source emerges enough from the background so that it makes sense to continue the measurement.

When we derived the last two relationships, we assumed a continuum source, which is satisfied for interstellar sources because usually they are surrounded with dust which produces a continuous spectrum. After a measurement time of about 1 second (about 10 interferogram points are determined in this time), therefore, first the dust concentration will be seen first. As the resolution increases, its structure becomes visible and finally, the lines of the interstellar gas cloud will emerge.

In addition, we should mention the fact that the last two expressions appear to be independent of the elementary measurement time, which would mean that useful results would be obtained even for infinitesimally small integration times. Of course, this is not the case, because the width of the spectral element is proportional to $1/t'$, according to (2.43). Therefore, very wide spectral elements are required for very small integration times, if (2.44a/45a) is to apply. The limit of validity is reached when the width of the spectral element equals that of the spectrum to be recorded. In this experiment, for $\Delta\sigma \approx 4500\ cm^{-1}$ and $v = 5 \cdot 10^{-3}$ cm/sec; this would be the case for $t' = 1/(4v \cdot \Delta\sigma) = 0.1$ sec.

2.4.5. Effects of instrumentation errors on the s/n ratio /38

Two instrumentation errors will have a detrimental effect on the noise in the calculated spectrum. The first one is based on the inexact adjustment of the phase difference in the interferometer and the second one is concerned with the fact that the telescope does not have constant alignment in time.

The calculation of the spectrum from the interferogram implies the assumption that the change in the phase difference of the interfering rays from one interferogram point to the other is exactly equal. The change in the phase difference is produced by displacement of the interferometer mirror, which will be constant only within certain tolerances which are known. If the displacement is produced by a micrometer spindle, then periodic errors will also occur in general.

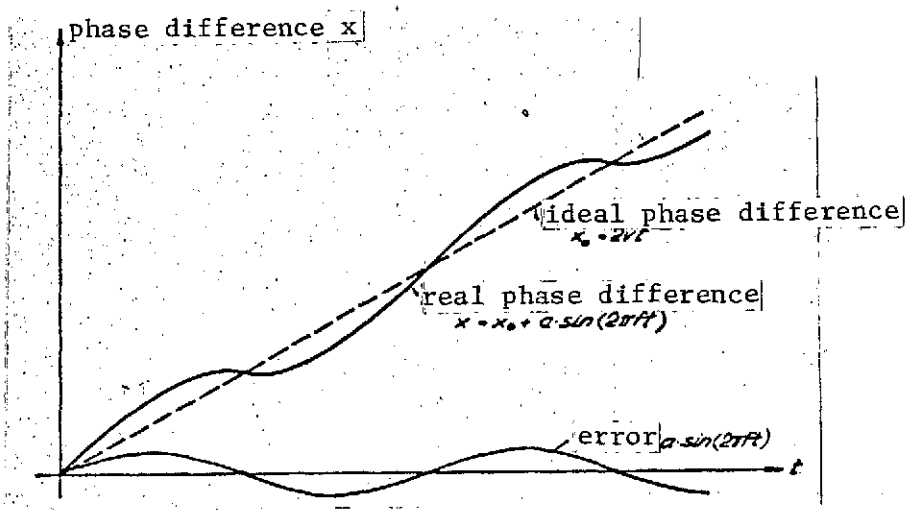

Figure 6. Time variation of phase difference for periodic errors in the interferometer advance.

First, we will investigate the influence of such periodic errors on the calculated spectrum. It is assumed that the spectrum consists of a delta line at the wave number σ_0, which produces the flux B_0 at the detector. If v is the advancing velocity of the interferometer mirror, then the phase difference at time t is given by:

$$x = 2vt + a \cdot \sin 2\pi ft,$$

where a is the amplitude and f is the frequency of the error. /39
The ideal phase difference is:

$$x_o = 2vt .$$

If this relationship is solved for t and substituted above, then we find:

$$x = x_o + a \sin(2\pi f x_o / 2v) .$$

The flux from the spectrum is:

$$B(\sigma) = B_0 \cdot \delta(\sigma - \sigma_0) \; ;$$

and we have the following for the interferogram:

$$F(x_0) = B_0 \cdot \cos 2\pi\sigma_0 (x_0 + a \cdot \sin(\pi f x_0 / v)) \; . \qquad (2.47)$$

The expansion of this expression, according to Bessel functions and the expansion of them with respect to $\sigma_0 a$, results in the following in the first approximation [7]:

$$F(x_0) = B_0 \{\cos 2\pi\sigma_0 x_0 + \tfrac{1}{4}\sigma_0 a [\cos 2\pi x_0 (\sigma_0 - f/2v) + \cos 2\pi x_0 (\sigma_0 + f/2v)]\}$$

The reverse transformation then results in:

$$B'(\sigma) = 2 \cdot \int_0^X F(x_0) \cdot \cos 2\pi\sigma x_0 \, dx =$$

$$= B_0 \cdot \left\{ X \cdot \frac{\sin 2\pi(\sigma - \sigma_0)X}{2\pi(\sigma - \sigma_0)X} - \frac{\sigma_0 a}{4} \cdot 2 \int_0^X dx_0 [\cos 2\pi x_0 (\sigma - \sigma_0 + f/2v) + \right.$$

$$\left. + \cos 2\pi x_0 (\sigma + \sigma_0 - f/2v) + \cos 2\pi x_0 (\sigma - \sigma_0 - f/2v) + \cos 2\pi x_0 (\sigma - \sigma_0 + f/2v)] \right\}$$

$$B'(\sigma) = X B_0 \cdot \{\operatorname{sinc}[2(\sigma - \sigma_0)X] + \frac{\sigma_0 a}{4} \cdot \operatorname{sinc}[2X(\sigma - \sigma_0 + f/2v)] + \qquad (2.48)$$

$$+ \operatorname{sinc}[2X(\sigma - \sigma_0 - f/2v)]\}$$

Here, we have ignored the terms which contain $\sigma + \sigma_0$ because their greatest values occur for negative wave numbers and they hardly influence the values with $\sigma > 0$.

Equation (2.48) shows that the calculated spectrum contains two satellite lines at the wavelengths $\sigma_0 \pm f/2v$, in addition to the real lines. Their amplitude relative to the central line is $\sigma_0 \cdot a/4$.

If the step of the spindle used for the interferometer drive equals Δz = 1 mm, then the main contribution of the periodic error has the local period of 1 mm and we find:

$$f = v/\Delta z, \quad \sigma_{\Delta z} = 1/2\Delta z = 5\,\mathrm{cm}^{-1}.$$

The satellite lines occur at a separation of 5 cm^{-1} from the central line. The approximation just considered is only correct /40 for $\sigma_0 a \ll 1$. In the experiment, the maximum wave number will be about 500 cm^{-1} and for $\sigma_0 a \leq 10^{-2}$, we find: $a \leq 0{,}2\mu$. If a is substantially larger, then the same analysis can be carried out but, in the expansion (2.47), it is necessary to consider terms of higher order.

In addition to this purely periodic error, statistical errors will also occur. Their distribution can be represented as a sum of periodic deviations and, in the limiting case, as an integral over them. This means that the two satellite lines are smeared to form sidebands. A new noise component is produced. The calculated spectrum shows the same behavior with respect to periodic fluctuations in the telescope alignment, as did the phase difference with respect to periodic errors.

The error is produced because the Fourier transformation of the interferogram points assumes that there is a constant flux from the source. If the alignment of the telescope is not stable over the entire measurement duration, then the flux will vary with time, because the part of the source inside the field of view of the detector will change in time. The change in the flux with alignment depends greatly on the source size and its relationship with respect to the field of view diameter. It is the smallest for point sources, as long as the source remains within the field of view and is relatively small for sources which are much larger than the field of view (as long as there

are no strong space gradients in intensity). For sources which are approximately as large as the field of view, or when the refraction image fills out the detector surface (which will occur in the vicinity of λ = 200 μ) it becomes critical. Then the percentage change in the flux is approximately determined by the ratio of the alignment error and field of view diameter.

The attitude control of the telescope is designed so that the optical axis of the instrument moves within a circle around /41
the nominal value, the circle of "limit cycles." If small perturbation moments affect the system, then the optical axis will slowly migrate through the limit cycle and finally come to rest. If the perturbation moments are large, on the other hand, then the axis will be affected by them and will come to rest at the edge of the limit cycle, where it will reverse its direction of motion. The velocity of this motion depends on the time constant of the control loop, as well as on the perturbing moments. No quantitative information is yet available on these relationships and the magnitude of the perturbation moments which can be expected.

For periodic orientation fluctuations of the telescope, it is possible to estimate the influence of the flux fluctuations on the spectrum. For this, we again consider a source spectrum which only consists of a delta function. The relative amplitude of the flux fluctuation at the detector is assumed to be $\varepsilon/2$ and is assumed to occur at the frequency f_r. Then the flux is approximately given by the following (source diameter = field of view diameter):

$$B(\sigma) = B_0 \cdot \delta(\sigma - \sigma_0) \cdot \left\{1 - \varepsilon/2 \left(1 + \cos(2\pi f_r t + \varphi)\right)\right\} \quad ,$$

where φ is the initial phase. If it is set equal to zero and t is replaced by x/2v, we obtain the following for the interferogram (in the case where the sensitive surface of the detector is homogeneous with respect to its detection behavior):

$$F(x) \sim B_o \cdot \{1 - \varepsilon/2 - (\varepsilon/2)\cdot\cos(2\pi f_r x/2v)\} \cdot \cos(2\pi\sigma_o x) \ .$$

The product of the two cosine functions is written as a sum and then the reverse transformation is carried out just like (2.48). Then we obtain:

$$B'(\sigma) = XB_o \cdot (1 - \varepsilon/2)\ \mathrm{sinc}[2(\sigma - \sigma_o)X] \qquad (2.49)$$
$$- (\varepsilon/4)\{\mathrm{sinc}[2(\sigma - \sigma_o - f_r/2v)X] + \mathrm{sinc}[2(\sigma - \sigma_o + f_r/2v)X]\}.$$

Again, satellite lines are produced at $\sigma_o \pm f_r/2v$. The frequency f_r should lie between 0.1 and 0.01 Hz. If we then set $v = 5 \cdot 10^{-3}$ cm/sec, then we find the following for the distance σ_r between the satellite lines and the central line:

$$\sigma_r = f_r/2v = 10\,\mathrm{cm}^{-1} \text{ to } 100\,\mathrm{cm}^{-1}.$$

Such large separations can very much facilitate the differentiation between true lines and ghost lines, if the telescope really would carry out motions with accurately defined frequency. However, we do not expect this. It is more likely that there is a frequency distribution which leads to a smearing of both satellite lines into sidebands. These can then be interpreted as noise, but they are different from the photon and detector noise, because they can be eliminated if the time variation of the alignment errors of the telescope is known. /42

If we assume that the relative amplitude $\gamma(f_r)$ of the alignment error is constant within the frequency interval $(f_o - \Delta f/2,\ f_o + \Delta f/2)$ and if it is assumed that it is equal to $\bar{\gamma}$, and if we assume that it is zero outside of this interval, then the amplitude of these sidebands can be estimated by integrating (2.49) over the frequency f_r:

$$B_r'(\omega) = -XB_o \cdot \frac{\pi}{4} \cdot \int_{f_o-\Delta f/2}^{f_o+\Delta f/2} df_r \cdot \{\operatorname{sinc}[2X(\omega-\omega_o-f_r/2v)] + \operatorname{sinc}[2X(\omega-\omega_o+f_r/2v)]\} . \quad (2.50)$$

The value of this expression is then calculated for the center of one sideband while ignoring the contributions of the other sidebands, for example, for $\omega = \omega_o + f_o/2v$:

$$B_r'(\omega_o+f_o/2v) \approx -XB_o \cdot \frac{\pi}{4} \cdot \int_0^{\Delta f/2} df_r \cdot \frac{\sin \pi X f_r v}{\pi X f_r v} = -B_o \cdot \frac{X}{2} \cdot \frac{v}{\pi} \cdot \int_0^{w} d\varphi \frac{\sin\varphi}{\varphi} .$$

In the experiment, we will have X ≈ 20 cm, v ≈ $5 \cdot 10^{-3}$ cm/sec and Δf ≈ 0.1 Hz. Thus, we find, for the upper integration limit, w = Δf · π · X/2v ≈ 200 π. Therefore, we can set w = ∞ and we find:

$$B_r'(\omega_o+f_o/2v) \approx -B_o \cdot \frac{\pi}{4} \cdot v . \quad (2.51)$$

At the present time, we cannot say much about the quantity $\bar{\gamma}$. As an upper limit, we can use the ratio of the limit cycle radius and field of view diameter, which will be in the area of 0.5. (This quantity determines the amplitude of the satellite line if the orientation fluctuation occurs with a fixed frequency.)

2.4.6. Digitalization noise

There is one last noise component which influences the signal-noise ratio in the spectrum, which is the digitalization noise [5]. It occurs when the measurement data, which are initially analog (voltages), are converted into digital values which are then suitable for further processing in computers. The reason for this is that the analog-digital converter assigns all analog values from the interval $(V_0 - \Delta V, V_0 + \Delta V)$ to the digital value V_0. The amplitude of the error produced in this way is $\Delta V = n_{Dig}$.

Now let us assume that the source spectrum consists of N' lines, which produce an average radiation flux B. The interferogram produces the maximum value $N' \cdot B$ for the phase difference $x = 0$ and a detector with the sensitivity S produces the signal $N' \cdot B \cdot S$. Now, the amplification factor $\tilde{G}$ of the amplifier connected behind the bolometer is adjusted so that the maximum permissible signal K is supplied to the analog-digital converter:

$$K = N' \cdot B \cdot S \cdot \tilde{G} .$$

In the calculated spectrum, the spectral lines then have an average height of:

$$s = B \cdot S \cdot \tilde{G} .$$

The noise in the digitalized interferogram is

$$n_I = \tilde{G} \cdot n + n_{Dig} , \qquad (2.52)$$

where n is determined by the dominating noise source of the measured values, which have not been digitalized. If the noise extends from $\sigma = 0$ to $\sigma = \sigma_M$ in the spectrum, and if it is not

correlated with the signal, then we have the following for the noise in the spectrum, as discussed in 2.4.1:

$$n_S = n_I\sqrt{N},$$

where N is the number of interferogram points. Therefore, we have:

$$n_S = (\tilde{G}\cdot n + n_{Dig})\cdot\sqrt{N}.$$

/44

For a few lines of average height, the amplification factor G can be made large and the noise is determined by $G \cdot n \cdot \sqrt{N}$. On the other hand, if many lines of average height are contained in the spectrum, then G must be relatively small and n_{Dig} can then become the dominating noise component. The digitalization noise therefore becomes important, as soon as

$$\tilde{G}\cdot n \leqslant n_{Dig}$$

or:

$$\frac{K}{n_{Dig}} \leqslant \frac{N\cdot B\cdot\tilde{G}}{n}. \qquad (2.53)$$

The left side of this inequality is the dynamic factor of the analog-digital converter and the right side is the s/n ratio for the interferogram point for the phase difference zero.

The digitalization noise becomes important as soon as the dynamic factor of the analog-digital converter becomes smaller than the s/n ratio for the central maximum of the interferogram.

If the digitalization noise dominates, then the s/n ratio in the spectrum cannot be improved by extending the measurement time.

3. Comparison of Lamella Grids and Michelson Interferometer /45

3.1. Division of the Wave Front in the Interferometer

The basic principle of all interferometers used for Fourier spectroscopy consists in the production of the phase difference between two coherent ray bundles. The interferometers of this type can be classified according to the way which they produce these bundles from the incident waves. There are those which use wave front division and those which use amplitude division.

The simplest example of the last group is the Michelson interferometer. There are others, some of which are quite complicated instruments, which also operate with amplitude division and which all include one element, the ray divider. It divides the incoming wave into two divergent ray bundles. Their amplitudes are distributed to the two new waves, while maintaining the total energy of the radiation. One of the two waves then obtains a definite phase difference, compared with the other (it is twice as large as the mirror displacement in the interferometer) and both are again reflected at the ray divider, which provides for their superposition. Therefore, two divergent ray bundles are produced and their flux is determined by the phase difference produced in the interferometer. Each of the two partial bundles provides the complete spectral information. For such an ideal interferometer, the sum of their fluxes equals the flux of the incoming radiation.

There are interferometers in which the spatial separation of the ray bundles is not done according to the principle of amplitude division, but using wave front division: these are the lamella grids. In this instrument, the reflecting surfaces are arranged next to each other and adjacent mirrors are displaced in the direction of their surface normals. Part of the incoming wave is reflected at a mirror and the part next to it continues until it is reflected at the displaced mirror. In this way, it receives a phase difference compared with the contribution first reflected. In this method, the wave front is split /46
up in space. The big advantage of this is that no ray divider is needed. If a ray divider is used, the useful spectral range of the interferometer is limited because of the material constant and the required high emissivity (about 0.5). Therefore, the lamella grid is probably better suited for the IR experiments than the Michelson interferometer. In order to arrive at a reasonable decision here, we will now compare the properties of both instruments.

3.2. Lamella Grid

As already mentioned, the lamella grid consists of two groups of mirror surfaces, arranged parallel to each other (shown shaded in Figure 7), which slide into each other. The surfaces of one group can be displaced with respect to the surfaces of the other, in the direction of their surface normals.

The displacement of the movable surfaces produces a change in the phase difference of the rays reflected by neighboring /47
surfaces. These rays first run next to each other, superimposed as the distance from the grid increases, and then interfere. Only at a large distance from the grid or in the focal plane of the collimator is the complete interference pattern produced.

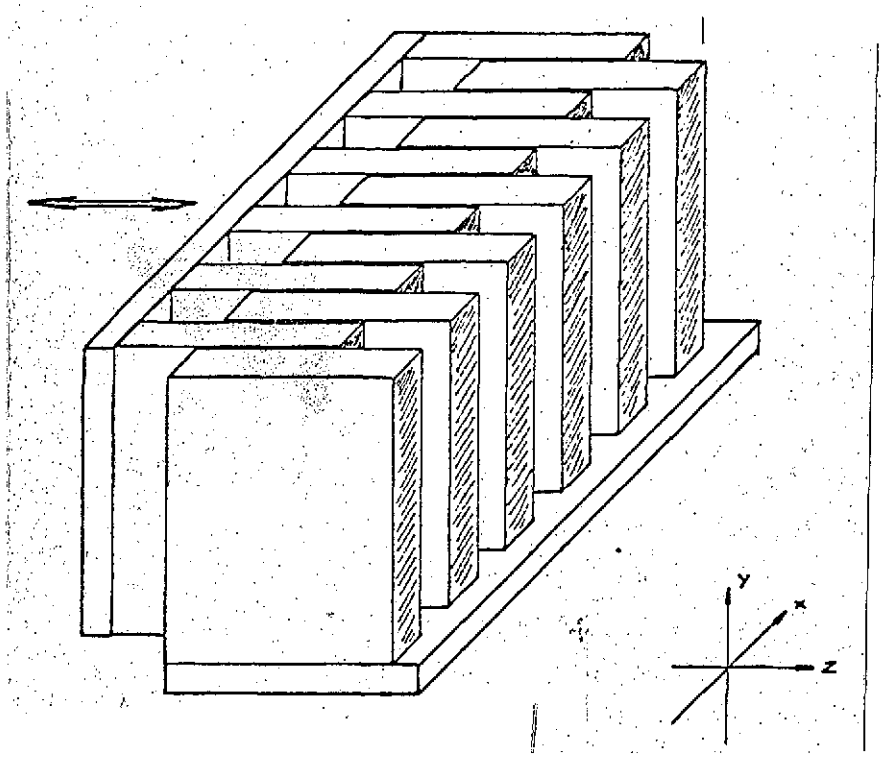

Figure 7. Sketch of a lamella grid.

Its intensity distribution will now be considered for the two-dimensional case. It is assumed that parallel rays impinge on the grid with the inclination α to the mirror normal and that all rays lie in one plane, which is perpendicular to the reflecting lamella surfaces (Figure 8).

We obtain the following expression for the phase difference of a ray reflected at a grid point (x, y) in the direction β (because of the narrow mirror surface, we can have $\alpha \neq \beta$, because of refraction effects), compared with the ray reflected in the same direction at the coordinate origin:

$$\delta = x \cdot (\sin\alpha - \sin\beta) - z \cdot (\cos\alpha + \cos\beta). \qquad (3.1)$$

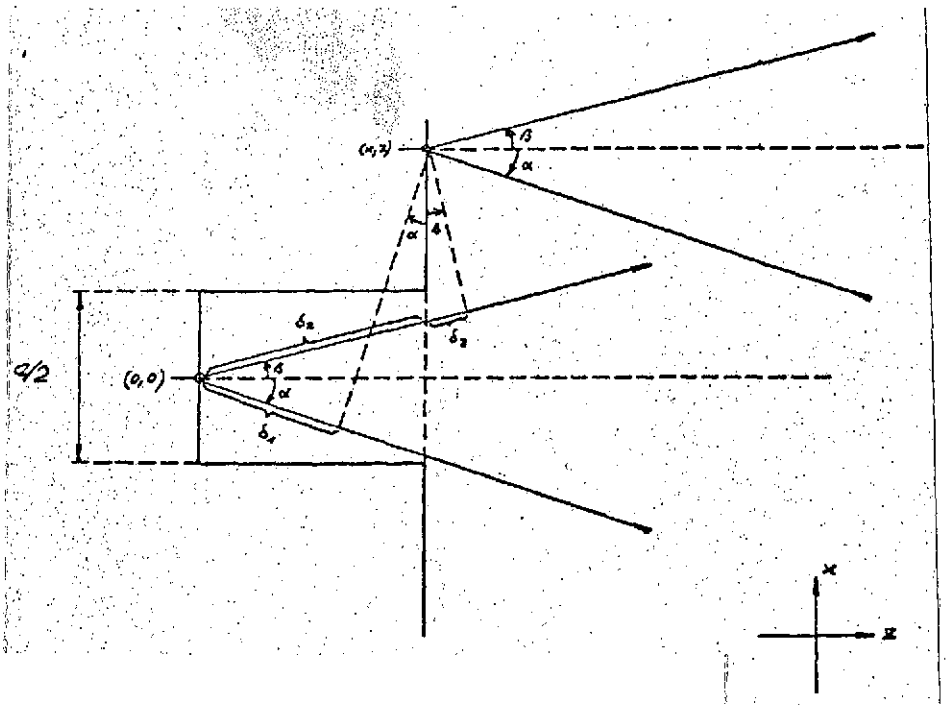

Figure 8. Production of the phase difference.

The generalization to the three-dimensional case results in:

$$\delta = \vec{x} \cdot (\hat{k} - \hat{r}) .$$

$\vec{x}$ is the reflecting grid location, $\hat{k}$ is the unit vector in the direction of the incident ray, $\hat{r}$ is the corresponding vector for the reflected ray. The phase difference is given by the following for both cases: /48

$$\Delta = 2\pi\sigma\delta$$

The amplitude of the field vector of the incoming radiation is normalized to one, and then we find the following for the radiation field at a very large distance from the grid or after focusing in the image plane [5]:

$$I \sim \frac{a^2}{2} \cdot \operatorname{sinc}^2[\sigma\psi_x a/2] \cdot \left(\frac{\sin(\pi\sigma\psi_x N a)}{\sin(\pi\sigma\psi_x a)}\right)^2 \cdot \{1 + \cos[2\pi\sigma(\psi_z z + \psi_x a/2)]\} \quad (3.2)$$

where $\psi_x = \sin\alpha - \sin\beta$, $\psi_z = \cos\alpha + \cos\beta$. The quantity a is the grid constant, z is the mirror shift, and N is the number of lamella pairs.

For the three-dimensional case, we have:

$$I \sim 2F_1^2 \cdot \mathrm{sinc}^2[\pi 2\psi_x a/2] \cdot \mathrm{sinc}^2[\pi 2\psi_y b] \cdot \left(\frac{\sin(\pi 2\psi_x N a)}{\sin(\pi 2\psi_x a)}\right)^2 \{1 + \cos[2\pi 2(\psi_z z + \psi_x a/2)]\} \quad (3.3)$$

Here b is the length of a lamella, F_1 is its surface area, and $\psi_i = \mathbf{k}_i - \mathbf{r}_i$. Changes occur with respect to (3.2) because of the various meanings of the ψ_i. The derivation of (3.3) is given in Appendix A.

Compared with the Michelson interferometer, we obtain relatively complicated formulas for the radiation field of the lamella grid. Therefore, it seems appropriate to briefly discuss the intensity distribution for the two-dimensional case. Here we are interested in the expression:*

$$I \sim \left(\frac{\sin(\pi 2\psi_x a/2)}{\pi 2\psi_x a/2}\right)^2 \cdot \left(\frac{\sin(\pi 2\psi_x N a)}{\sin(\pi 2\psi_x a)}\right)^2 \{1 + \cos[2\pi 2\psi_z z + \pi 2\psi_x a]\}$$

as a function of z, α and β.

If we now assume normal incidence, then we have the following for small angles and $\varphi = \beta - \alpha$

$$\psi_x = \sin\alpha - \sin\beta \approx -\sin\varphi \approx -\varphi$$

In addition, we use the abbreviation:

$$\pi 2 a \psi_x \approx -\pi 2 a \varphi = -\varphi v.$$

*It describes the intensity distribution in the plane of the grid structure.

Therefore, we obtain: /49

$$I \sim \left(\frac{\sin\varphi\psi/2}{\varphi\psi/2}\right)^2 \cdot \left(\frac{\sin N\varphi\psi}{\sin\varphi\psi}\right)^2 \cdot \{1 + \cos(2\pi\sigma\varphi_x z - \varphi\psi)\} \qquad (3.4)$$

Figure 9 shows the variation of the three factors in this product for N = 20 and $2\pi\sigma\varphi_x z = 2n$ where n = 0, 1, ... (constructive interference of zero order). The side maxima of the second term are not shown, because for the selected N, their amplitudes are smaller than 0.05 of the amplitude of the main maxima. In addition, N side maxima occur between two main maxima and they can therefore contain a considerable part of the radiation flux (about 9.5% for the selected example).

The first factor in (3.4) describes the refraction at a lamella surface and the second describes the influence of the interference between the ray bundles which are reflected by the individual lamellae. The third describes the modulation caused by the interferometer properties of the grid. /50

The refraction term $\sin(\varphi\psi/2)/(\varphi\psi/2)$ has maxima for $\varphi\psi/2 = 0$ and $\varphi\psi/2 = (2n + 1)\pi/2$, where n are whole numbers. Its zeros are located at $2\varphi\psi = n\cdot\pi$.

The grid term $\sin(N\varphi\psi)/\sin(\varphi\psi)$ has main maxima for $\varphi\psi = n\pi$ and vanishes for $N\varphi\psi = m\pi$, as long as m/N is not a whole number. This can be summarized in the following table:

	Refraction	Grid
I = 0	$\varphi\psi = 2n\pi$; $n \in \mathbb{Z}, \neq 0$,	$\varphi\psi = m\pi/N$; $m/N \in \mathbb{Z}$
I maximal	$\varphi\psi = \frac{1}{2}(2n + 1)\pi$; $n \in \mathbb{N}$	$\varphi\psi = n\pi$; $n \in \mathbb{Z}$

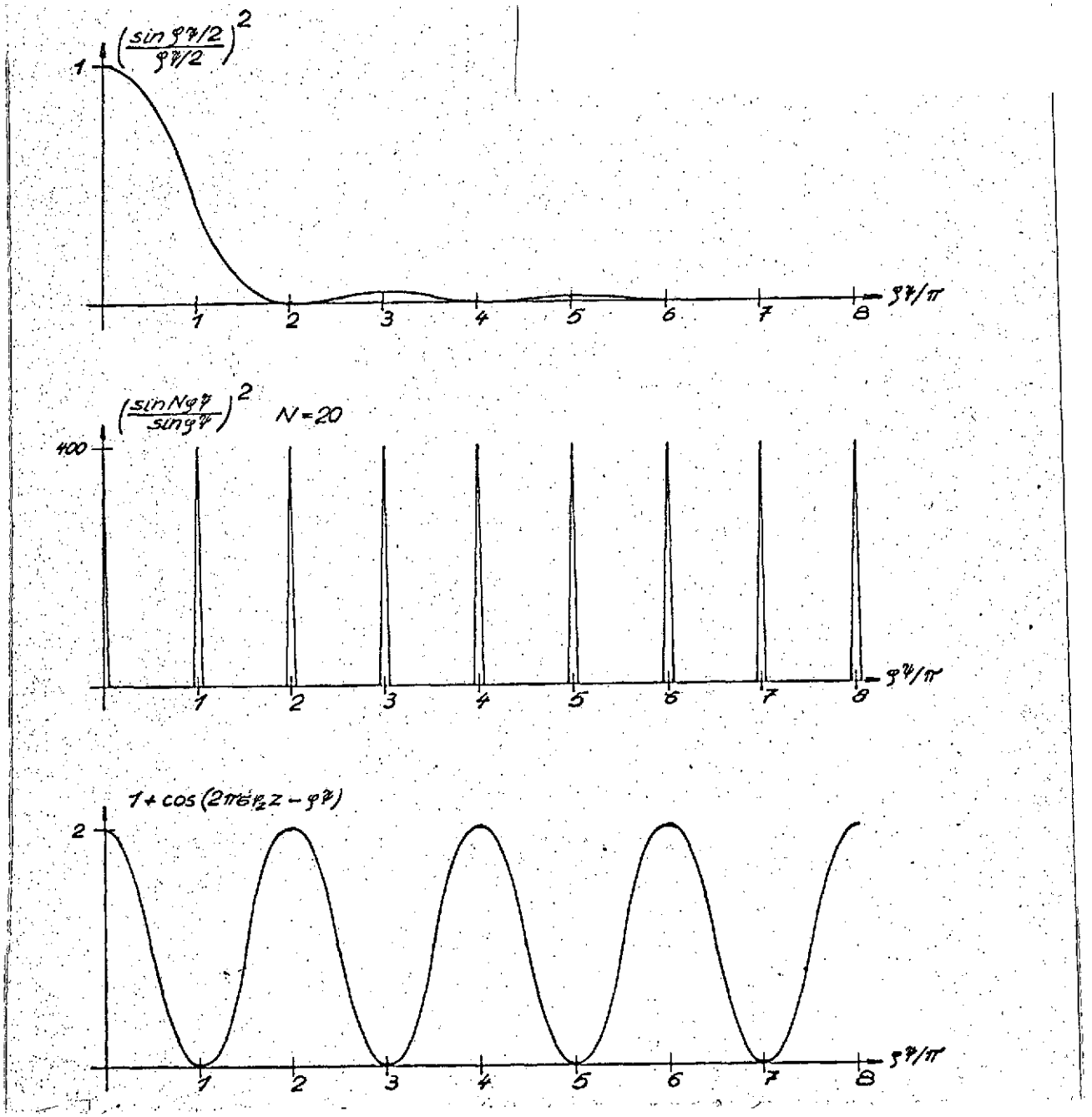

Figure 9.· The factors of (3.4) $\varphi = \pi\delta a$, $\psi = \beta - \alpha$

From this we can see that all even orders of the spectrum vanish with the exception of the zero order, because the refraction term has zeros at the corresponding rotations. Therefore, we only have the zero, first, third, etc., order.

The interference term can restrict a number of orders which occur even more. It is given by:

$$1 + \cos(2\pi\mathcal{G}_z z - \varphi\psi).$$

Since

$$\mathcal{G}_z = \cos\alpha + \cos\beta = 1 + \cos\beta$$

for perpendicular incidence of radiation and since also β can be assumed to be very small, the first part of the argument can first of all be assumed to be constant. Then the variation of the argument with the angles is practically entirely due to the term $\varphi\psi$. Now it is assumed that the grid shift z is adjusted so that for $\beta = 0$ (that is, also for $\psi = 0$), there will be constructive interference of zero order for the wavelength under consideration. The first zero of the interference term is then found for $\varphi\psi = \pi$, which is exactly the direction of the first main maximum of the grid term. The other zeros follow, separated by 2π and they coincide with the other maxima of uneven order. /51 This means that the grid almost acts like a mirror of the same dimensions as a grid in the case of constructive interference of zero order. Only one main maximum of the grid term occurs, which is exactly as wide as that of the refraction image of a slit having width Na. In contrast to the mirror, there are also side maxima.

If the grid is in a position which produces destructive interference for zero order reflection, then it can easily be seen that the second order will vanish but all uneven orders will appear with maximum intensity. This should already be expected because of the conservation of radiation flux. Figure 10 shows the cases of intensity distribution discussed, where again we have not shown the side maxima of the grid term.

The radiation field behind the lamella grid is not only determined by the interferometer properties, but also by the grid properties of the instrument. Of course, this can be felt in /52
the relationship between the useful solid angle and the resolution and, therefore, is involved in the formula for the light yield, which we will now derive.

For this, it is sufficient to consider the interference term:

$$1 + \cos(2\pi\sigma(\varphi_z z + \varphi_x a/2)).$$

Written out, the second factor of the argument is:

$$\varphi_z' z + \varphi_x a/2 = z(\cos\alpha + \cos\beta) + a/2\cdot(\sin\alpha - \sin\beta)$$

In general, all angles which occur are small. If, in addition, we set $\psi = \beta - \alpha$, then we can write the following for the last expression [5]:

$$2z\cdot\cos\alpha - a/2\cdot\sin\psi$$

and the variable part of the interference term finally is given by

$$\cos(2\pi\sigma(2z\cdot\cos\alpha - a/2\cdot\sin\psi)).$$

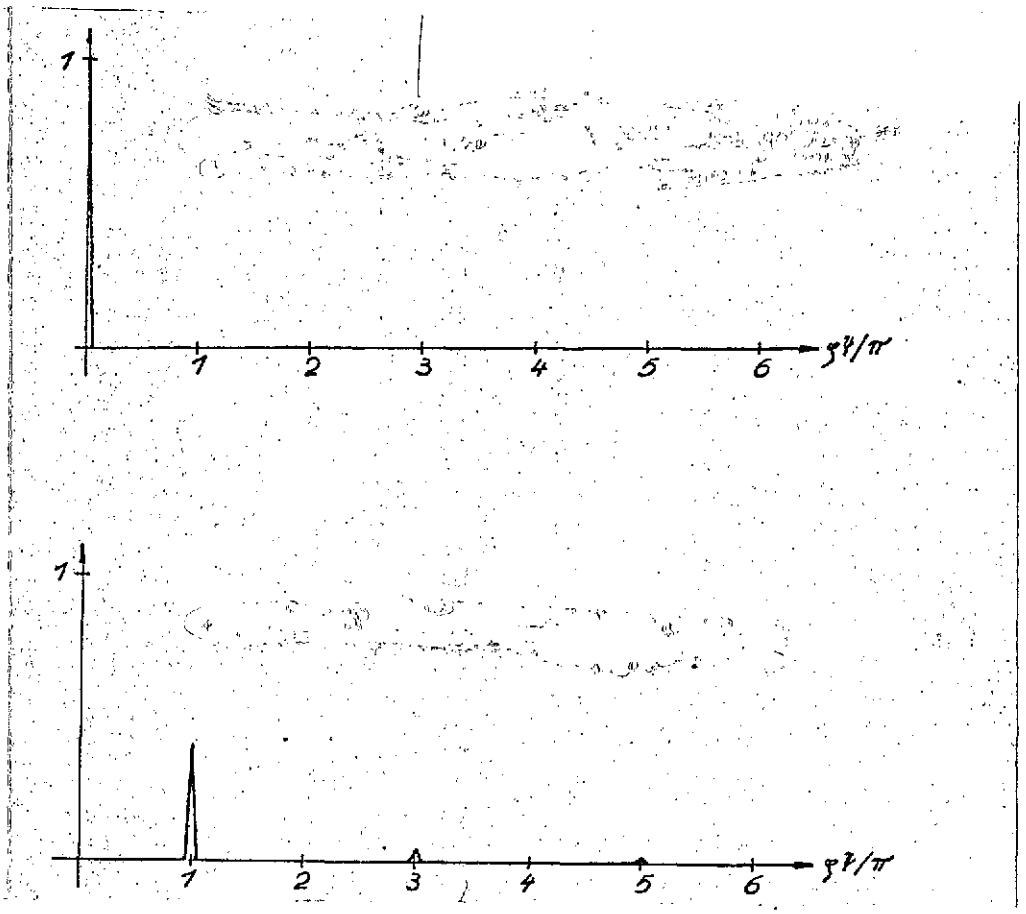

Figure 10. Intensity distribution at a large distance from the grid, according to (3.4) in relative units.

top- constructive interference of zero order; bottom- destructive interference of zero order.

In order to be able to well measure the modulation as a function of the grid shift, neither of the two sum terms of the argument should vary by more than π when the ray direction varies within the angular range filled by the light bundle. (Equivalent to this, we have the requirement that the detector should only see rays for which the phase difference is changed by less than $\lambda/2$, because of the direction variation. This corresponds to the size of the central spot in the Michelson interferometer.) This produces the following conditions:

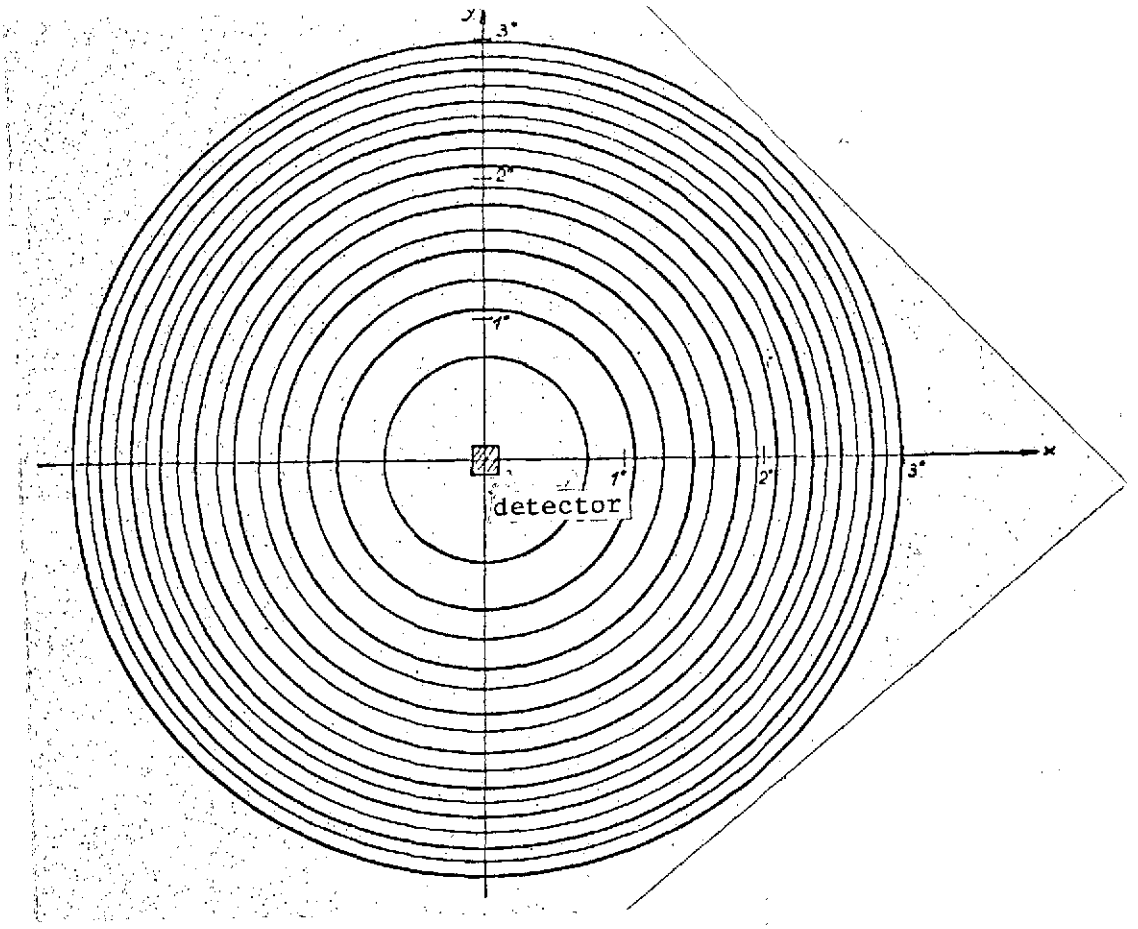

Ring system of a Michelson interferometer for 15 cm phase difference and $\sigma = 400 cm^{-1}$. Coordinates: direction of radiation reflected by dispersion element.

(1) $$4z\sigma(1 - \cos\alpha_G) = 2X\sigma(1 - \cos\alpha_G) \leq 1 \qquad (3.5)$$

(2) $$2a\sigma \cdot \sin\psi_G \leq 1 \qquad (3.6)$$

The factor 2 in (3.6) is caused because ψ varies from $-\psi_G$ to $+\psi_G$ and the sin varies by 2 sin ψ_G.

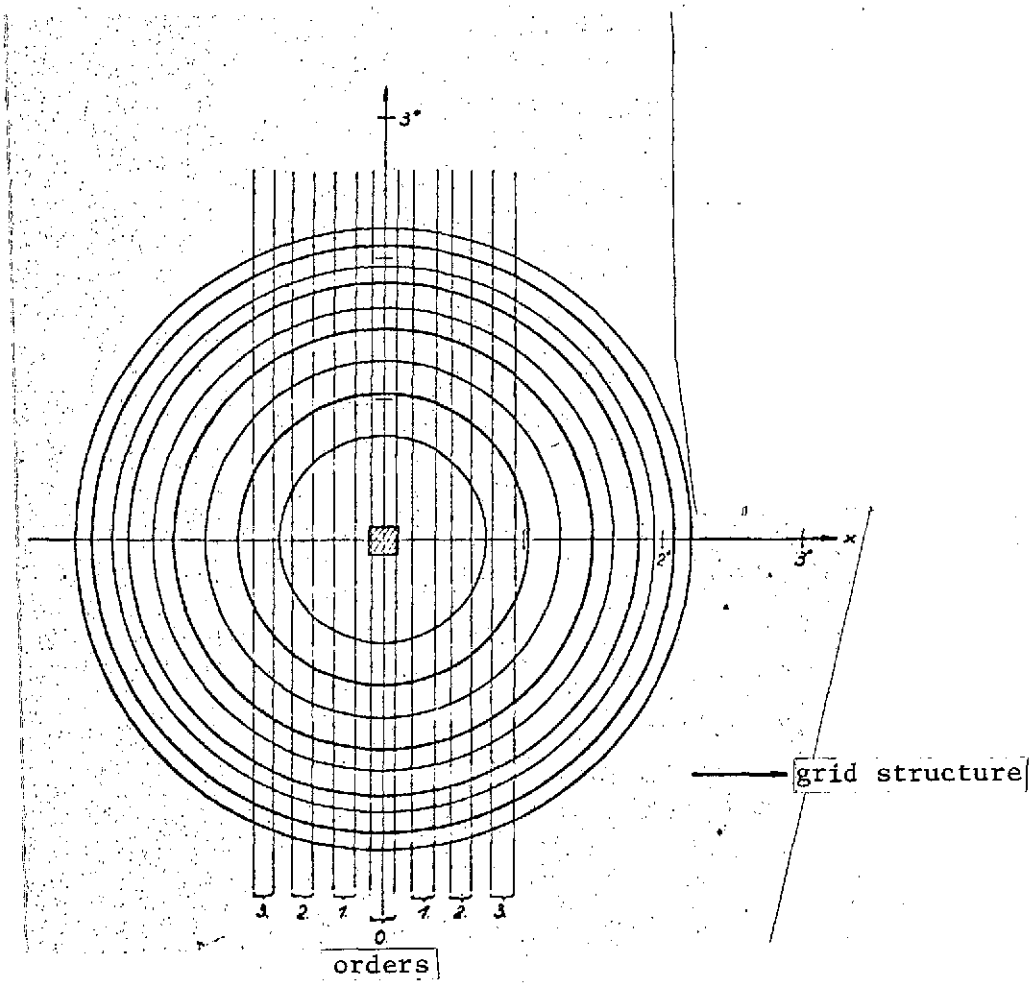

Intensity distribution behind a lamella grid for 15 cm phase difference and $(\sigma = 400\,cm^{-1})$ in the approximation $(z/a \gg 1)$. The width of the orders is determined by the ray divergence at the grid (= 10'), the grid constant (a = 0.5 cm), and the wave number. In the y direction, the intensity distribution is modulated in the orders by the Haidinger rings.

The first condition applies when the interferometer properties of the grid dominate and it results in the following (just like for the Michelson interferometer:

$$\alpha_G \leq \sqrt{1/2x} \qquad (3.7)$$

α_G is one-half of the ray divergence at the grid. For $\sigma = \sigma_M = 500\ cm^{-1}$ and X = 20 cm, we find $\alpha_G \leq 0.01 \triangleq 0.57°$. The maximum ray divergence at the grid would, therefore, amount to more than 1°. /53

The second condition limits the ray divergence if the grid properties of the instrument dominate. Since the angle ψ_G is again assumed to be small, we find that it simplifies to:

$$2 \cdot \sin \psi_G = 1/a\sigma = 2\psi_G \qquad (3.8)$$

For $\sigma = 500\ cm^{-1}$ and a = 0.5 cm, we find $\psi_G = 2 \cdot 10^{-3} \triangleq 6{,}87' \triangleq 0{,}11°$ which is much smaller than the limiting value found from (3.5).

In a plane perpendicular to the grid structure, the grid properties do not play a role and the ray divergence is limited by α_G (Figure 11). In the plane parallel to the grid structure, the condition (3.8) results in a greater restriction than (3.7) for a grid shift which is not too large. The maximum ray divergence is then specified by $2\psi_G$. It is only when $\alpha_G > \psi_G$ that the interferometer properties limit the ray divergence in this direction as well. For a = 0.5 cm and $\sigma = 500\ cm^{-1}$, this case only occurs when the grid shift is greater than 2.5 m. Therefore, the maximum ray divergence in one direction will practically always be determined by α_G and, in the other direction, it will practically always be determined by ψ_G.

If these angles are small, then the maximum useful solid angle is approximately: /54

$$\Omega \approx \pi \alpha_G \psi_G = \pi \cdot \frac{1}{16X^2} \cdot \frac{1}{2a}$$

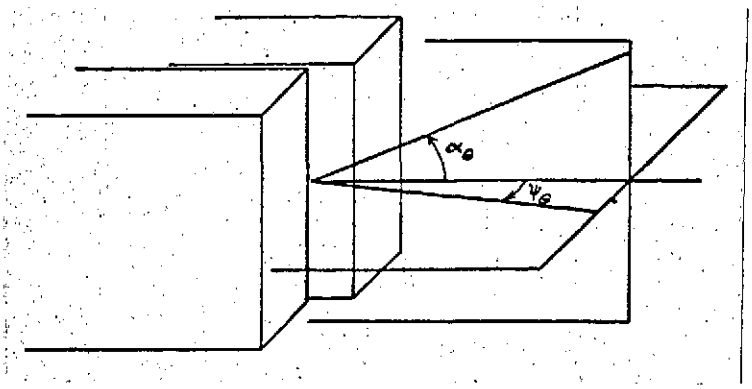

Figure 11. Definition of maximum permissible ray divergences at the lamella grid.

If we set $\delta\sigma_m = 0{,}681/X$ and $\sigma = \sigma_M \cdot \text{ein}$, then we find

$$\Omega = \pi \cdot \frac{1}{\sqrt{\sigma_M \cdot 0{,}681/\delta\sigma_m}} \cdot \frac{1}{\sigma_M a} = \frac{\pi}{\sqrt{0{,}681}} \cdot \frac{1}{\sqrt{R_M}} \cdot \frac{1}{\sigma_M a} \approx \frac{4{,}6}{\sqrt{R_M}} \cdot \frac{1}{\sigma_M a} \cdot \quad (3.9)$$

and using $T \cdot E = L = 4{,}6 \cdot T \cdot A/(\sigma_M a \cdot \sqrt{R_M})$, we obtain the following, in analogy to (2.26):

$$L \cdot R_M = 4{,}6 \cdot T \cdot A \cdot \sqrt{R_M}/(a \cdot \sigma_M) \quad . \quad (3.10)$$

In general, the incoming radiation is limited by a circular cone surface and not by the surface of an elliptical cone, as assumed here. Therefore, L will either be smaller or the modulation will be poorer. For the IR experiment, this is not very important because the ray divergence at the grid will be much smaller than would be possible, according to (3.7) and (3.8) (see Section 3.5).

3.3. Degree of Modulation

The degree of modulation of an interferometer for prescribed ray geometry and wavelength of radiation to be investigated can be defined experimentally as follows:

Quasi-monochromatic radiation falls on the dispersion element. The phase difference is first adjusted so that the signal at the detector output takes on a maximum value of F_M. This value is measured and, finally, the phase difference is changed until the minimum signal is reached, and its value F_m is also measured. The degree of modulation is then defined as:

$$M = \frac{F_M - F_m}{F_M + F_m} .$$

For the Michelson interferometer, M depends on the ray divergence at the interferometer, as well as on the wave number and on the phase difference. In the case of the lamella grid, it is also determined by the grid constant and the number of lamella pairs.

In order to carry out the experiment, it is important for /55
a large maximum radiation flux of the source to reach the detector and there must be a good modulation of this flux. Therefore, M must be close to one. The flux at the telescope is determined by the solid angle range $E = F_i \Omega_i$ or by $(D_i \cdot \alpha_i)^2$, where D_i is the diameter of the imaging surface of the instrument and α_i is one-half of the ray divergence of the radiation which is incident there. α_i is defined by the field of view diaphragm or by the sensitive surface of the detector, as well as by the imaging equations of the optics. D_i is then specified by $D_i \alpha_i = \text{const}$, if a diameter is specified. The only diameter which is specified is the one of the main mirror, 1 m. In order to now obtain the maximum radiation flux, the field of view of the telescope would have to be made as large as the diameter of the interstellar sources being investigated. However, since these sources are quite large, this would lead to a large ray divergence at the

interferometer and, therefore, to possibly small degrees of modulation. Therefore, the optimum ray divergence at the grid and, therefore, the optimum field of view diameter would have to be found (which is also determined by other conditions, see Section 4). This can only be done when the variation of the degree of modulation is known quantitatively as a function of the ray divergence. We will now determine this.

Degree of Modulation of the Michelson Interferometer

In the last chapter, we already determined an expression for the interferogram of an extended quasi-monochromatic source for the Michelson interferometer (2.17):

$$F(x_0) \sim B(\sigma)d\sigma \cdot \Omega \cdot \left\{1 + \operatorname{sinc}\left[\frac{\sigma x_0}{2\pi}\cdot\Omega\right]\cdot\cos\left[2\pi\sigma x_0(1-\Omega/4\pi)\right]\right\}$$

For the maximum or minimum radiation power arriving at the detector, we find

$$F_m \sim 1 - \operatorname{sinc}\left(\frac{\sigma x_m}{2\pi}\Omega\right); \qquad F_M \sim 1 + \operatorname{sinc}\left(\frac{\sigma x_M}{2\pi}\Omega\right).$$

The subscripts m and M indicate that x is first to be taken at a point which produces destructive interference at the center of the interference figure, and then at a distance of $\lambda/2$ from this, that is, for constructive interference. The estimation (3.7), which also applies for the Michelson interferometer, showed that the ray divergence cannot exceed 1° by much for the requirements formulated. Therefore, it follows that Ω must be smaller than 10^{-4} sr. Since σX changes by 0.5 in the transition from constructive to destructive interference, the argument of sine changes by $\Omega/4\pi \approx 10^{-5}$, which can be ignored in the determination of the degree of modulation. Therefore, the degree of modulation can be defined for a certain phase difference and we find: /56

$$M_X = \text{sinc}\left[\frac{\Delta x}{2\pi}\Omega\right]$$

For the experiment, we are interested in the wave number range between 50 and 500 cm^{-1} and the maximum phase difference becomes smaller than 20 cm. Figure 12 shows the variation of the degree of modulation in the spectral range for a phase difference of 10 cm for various ray divergences at the interferometer.

Degree of Modulation of the Lamella Grid

The degree of modulation of the lamella grid must be calculated numerically because the refraction and grid effects complicate the formula for the radiation flux so much that the integration over the incident and reflection angles cannot be done analytically.

In the case of the Michelson interferometer, only one angle is involved in the calculation (because the reflection angle equals the incident angle according to the reflection laws of geometric optics). The exact calculation of the lamella grid requires the use of four angles, and two of them determine the incident direction and two others determine the reflection direction. It is because of refraction effects that the laws of geometric optics can no longer be used. In addition, there is shading of part of the lamella surface if the direction vector of the incident rays has a component which is not in the plane of the side surfaces of the lamella. The exact solution of the three-dimensional problem would require the numerical calculation of a four-dimensional integral over the four angles, which would /57 lead to unrealistic calculation times. For this reason, we must reduce the calculation to a two-dimensional problem.

In order to obtain an idea on the variation of the modulation degree as a function of wave number, we will first estimate its variation. The maximum wave number, for which it is still greater than 0.95, is important. (It becomes exactly equal to 1.0 only for an infinitesimally small field of view and an infinitesimally small detector surface area when the refraction at the telescope optics can be ignored, because side maxima occur and because of the finite flux in the vicinity of a minima in the case of destructive interference.) This wave number σ_{kr} is determined by the fact that, for large wave numbers, the refraction pattern becomes so narrow that not only the zero order but also higher orders of the spectrum appear in the field of view of the detector. Therefore, for σ_{kr}, the refraction contribution $2\pi\sigma_{kr}\, a/2$ in the modulation term $(1 + \cos\{2\pi\sigma(\varphi x - \varphi a/2)\})$ of (3.2) becomes exactly equal to π and this wave number is determined by (3.6) if the equal sign is used:

$$2a\sigma_{kr}\sin\varphi_G = 1$$

or

$$\sigma_{kr} = 2a\varphi_G$$

For $\sigma \gg \sigma_{kr}$, the degree of modulation should be constant and be approximately equal to 1, and it should decrease for smaller wavelengths. The following table shows a few values of σ_{kr} as a function of the grid constant a and the ray divergence $2\varphi_G$ at the grid:

		60	40	30	20	10	$2\varphi_G$/arc min.
a/cm	1,5	261,8	174,5	130,9	87,3	43,6	
	1,0	174,5	116,4	87,3	58,2	29,1	
	0,5	87,3	58,2	43,6	29,1	14,5	σ_{kr}/μ

The shading of lamellae displaced backwards is also of interest here, caused by the ones in front of them, because this determines the fraction of the radiation which is not modulated.

If a bundle of parallel rays falls on a lamella grid with /58
the incident angle ψ, and if the shift is z, then the area shaded for this bundle is given by the following (Figure 13):

$$2\Delta f = 2z \cdot \tan\psi \approx 2z\psi \qquad (3.15)$$

For a grid shift of 5 cm and a grid constant of 0.5 cm, the shading for a ray divergence at the grid of 60' (10', 5') amounts to 35% (11%, 6%) of one lamella surface area. These numbers are only correct for the plane problem. In the three-dimensional case, the flux from a certain direction must be weighted by a factor which is proportional to the inclination with respect to the optical axis. The shading, in general, leads to a reduction in the degree of modulation. However, since it is not a linear term in the intensity distribution [see (3.21)], the non-modulated part of the flux is not proportional to the shaded surface area.

As a further effect, which restricts the operation of the lamella grid, we should mention the wave guide property of this instrument. If the wavelength of the incoming radiation is on the order of the grid constant, then the grid behaves like a waveguide for the radiation reflected at the lamella surfaces displaced backwards. The effect of these circumstances on the emitted spectrum depends on the wavelength, the polarization, and the mode of the incoming wave, as well as on the lamella width. If a plane monochromatic wave impinges on the grid, for which the electrical field is perpendicular to the side surfaces of the lamellae, then an effect occurs. On the other hand, if it

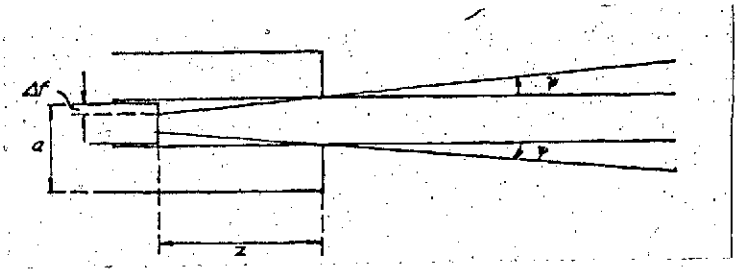

Figure 13. The extinction at the lamella grid.

is parallel to the surfaces, then the wavelength changes according to the relationships:

$$\lambda_w = \frac{\lambda_0}{\sqrt{1-(\lambda_0/a)^2}} \qquad (3.16)$$

where λ_w is the wavelength in the waveguide, λ_0 is the vacuum wavelength, and a is the grid constant [13]. In order for this relationship to be valid, the edge effects at the inlet aperture of the waveguide must be negligible, which means that the ratio of the length to the width of the waveguide is sufficiently large. This condition is satisfied for lamella grids with a shift of 10 cm and a grid constant of 0.5 cm. Relationship (3.16) applies for the largest possible change in wavelength, which occurs when the wave propagates in the conductor in such a way that the vector of the electrical field is parallel to the lamellae and this field only vanishes at the side surfaces of the lamellae ($TE_{0.1}$ mode). For other modes, this change will be smaller. For a vacuum length of 200 μ and a grid constant of 0.5 cm, we have: $\lambda_w/\lambda_0 = 1.00008$. The change in the wavelength, therefore, is below the resolution limit of 0.02 μ. As long as the wavelength is not greater than 200 μ and the grid constant is not smaller than 0.5 cm, the waveguide property of the lamella grid does not play a role, but this effect rapidly becomes critical when the wavelength is increased. In the

numerical treatment of the problem, this effect is not considered.

Now we will develop an analytical approximation for the variation of the modulation degree of the lamella grid, assuming that only the refraction term (3.6) is responsible for the change in the phase difference with reflection direction. When we determined the maximum light yield, we already showed that the interferometer properties of the grid dominate only for very large grid shifts. A more accurate estimation for the range of validity for the following approximation is obtained when we require that the refraction term (3.6) be greater than the interferometer term (3.5):

$$2X\cdot(1-\cos\alpha_c) \leqslant 2a\cdot\sin\eta_c$$

or

$$2X\,\alpha_c^2/2 \leqslant 2a\,\eta_c .$$

If we set the two angles equal to each other, we find:

$$\eta_c \leqslant 2a/X . \qquad (3.17)$$

If this inequality is satisfied, then the approximation solution applies.

In the following developments, we will consider the linear problem. In addition, the side maxima of the grid term are ignored, which makes sense for $N \gtrsim 10$, because then they are sufficiently small. (Maximum 4% of the main maximum for N = 10.) /60

Under these assumptions, the degree of modulation equals 1, as long as the first order spectrum does not reach the field of view of the detector. If the diameter of the detector is made just large enough so that the field of view of the telescope

is exactly imaged onto it, then the spectrum of first order lies outside of the field of view of the detector, as long as the refraction in the optics can be ignored, if the following holds:

$$R - r - \psi_G > 0$$

R is the distance between two maxima of the grid term, that is, of two spectra. r is one-half the width of such a maximum and ψ_G is again one-half of the ray divergence at the grid and, therefore, also the radius of the field of view at the detector (Figure 14). From (3.2), we find: $R = 1/a\sigma$ and $r = \psi_G = 1/Na\sigma$. If these values are substituted in the above, and if we solve with respect to the wave number, we obtain the wavelength down to which the degree of modulation equals 1 in this approximation:

$$\lambda_1 = \frac{2 \cdot Na\psi_G}{N - 1} \qquad (3.18)$$

For $\psi_G = 30'$, $N = 20$, $a = 0.5$ cm, we have for $x_0 = 10$ cm $\psi_G = 8.7 \cdot 10^{-3}$ rad and $2a/x_0 = 0.05$, which means that (3.17) is satisfied, and therefore, the approximation can be used. For the given values, we have $\lambda_1 = 92\ \mu$. In addition, (3.18) agrees quite well with the earlier estimation (3.14). In the latter, however, we ignored the widths of the maxima and, therefore, for $N \gg 1$ (3.18) becomes (3.14).

For wavelengths smaller than λ_1, the degree of modulation /61 should be determined by the linear increase of the minimum intensity for constant maximum intensity. This is brought about because R decreases linearly with wavelength and the maximum of first order therefore wanders into the field of view of the detector in approximately a linear manner. (This is only correct for ray divergences which are large, compared to the width of the maximum, because otherwise, the shape of the maximum is felt.)

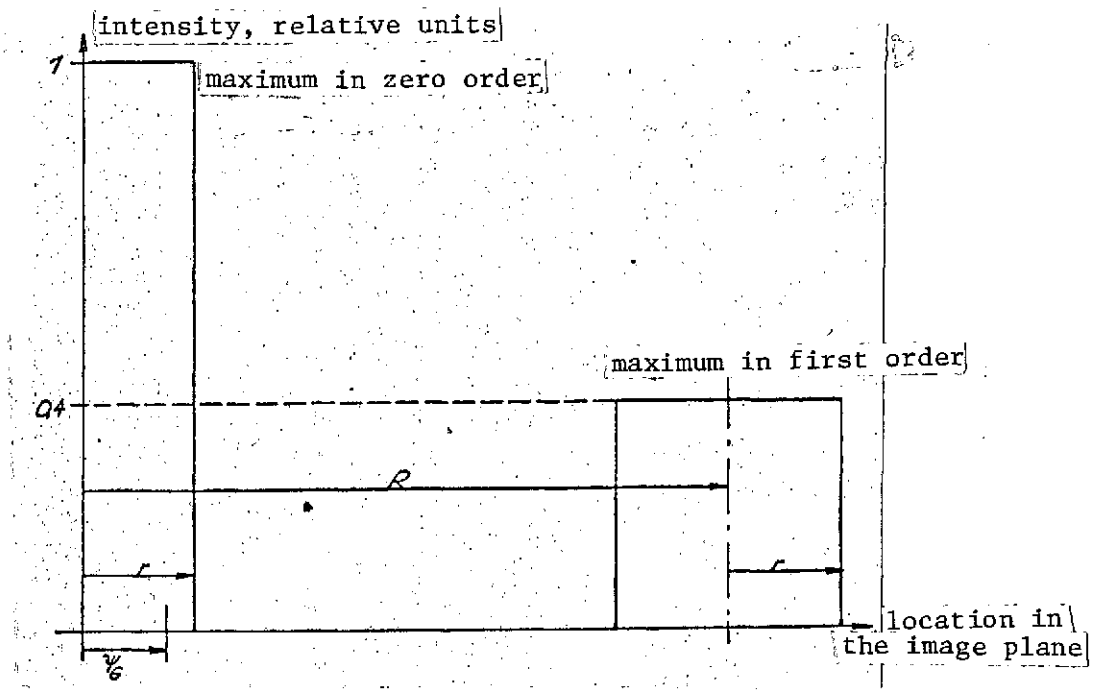

Figure 14. Definition of λ_1.

As soon as the third order also reaches the field of view of the detector, the decrease in the degree of modulation should become steeper. This would be the case for

$$3 \cdot R - r - \psi_0 = 0$$

or

$$\lambda_3 = \frac{2 \cdot Na\psi_0}{3N - 1} \qquad (3.19)$$

and we find, for

$$\psi_0 = 30', \; N = 20, \; a = 0{,}5 \text{ cm}: \; \lambda_3 = 30 \; \mu$$

and for

$$\psi_0 = 30', \; N = 10, \; a = 1 \text{ cm}: \; \lambda_3 = 60 \; \mu$$

Now we will approximately determine the degree of modulation /62 between λ_1 and λ_2 analytically. The flux contained in the zero order of the spectrum is assumed to be constant and is normalized to the following:

$$I_o = \psi_G$$

The amplitude of the spectrum of first order is given by

$$I_1 = \mathrm{sinc}^2\,(1/2) = 1/(\pi/2)^2 \approx 0{,}4$$

The following fraction of this reaches the field of view of the detector:

$$\psi_G + r - R = 2\psi_G - \frac{N-1}{Na}\,\varkappa$$

The maximum flux from the first order on the detector is, therefore (if the intensity distribution is rectangular, as is assumed in Figure 14):

$$I_{1D} = 0{,}4\cdot\left(2\psi_G - \frac{N-1}{Na}\cdot\varkappa\right)$$

In addition, we assume that $F_{Max} = I_0$ and $F_{min} = I_{1D}$. Then, we find the following for the degree of modulation:

$$M = \frac{F_M - F_m}{F_M + F_m} = \frac{0{,}2\cdot\psi_G + 0{,}4\cdot\varkappa(N-1)/Na}{1{,}8\cdot\psi_G - 0{,}4\cdot\varkappa(N-1)/Na} \qquad (3.20)$$

For $\psi_G = 30'$, N = 20, and a = 0.5 cm, this expression yields the following:

s/μ	M	Values from the numerical calculation
200	1,0	0,90
90	0,99	0,90
85	0,89	----
80	0,81	0,81
70	0,68	0,65
60	0,56	0,52
50	0,47	0,39
40	0,38	0,30
30	0,30	0,20

Figure 15 shows these values, together with the numerically calculated values (see below) for the same grid data and the same ray divergence. One can see that the approximation solution is a good description of the numerically calculated curve for wavelengths which are not too small. The deviation becomes the smallest in the region where the maximum of first order just reaches the field of view of the detector, because there, the flux concentrated in the side maxima is the smallest, compared with the flux absorbed by the detector. In the region around λ_3, the deviation again becomes large because there, all side maxima between the first and third main maxima are imaged onto the detector, but are ignored in the approximation. /63

The approximation given allows one to understand the creation of the degree of modulation for the lamella grid. It is desirable to get a better idea of the degree of modulation for selecting the optimum grid constant and ray divergence. In particular, we are also interested in the variation for the three-dimensional problem, that is, for area sources. For this reason, we will now carry out the numerical calculation of the

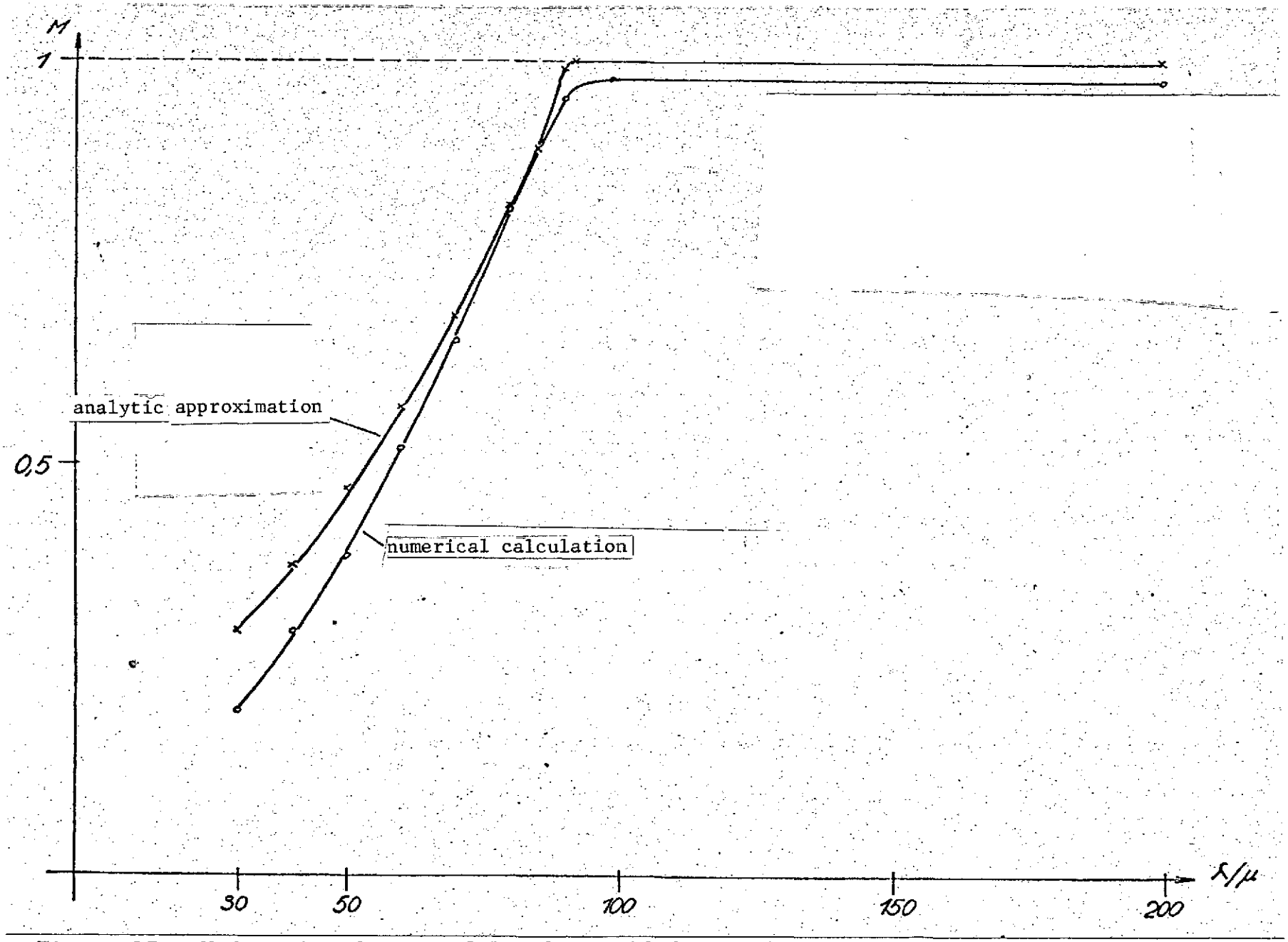

Figure 15. Modulation degree of lamella grid for a linear source. Ray divergence at the grid $2\gamma_G = 1°$ $a = 0{,}5cm$, $N = 20$

degree of modulation. This starts with a formula for the intensity distribution in the interference pattern, which is similar to the distribution (3.2), but which considers the shading of the lamella surfaces.

Let us assume that the grid constant a, the number N of the lamella pair, the initial grid shift z, the wave number σ of the incident radiation, and the ray divergence $2\psi_G$ at the grid are given. In addition, we assume that all rays which leave the grid with an inclination of less than ψ_G with respect to the surface normal of the lamellae are absorbed by the detector. Using these data, it is possible to determine the radiation flux through the detector surface.

The first calculations for the two-dimensional problem with a linear source are performed, assuming that the source has the position given in Figure 16. First, the grid shift z is adjusted so that the flux at the detector becomes a maximum. This is the /64 case when, in the zero order of the spectrum, there is constructive interference, that is, when the grid shift is a whole multiple of one-half of the wavelength of the radiation under consideration. The flux corresponding to this grid position is determined by the double integral

$$F_M = \int_{-\gamma-\eta}^{+\gamma+\eta} d\alpha\, d\beta \cdot I(\alpha, \beta, \sigma, z_m)$$

where I is the intensity distribution derived in Appendix B:

$$I = \frac{2}{(k\varphi_x)^2} \cdot \left(\frac{\sin(Nk\varphi_x a/2)}{\sin(k\varphi_x a/2)}\right)^2 \cdot \{2 - \cos[k\varphi_x (AU_1 - AL_1)] - \cos[k\varphi_x (AU_2 - AL_2)]$$
$$+ \cos[k\varphi_x (AU_2 - AU_1) + k\varphi_z \cdot z] + \cos[k\varphi_x (AL_2 - AL_1) + k\varphi_z \cdot z]$$
$$- \cos[k\varphi_x (AU_2 - AL_1) + k\varphi_z z] - \cos[k\varphi_x (AL_2 - AU_1) + k\varphi_z \cdot z]\} \qquad (3.21)$$

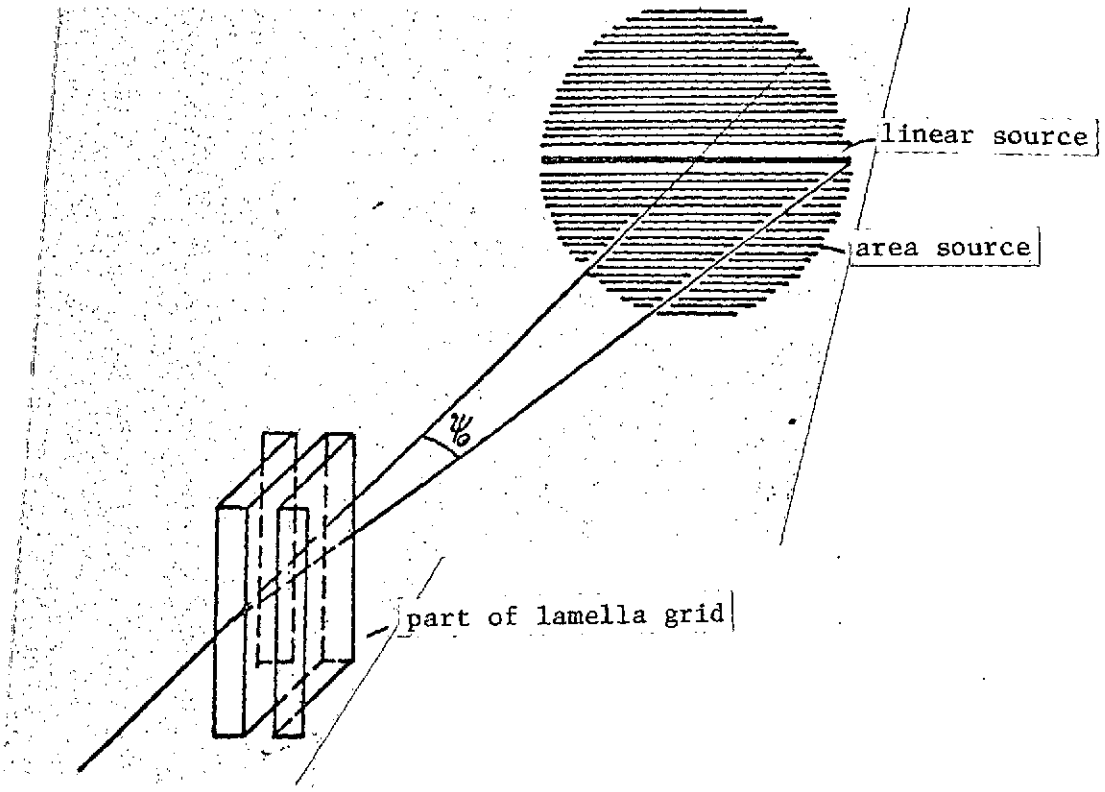

Figure 16.

After this, the grid shift is changed by $\pm \lambda/4$ and, in the zero approximation of the spectrum, there is destructive interference. The corresponding double integral then results in the minimum flux F_m.

From F_M and F_m, one then calculates the degree of modulation according to the definition equation (3.12). (See Appendix D for the calculation.)

The results of the calculation are given by the curves of /65
Figure 17 for various parameters. In addition, we show the variations of F_M and F_m for a few cases in Figure 18.

The calculation carried out in this way is exact for linear sources and can be looked upon as an approximation for the area sources. A better model for area sources is obtained by weighting the rays with an incidence angle of α with respect to the grid normal with this angle, which simulates the spatial expansion of the source. When one transfers from a linear to a circular source, the inclination angle α becomes the semi-opening angle of a cone along whose generating surface the incident rays pass. The flux is proportional to the circumference of the base area of the cone (see Figure 16). The results of this calculation are given in Figures 19 and 20.

In the case of the linear model, the influence of the edge rays was undervalued. In the calculation for the area sources, it is overvalued, because the flux contained in them is correctly considered, but one does not consider the fact that the grid does not have any radial symmetry. Therefore, the edge effects parallel and perpendicular to the grid structure are different. The actual degree of modulation will, therefore, lie between the values calculated for the linear and circular sources.

With this data, it is now possible to compare the lamella grid with the Michelson interferometer, as to their suitability for a balloon experiment.

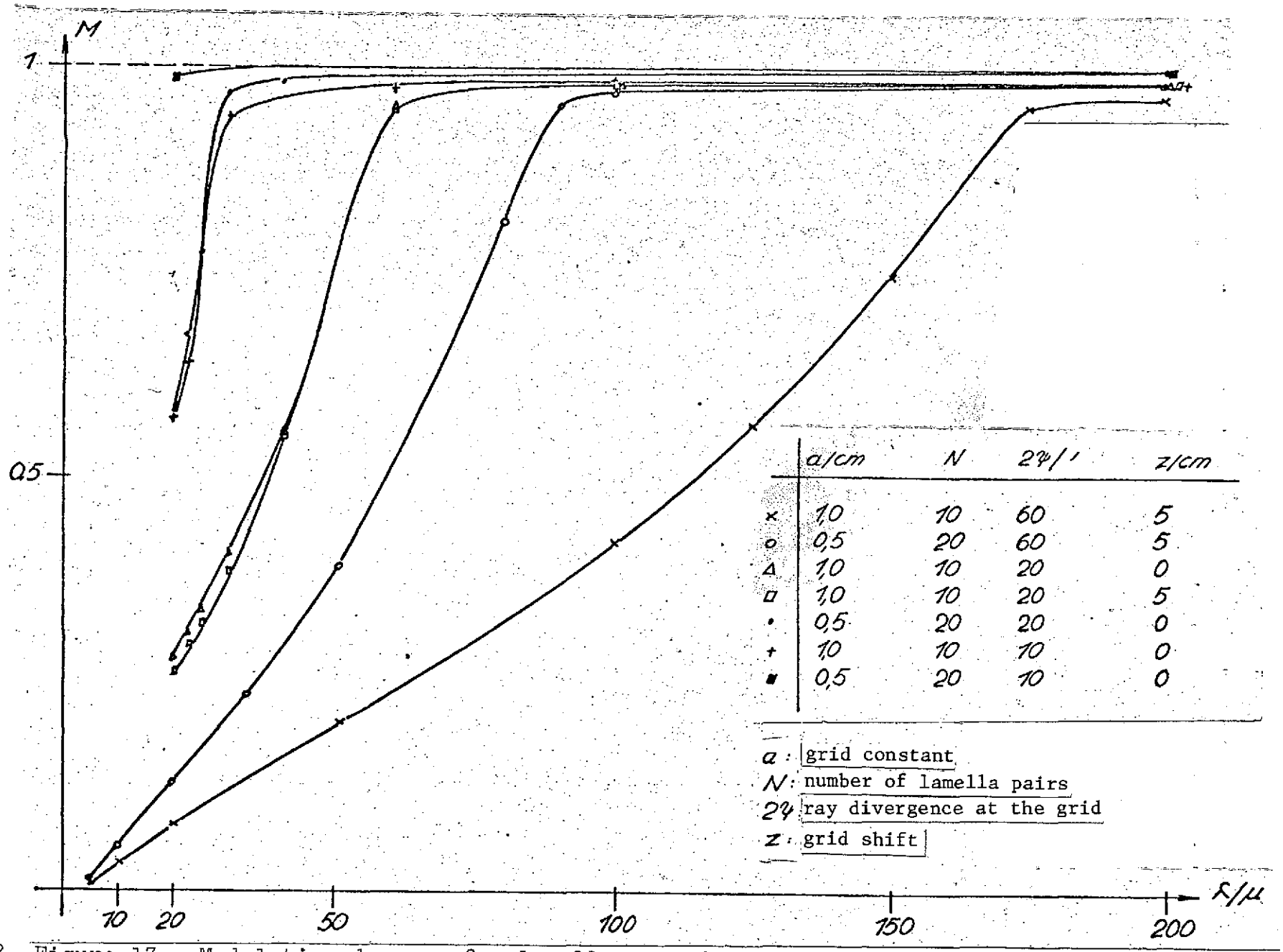

Figure 17. Modulation degree of a lamella grid for a linear source.

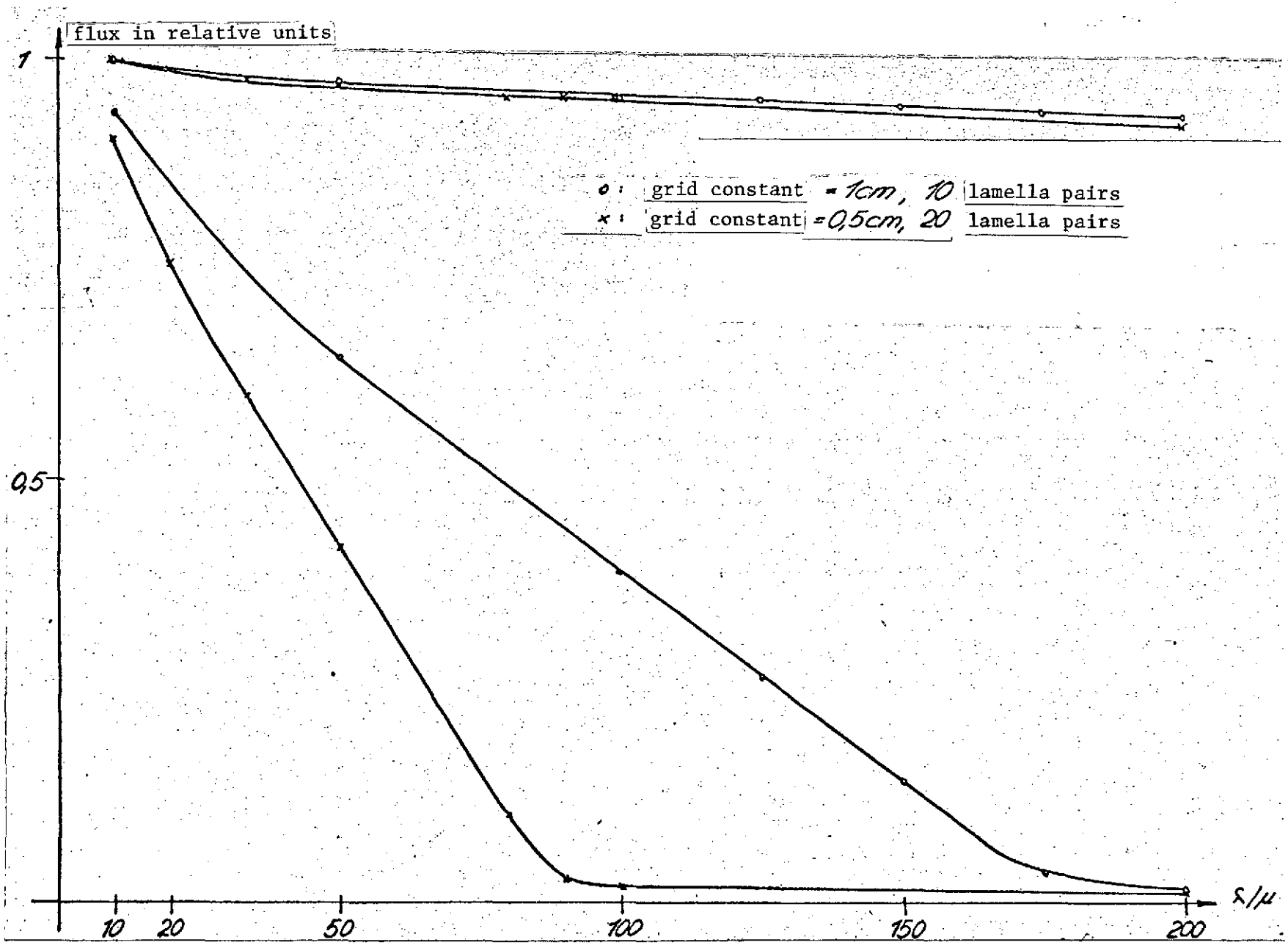

Figure 18. Minimum and maximum fluxes at the detector for a linear source and 60' ray divergence of the grid.

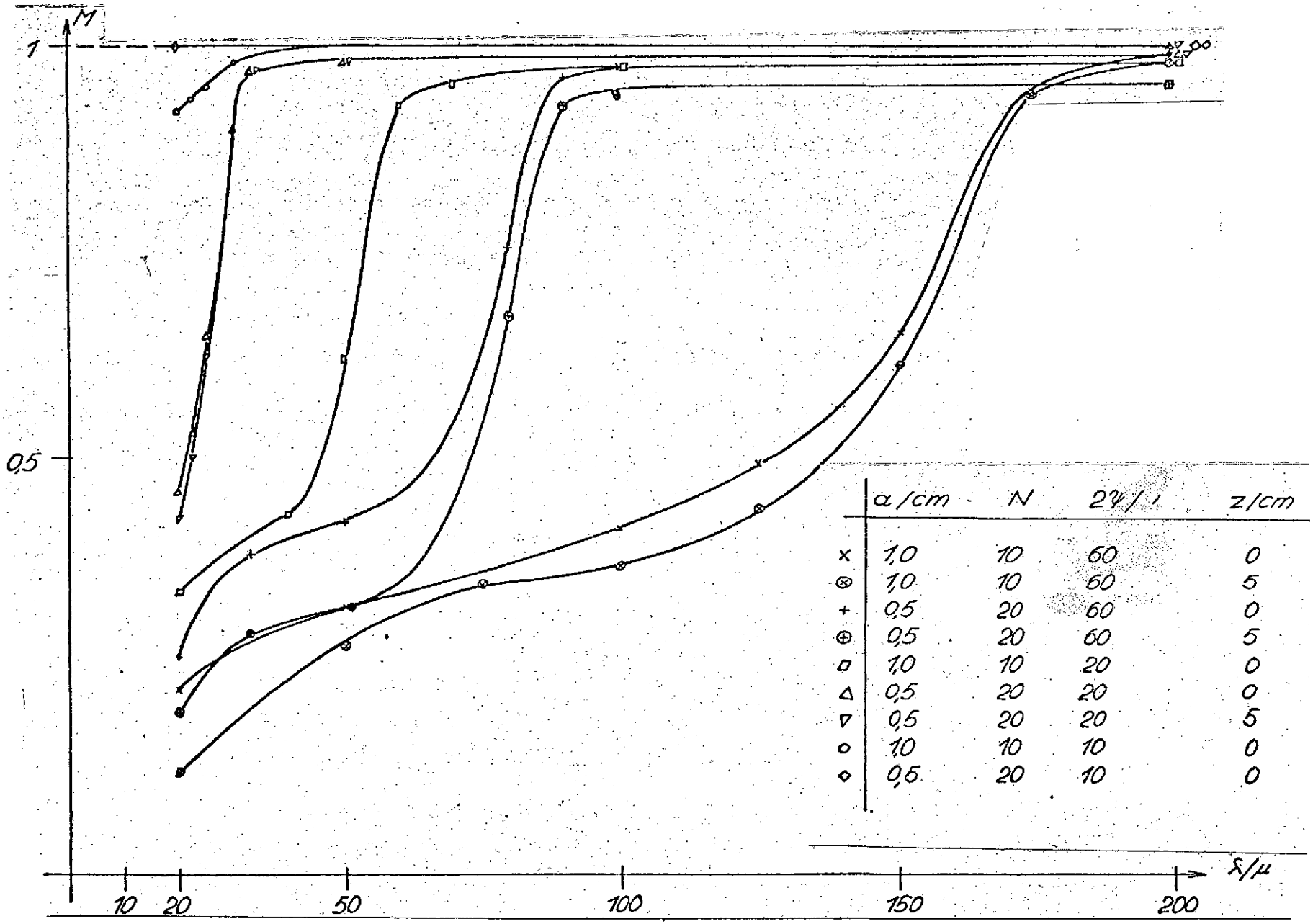

Figure 19. Modulation degree of lamella grid for a circular source.

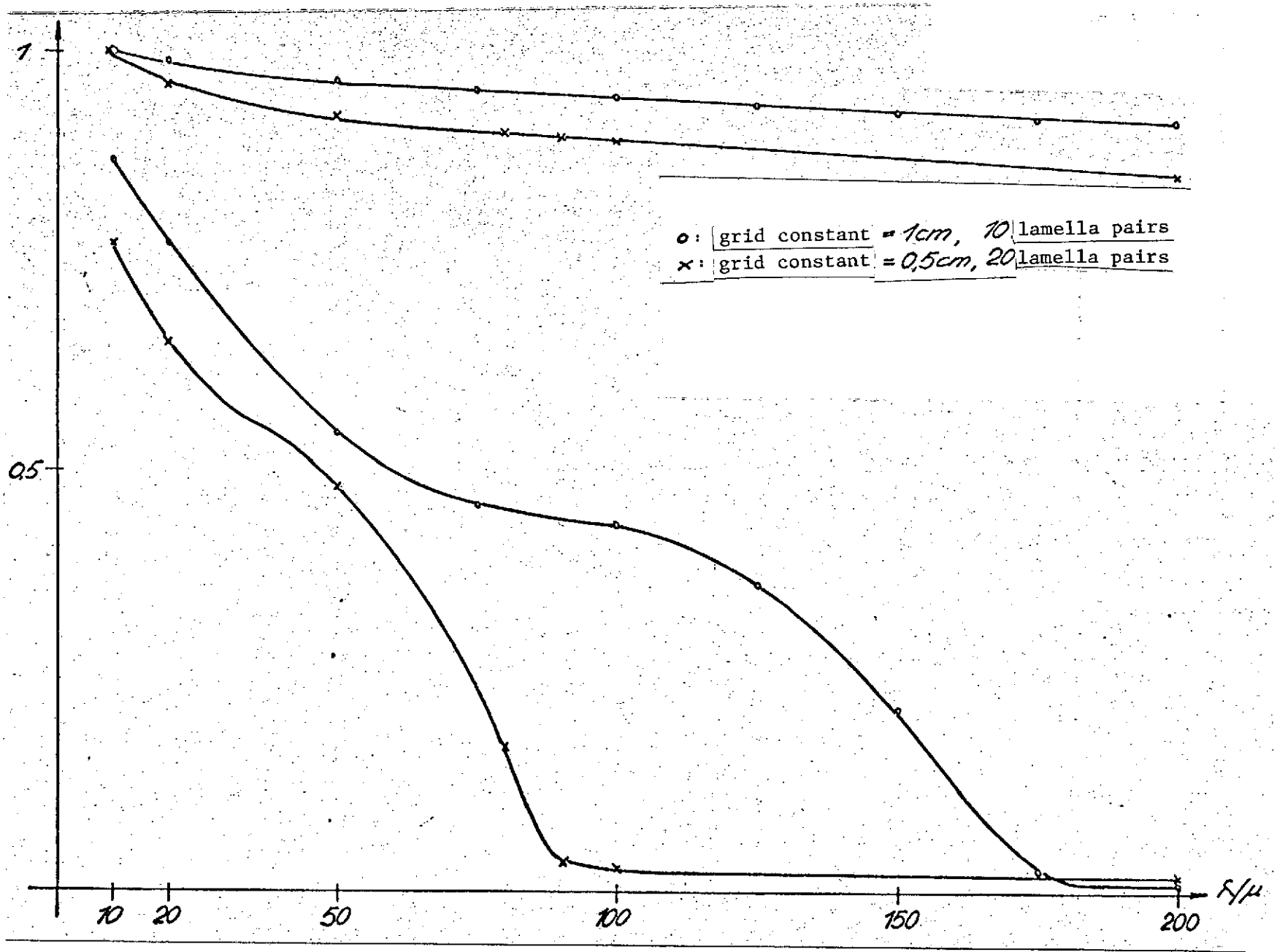

Figure 20. Minimum and maximum fluxes at the detector for a circular source and 60' ray divergence of the grid.

3.4. Comparison of Michelson Interferometer and Lamellae Grid

Degree of Modulation

The previous results could lead one to believe that the Michelson interferometer is better suited for the IR experiment than the lamellae grid because of its very flat variation of the degree of modulation. The variation found in Figure 12 is based /66 on the assumption of an ideal ray divider with a reflectivity and transmission of 0.5. Unfortunately, these ideal values can only be approximately realized in relatively narrow spectral ranges and, even then, they are different for the different polarization directions of the incident radiation [2, 14]. The variation of the degree of modulation of a Michelson interferometer which can be realized is much different from the one calculated here. It is not to be expected that it is monotonic over the entire wavelength range between 20 and 200 μ. In order to cover the entire spectral range, several ray dividers would have to be used which would lead to a reduction in the multiplex gain.

One advantage of the Michelson interferometer is the fact that its degree of modulation is much less sensitive on the ray divergence at the instrument than that of a lamellae grid. Its ray divergence could be greater for the same degree of modulation (for ideal ray dividers) than for the lamellae grid. Because of the fact that the solid angle range is constant, it would then be possible to reduce the diameter of the interferometer compared with that of the grid. The diameter of the main mirror is 1 m. If, in addition, we assume a field of view diameter of 1', then the solid angle range is: $E = 2.6 \cdot 10^{-4}$ cm^2 sr. The ray

divergence at the grid is a maximum of $\psi_G = 1/2a\sigma_M = 2 \cdot 10^{-3}$ rad, according to (3.8) for $\sigma_M = 500$ cm^{-1} and a = 0.5 cm. Because of the fact that the solid angle range is constant, we therefore find a diameter of 7.2 cm for the lamellae grid. According to (3.6), the ray divergence at the Michelson interferometer can amount to 0.01 rad for the same wave number and a phase difference of 20 cm, which results in a diameter of 1.45 cm. The Michelson interferometer could therefore be considerably smaller than the lamellae grid because of the better (theoretical) variation of the degree of modulation.

On the other hand, the lamellae grid has the advantage of a monotonic variation of the degree of modulation, which can compete with that of an ideal Michelson interferometer for sufficiently small ray divergence at the grid for $\lambda > 20$ μ. The latter is determined by no material constants and is, therefore, easier to produce than the ideal degree of modulation of the Michelson interferometer. /67

Light yield

The light yield is defined as a product of the solid angle range and the transmission. The transmission is close to 1 for both interferometers, if the degree of modulation is close to 1.* According to Figures 18/20, it remains about constant for the grid, if the degree of modulation is changed, because I_M remains approximately unchanged. The same is true for the Michelson interferometer, if the modulation decreases because of the excessive ray divergence. However, it is reduced based on the

*We use the definition (2.20) for the transmission; the average transmission is about 0.5.

optical properties of the ray divider and the transmission becomes less than 1. In addition, when the radiation passes through a real ray divider, a part of the flux is always absorbed which also reduces the transmission. A similar effect is produced in the lamellae grid by the shading of the lamellae, which reduces the degree of modulation, as well as the transmission. Some of the curves in Figures 17/19 were calculated for the grid shift of 0 and 5 cm and the influence of the shading can be seen. The flux concentrated in the side maxima can also lead to a reduction in the transmission for the lamellae grid, when these maxima are not imaged onto the detector. According to the estimation made above, they contain only about 10% of the flux of one main maximum and, therefore, this effect is not very large (it brings about a decrease in I_M at the higher wavelengths shown in Figures 18/20). Therefore, we should expect that the transmission for the lamellae grid will always be above 0.8 and that it will be similar for the Michelson interferometer, as long as the ray divider is optimum for the considered wavelength.

The solid angle range could be made considerably larger for /68
a Michelson interferometer than for the lamellae grid for the same effective surface area. The maximum ray divergence given above is greater for the Michelson interferometer by a factor of 5 than for the grid. Therefore, for the same surface area, the radiation flux could be 25 times greater than for the grid. Since the diameter of the main mirror is constant, it would be necessary to have a corresponding enlargement of the field of view diameter, which makes sense only as long as the diameter does not exceed the size of typical sources. Otherwise, only the perturbation radiation from the atmosphere and from the mirrors of the telescope optics would be increased, which would have detrimental effects on the s/n ratio. The advantage of the Michelson interferometer for the IR experiment is not so much

its large solid angle range, but more that it can be made considerably smaller than the lamellae grid.

Eigen Radiation

The eigen radiation of the lamellae grid equals that of the mirror. The eigen radiation of the Michelson interferometer is determined by the radiation of the mirror and the ray divider. A good mirror can have an emissivity of $\varepsilon \approx 0.01$, whereas the emissivity of a real ray divider is $\varepsilon \lesssim 0.1$.* For the same temperature, the radiation intensity of the ray divider is about 10 times greater than that of a very good mirror. The total radiation is proportional to εT^4 for the same temperature and solid angle range. If the flux from the ray divider is not to be greater than that from the mirror, then its temperature can be dropped, according to the following:

$$\varepsilon_{st} \cdot T_{st}^4 = \varepsilon_{sp} \cdot T_{sp}^4$$

or (for $\varepsilon_{st} = 0,1$)

$$T_{st} = T_{sp} \cdot (\varepsilon_{sp}/\varepsilon_{st})^{0,25} = 0,56 \cdot T_{sp} \qquad (3.22)$$

The normalized noise power is proportional to $\sqrt{\varepsilon T^5}$ if no filter is inserted in the radiation path. If it is to be the same for the mirror as for the ray divider, then we must have:

$$T_{st} = T_{sp} \cdot (\varepsilon_{sp}/\varepsilon_{st})^{0,2} = 0,63 \cdot T_{sp} \qquad (3.23)$$

*Of course, it depends on the material and the thickness of the ray divider.

As long as the mirrors are at the temperature of the surrounding (250° K at an altitude of 35 km), (3.22) can be satisfied if T_{st} = 129° K. This is just above the temperature of boiling nitrogen and can, therefore, be done using a nitrogen cooling system. If the entire telescope is at the temperature of nitrogen (about 70° K), then we would have to have T_{st} ≐ 39° K. Since the ray divider would have a diameter of only 1 cm, the cooling could be done with a little bit of complexity. On this point, a lamella grid would be more advantageous, because it does not introduce such difficulties. /69

Sensitivity with Respect to Inhomogeneities in the Ray Path

If inhomogeneities in the ray path of the telescope occur, for example, because part of a collimator mirror has deposits, then the interferometer is no longer uniformly illuminated. This has no consequences for the Michelson interferometer, because the radiation coming from the surface with the deposits is divided by the ray divider and, after reflection at the interferometer mirrors, they interfere with themselves. In the case of the lamellae grid, on the other hand, the surface with deposits will illuminate another lamella than the adjacent clear mirror surface in the most unfavorable case. The radiation bundles reflected by the lamellae will interfere but, because of the different emissivities of the mirror surfaces from which they depart, they will have different amplitudes and, therefore, can no longer destroy each other. In the worst case, one lamella is not illuminated at all (if there is more than one lamella, the contributions with reduced amplitude partially cancel again). The radiation from the adjacent completely illuminated lamella is not modulated and the degree of modulation will drop. When such inhomogeneities occur in the ray path,

there will be, in the worst case, a small reduction ($\approx 1/2N$, N is the number of lamellae pair) in the degree of modulation for the lamellae grid, and this is not critical.

Control /70

Another point which must be considered when selecting the dispersion element is the controllability of the interferometer shift.

The Michelson interferometer is more favorable on this point, because it can be made smaller and lighter than the lamellae grid. This means that the part in motion is also light and can be more easily controlled than in the case of the lamellae grid. (The weight of a mirror with a diameter of 1 cm is on the order of 10 p, whereas the weight of a lamellae collection with a side length of 10 cm is on the order of 1 kp.) This argument is especially important for the balloon experiment, because the position of the interferometer is not fixed in space.

Because of the smaller areas, the requirements for adjusting the individual parts of the interferometer with respect to each other are considerably reduced for the Michelson interferometer, compared with the lamella grid. In addition, in the case of the Michelsol interferometer, the movable mirror can be replaced by a system of two curved mirrors (cat's eyes),* of which one is used for fine control of the phase difference with a very small time constant (about 1 msec) [15]. These possibilities do not exist for the lamella grid and, in this case, it is always necessary to move about one-half of the relatively large grid mass.

*In addition, cube corner reflectors can be used which greatly reduce the sensitivity against small tipping motions of the reflectors.

Non-Imaging Elements

For the IR experiment, there shall be the possibility of using the dispersion element in conjunction with a light conductor or an off-axis mirror. Now, a light conductor produces no optical imaging at all any more, and a mirror with a large off-axis angle and large aperture ratio will only produce poor images. Both systems disturb the phase relationship of the incoming rays, at least in part. This means that the interference pattern and, therefore, the modulation of the radiation should be disturbed. On the other hand, light conductors are successfully being used in conjunction with interferometers [13]. Up to the present, we were not able to clarify why light conductors can be used in interferometry. Only model calculations for the behavior of the degree of modulation indicate that the results will probably be very similar for both types of interferometers (Michelson interferometer and lamella grid). A better theory of the light conductor will have to be developed for the final resolution of this problem. For the present time, we must assume that both dispersion elements show the same behavior, if a non-imaging element is used in the ray path. /71

Decision

Summarizing, we can say that the advantage of the Michelson interferometer lies in its small dimensions and the resulting easy controllability and the relatively low requirements for adjustment. The disadvantage of it is the use of the ray divider, which then limits the useful spectral range of the instrument because of its material properties. On the other hand, the lamella grid can be used to exploit a large spectral range if the ray divergence is not too large (one of the first instruments

of this type could process a spectral range between 15 to 4000 μ [16]). This advantage must be bought with the relatively high dimensions of the instrument and the correspondingly high requirement for control technology and adjustment. However, when these purely technical problems are solved, then the lamella grid will be superior to the Michelson interferometer, as far as the requirements of this experiment are concerned. For this reason, we believe that the lamella grid is the dispersion element which is best suited for the IR experiment.

3.5. Dimensioning and Tolerances of the Lamella Grid /72

The dimensions of the lamella grid are found from the following considerations:

i) The width of the main maxima of the spectra caused by refraction effects for parallel incident radiation should not be greater than the finite magnitude of the width of the maxima of the field of view or of the sources, because otherwise, the refraction losses become too large. The width $2\psi_M$ of the main maximum for the maximum wavelength is the following, according to (3.2):

$$2\psi_M = \delta_M/Na = \delta_M/D \qquad (3.24)$$

On the other hand, because of the fact that the solid angle range is constant, we have:

$$\alpha \cdot D = 2{,}9 \cdot 10^{-2}\ \text{cm rad}$$

for a 1 m main mirror diameter and a 1' field of view diameter. D is the ray diameter at the imaging surface of the optics and α is the divergence of the incident radiation. If we set the

width of the maximum $2\psi_M$ equal to the ray divergence at the grid $2\psi_G$, then (3.24) can be written as follows:

$$2\delta_M = Na \cdot 2\gamma_G = 2{,}0 \cdot 10^{-2}\text{cm rad.} \qquad (3.25)$$

ii) According to (3.18), the minimum wavelength is the following with a degree of modulation of approximately 1:

$$\delta_m = 2\gamma_G \cdot a$$

(this is only exact for sufficiently large N). If we solve with respect to a, we find the following from this relationship:

$$a = \delta_m / 2\gamma_G \qquad (3.26)$$

and substituted into (3.25):

$$2\delta_M = N\delta_m \qquad (3.27)$$

For λ_m = 20 μ and λ_M = 200 μ, it follows that:

$$N = 2\delta_M / \delta_m = 20. \qquad (3.28)$$

iii) In order to be able to have a mechanically stable construction of the lamella grid and optically perfect machining of the lamella, the grid constant cannot be smaller than 0.5 cm. For this lower limit, /73

$$a = 0{,}5\text{cm} \qquad (3.29)$$

we then find:

$$D = Na = 10\text{cm} \qquad (3.30)$$

These dimensions of the grid seem quite reasonable and the instrument is still manageable and does not become too heavy for the balloon experiment. The thickness of the lamellae is 2.5 mm and is still large enough so that they have sufficient mechanical stability.

If we substitute the value for D determined in (3.25), we find the following for the ray divergence at the grid:

$$2\gamma_G = 2{,}9 \cdot 10^{-3}\,\mathrm{rad} = 10'. \tag{3.31}$$

Figure 19 shows that the instrument operates with a degree of modulation of approximately 1 down to 20 μ, if the specifications given above are adopted.

iv) The grid shift is specified as follows by the required resolution, according to (2.7):

$$\delta\sigma = 0{,}681/X = 0{,}681/2z .$$

X here is the maximum phase difference and z is the corresponding grid shift. The quantity δσ takes on the smallest value for constant resolution for the smallest wave number. Since a resolution of greater than or equal to 10^3 is required, we must have

$$\sigma_m/\delta\sigma = 10^3 ,$$

which means that

$$\delta\sigma = 0{,}05\,\mathrm{cm}^{-1}.$$

This means that the required grid shift is:

$$z_1 = 0{,}681/2\delta\sigma = 6{,}81\,\mathrm{cm} . \tag{3.32}$$

The movable part of the grid must, therefore, be capable of being displaced by at least 6.8 cm, with respect to the part at rest, in order to provide a resolution of greater than 10^3 over the entire spectral range. However, a somewhat greater grid shift should be possible, because according to the definition used for the resolution, the separation of two (*) separated by $\delta\sigma$ only starts at the calculated value of the shift, which /74 means that it is practically no longer visible. (The depression between the lines in the calculated spectrum is still zero.) Since the resolution is reduced when filter functions and apodization functions are used, it seems that a maximum grid shift of 8 cm is appropriate.

v) The width of a spectral element is $\Delta\delta = 1/2\ X = 0.0367\ cm^{-1}$ and the spectral range extends over approximately 500 cm^{-1}, which results in the number of spectral elements of N = 500/0.0367 = 13624. The number of interferogram points is just as large. They are distributed over a grid shift of 6.81 cm and follow each other at distances of 6.81 cm/N = 5 μ. The movable part of the grid must be displaced each time by 5 μ between the determination of two interferogram points.

We already mentioned above that the grid shift should be made greater than 6.81 cm. Now we must realize that, for the Fourier transformation programs according to Cooley-Tukey, the number of transformed points must always be a power of two. (If less values are measured, then the other positions can be filled with zeros.) The next power of two greater than 13624 is 2^{14} = 16384. This number of points can be exploited if the grid shift were increased to $2^{14} \cdot 5\mu$ = 8.192 cm. Then it is also possible to achieve the required resolution, even when

*[Translator's note: Word omitted.]

apodization functions are used [17].

Finally, we obtain the following data for the grid:

Number of lamella pairs:	$N = 20$
Grid constant:	$a = 0.5$ cm
Optimum ray divergence:	$2\psi_G = 2.9 \cdot 10^{-3}$ rad = 10'
Maximum grid shift:	$z = 8.2$ cm
Step:	$\Delta z = 5$ μ

Tolerances /75

The tolerances of the lamella grid must be oriented towards the smallest wavelengths being measured, that is, towards λ_m = 20 μ. The basic requirement is that the sum of all possible errors occurring at the lamella grid produce a phase difference of less than $\lambda_m/10$ = 2 μ for parallel incident rays.

For this purpose, the surfaces of the lamellae must be machined so that, at the position with the grid shift z = 0, no points of the grid surface deviate from the ideal plane by more than 0.5 μ. The position of this plane in space is not as critical.

In addition, when the movable lamellae family is displaced, no point on the plane of this family should deviate from the adjusted shift by more than 0.5 μ. The advance of the grid must be controlled with the same accuracy of ±0.5 μ and it should be possible to measure it within this accuracy.

If these tolerances are maintained, then the instrument should reach the calculated degree of modulation down to wavelengths of 20 μ.

Remarks for the Construction*

When constructing the grid, one must be especially careful that the tolerances can be maintained for arbitrary positions of the instrument in space. This can only be done if the individual lamellae have sufficient stiffness and the entire instrument has great mechanical strength. The guides of the movable part must be very precise, which is difficult to bring about for the required accuracy. This problem is very important for the operation of the grid.

Since the telescope is to be cooled later on to the temperature of boiling nitrogen, it is useful to design the grid now, so that it can still operate at this temperature. This /76
leads to the requirement for building the instrument from a material which has approximately the same coefficient of expansion, so that the ground surfaces will not deform when there are temperature changes. A glass ceramic material with a low coefficient of expansion (Zerodur) seems to be especially suitable for this. One must then consider the various expansions of the materials in the transition to the metal parts of the grid guides. At 70° K, the drive system will also present some problems. The motor cannot operate at temperatures substantially below 270° K, because otherwise, the lubricant freezes. There is a micrometer spindle between the motor and the grid, and its length change with temperature must be considered. In order for the heat flux between the motor and the grid to remain small, which would produce temperature gradients in the grid, there must be a heat insulating layer between these two components.

---

*The information on the problems presented here [is] due to J. Stoecker.

If the micrometer spindle is cold, then the step of the grid advance will be smaller than is the case at room temperature, which means that it is very important to accurately measure the grid shift in each case. An optical system would be ideal for this, for example, a laser interferometer or a Moiré system, which both reach very high measurement accuracies and depend very slightly on the surrounding conditions. On the other hand, both systems require light sources, they have a high degree of energy consumption, and produce relatively large amounts of heat and they also cannot be operated at temperatures much above 270° K. Finally, the radiation of the grid, which is point shaped in the case of a laser interferometer, leads to temperature gradients and, therefore, deformations in the lamellae. Therefore, a system of the firm Haidenhain, based on the induction principle and which is fixed in the zerodur body of the grid, seems appropriate for the IR experiment. At the present time, the accuracy of this system is still too small, but one instrument should be built by the end of 1974 which can measure distances with an accuracy of 0.5 μ. /77

Another problem is the separation of the incoming rays and the rays reflected by the grid. The simplest solution would be to have the grid oblique with respect to the incident radiation so that the normals of the lamellae surfaces would have an inclination with respect to the axis of the incident ray bundle. The inclination of the grid would have to be perpendicular to the lamellae structure, because otherwise, the lamellae surfaces in the back would be shaded. In this arrangement (Figure 21), we must consider the fact that the displacement of the movable lamellae is perpendicular to the directions of the incident or reflected rays, and, therefore, with increasing shift, they wander outside of the bundle of the incident radiation. In

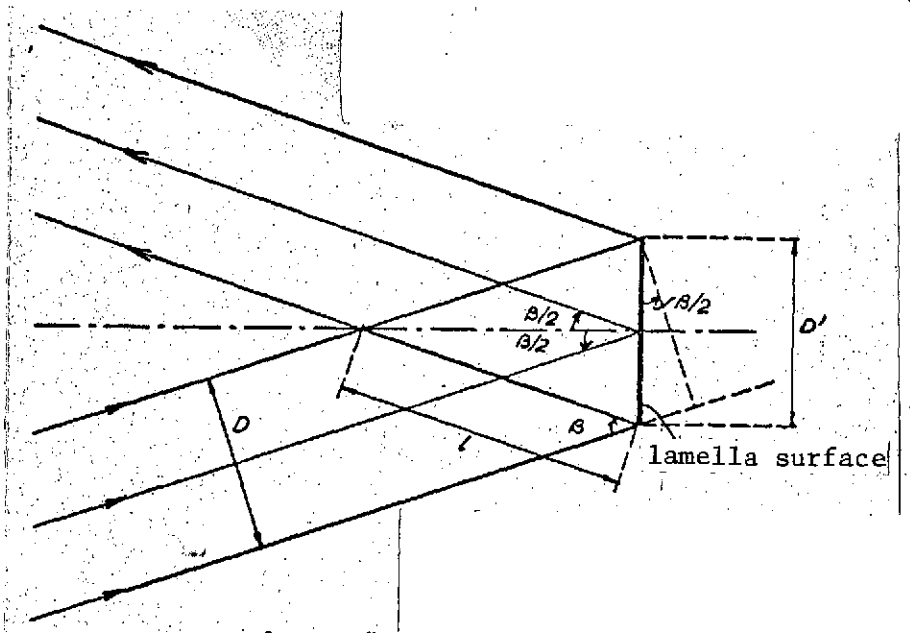

Figure 21. Spatial separation of reflected and incoming rays.

order to obtain smaller losses, the grid would have to be over-dimensioned, which would have a detrimental effect on the stability. In addition, there is no possibility here of specifying the grid inclination in a reproducible way. However, this is very important because the inclination determines the produced phase difference. For the arrangement discussed here, it is given by

$$x = 2z \cos(\beta/2) .$$

Therefore, it is more advantageous to have an oblique surface on the lamellae and to adjust the grid in such a way that the motion of the lamellae is parallel to the axis of the incoming radiation (Figure 22). The reflection direction is then uniquely determined by the inclination of the lamellae surfaces. If the angle between the normals of these surfaces

/78

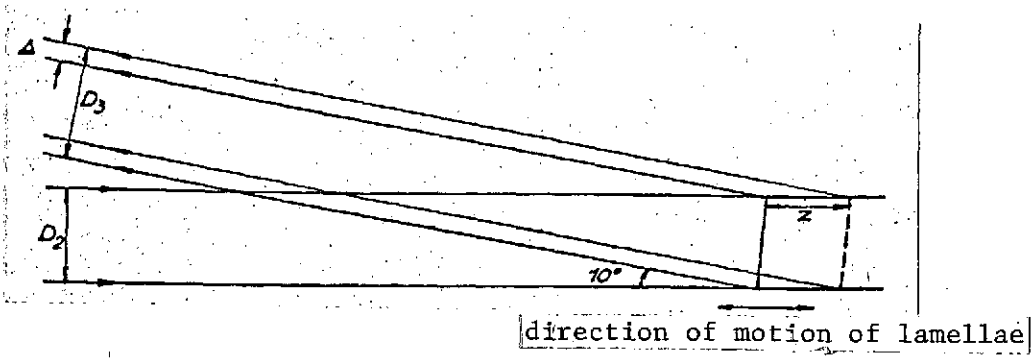

Figure 22.

and the direction of motion is β/2, then the reflection occurs at an angle β with respect to these normals and the phase difference for the grid shift z is:

$$x = z \cdot (1 + \cos\beta)$$

The reflected ray bundle has the diameter D_2 of the incident bundle for z = 0 and for a finite grid shift, it is wider by $\Delta = z \cdot \sin\beta$, which must be considered when dimensioning the collimator mirror, which follows the grid.

If β/2 = 5° is selected, then Δ = 1.7 cm for a 10 cm grid shift and for separating the incident and reflected radiation, and for a 10 cm ray cross section, a path of about 60 cm is required. This means that neither the collimator mirror nor the path required for separating the rays become excessively large. Considering the ray divergence at the grid, we find a collimator mirror diameter of D_3 = 12 cm.

We should also like to mention that β can be freely selected within certain limits. Therefore, relatively wide tolerances are allowed for the manufacturing process (about 0.5°). The

value obtained must be known to within a few minutes of arc in order to carry out the correction for the phase difference, according to (3.33).

4. Optical Structure of the IR Telescope /79

The establishment of the unknown data for the telescope optics (optical system, focal length, and diameter of the mirrors) and of the detector (time constant, noise power) determines the requirements for the overall payload (uncooled or cooled optics, weight distribution in the balloon gondola, alignment accuracy of telescope). In order to arrive at meaningful decisions, the purpose of the IR experiment must be discussed in more detail. The radiation fluxes to be measured and the spatial extension of the interstellar sources must be considered most important. Therefore, we will first investigate the fluxes which occur at the detector, because of the various sources, as well as their noise power levels.

4.1. Radiation Sources

4.1.1. Interstellar sources

The objects of interest are, for the most part, extensive sources, that is gas and dust clouds, as well as galaxies. The breadths of these objects ranges between seconds of arc up to several minutes of arc.

Here we will only consider interstellar clouds, because they were first investigated. As a typical example, we will consider a gas cloud with a diameter of 1 pc = $3 \cdot 10^{18}$ cm and a temperature of 100° K. The electromagnetic radiation in the infrared then primarily comes from thermally excited molecules. The intensity of the lines is approximately given by the value of

the Planck curve at the corresponding frequency and temperature, multiplied by the line width for media which are optically dense for the line center. For a typical density of 10^5 cm^{-3}, the cloud will, for example, be optically dense for the line radiation of CH, OH, CN, if the corresponding transitions do not start at excessively high rotational levels ($J \lesssim 4$).

The number of photons emitted by a black body at temperature /80
T at a wavelength λ is:

$$\frac{di}{d\nu} = \frac{2}{\lambda^2} \cdot \frac{1}{e^{hc/kT\lambda} - 1} \left[\frac{\text{Photons}}{cm^2 sr\, s\, Hz}\right]. \qquad (4.1)$$

The line width is determined by the Doppler width of the thermal motion of molecules:

$$\Delta\nu = \frac{v_0}{\lambda}\,; \quad v_0 = \sqrt{\frac{8kT}{\pi m}}. \qquad (4.2)$$

(if microturbulences occur, then v_D can be even larger).

Therefore, we have the following for the photons emitted per line:

$$i = \frac{2}{\lambda^2} \cdot \frac{1}{e^{hc/kT\lambda} - 1} \cdot \frac{v_0}{\lambda} = \frac{2}{\lambda^2} \cdot \frac{1}{e^{1,44/\lambda T} - 1} \cdot \frac{v_0}{\lambda} \left[\frac{\text{Photons}}{cm^2 sr\, s}\right]$$

where λ must be substituted in centimeters. The typical molecular weight is around 20 and, therefore, with $m = 20\ m_p = 3.34 \cdot 10^{-23}$ g, we have:

$$v_D = 3{,}2\ 10^4\ cm/s.$$

Therefore:

$$i = \frac{6.4 \cdot 10^4}{\lambda^3} \cdot \frac{1}{e^{1,44/\lambda T} - 1} \left[\frac{\text{Photons}}{cm^2 sr\, s}\right]$$

or:

$$i = \frac{1{,}27 \cdot 10^{-18}}{\lambda^4} \cdot \frac{1}{e^{1{,}44/\lambda T} - 1} \left[\frac{W}{cm^2 sr}\right]. \qquad (4.3)$$

The maximum of this distribution is at $hc/kT\lambda = 3.93$, so that for a cloud temperature of T = 100° K, a wavelength of 36.5 μ results. One obtains the following intensities as a function of wavelength:

100μ	$1{,}99 \cdot 10^{10}$	$\frac{\text{Phot.}}{cm^2 sr\ s}$	$3{,}95 \cdot 10^{-11}$	$\frac{W}{cm^2 sr}$
90μ	$2{,}22 \cdot 10^{10}$		$4{,}90 \cdot 10^{-11}$	
36,5μ	$2{,}60 \cdot 10^{10}$		$1{,}43 \cdot 10^{-10}$	
28,2μ	$1{,}74 \cdot 10^{10}$		$1{,}22 \cdot 10^{-10}$	.

The intensities to be expected, therefore, lie in the range between 10^{-10} and 10^{-11} W/cm² sr per line for typical sources.

For hydrogen, one of the most important molecules, such a cloud is not optically dense. For the 28.2 μ line, we then obtain:

$$i = \frac{A}{4\pi} \cdot \int n^* ds$$

where A is the Einstein coefficient and n is the density of the excited H_2 molecules. The differential equation for the number of excited molecules in the first rotational state is: /81

$$\frac{dn^*}{dt} = kn^2 - k'nn - An^*,$$

where $k' = 10^{-12} cm^3/sec$ [18], $k = k'(2J + 1) \cdot \exp[-J(J + 1)BHc/kT]$, $A = 10^{-12}\ sec^{-1}$. In equilibrium, we have $dn^*/dt = 0$, and by solving with respect to n*, we find

$$n^* = \frac{k}{k' n + A} n^2$$

For $A \ll k' \cdot n$, it follows that:

$$n^*/n = (2J + 1) \cdot \exp(-J(J + 1)Bhc/kT)$$

and

$$i = \frac{A}{4\pi} \cdot \exp(-J(J + 1)Bhc/kT) \cdot nl \; . \qquad (4.4)$$

If the density is again 10^5 cm^{-3}, with $J = 2$, we find for $\lambda = 28.2$ μ:

$$i = nl \cdot 1{,}15 \cdot 10^{-11} \cdot e^{-475/T} = 3 \cdot 10^{10} \; \frac{\text{photons}}{\text{cm}^2 \text{sr s}}$$

or

$$i = 2{,}1 \cdot 10^{-10} \; \text{W/cm}^2 \text{sr} \; .$$

If we again ignore absorption by the dust, then the intensity has the same order of magnitude as that of the lines for which the gas cloud is optically dense. The reader is referred to [26] for the influence of the dust on the intensity.

The interstellar sources which are of primary interest because they are the strongest produce intensities on the order of 10^{-10} to 10^{-11} W/cm^2 sr per line. These radiation power levels must at least be detected in order for the experiment to produce results. Later on, an attempt will be made to also measure lower intensities.*

*In addition, we can also investigate bright sources, such as H II regions [27], planets, and interstellar dust.

4.1.2. The atmosphere and the telescope optics considered as a radiation and noise source

The atmosphere is one of the most important sources of perturbation radiation. According to a private communication of F. Low, it has an average emissivity of $\varepsilon = 0.01$ in the far infrared, at an altitude of 35 km. There, the temperature is about 230° K. According to the Wein displacement law, the maximum of the radiation intensity of a black body (referred to wave numbers) at the temperature T occurs at the wavelength

$$\lambda = 2{,}9 \cdot 10^{-3}\ \text{m} \Big| \quad \text{degree/T}.$$

For T = 230° K, we have $\lambda_M = 12.6\ \mu$ and this is close to /82 the wavelength region being investigated. Therefore, as a zero approximation, we can assume that the total radiation flux is recorded by the detector, which is essentially true, if there is no filter at the radiation input point. At 230° K, the flux from the spectral range $\lambda \geq 20\ \mu$ is about 0.44 and from $\lambda \geq 30\ \mu$ it is about 0.19 of the total flux, the intensity of which is given by:

$$i = \varepsilon \cdot \frac{\sigma}{\pi} \cdot T^4 \Big| \qquad (4.5)$$

At T = 230° K, we have $i_{At} = 5.0 \cdot 10^{-5}$ W/cm² sr. This flux density is divided up among about 100 lines [23], so that the intensity per line is about $5 \cdot 10^{-7}$ W/cm² sr. This is three to four powers of ten more than the intensity per line from a typical interstellar cloud. One of the main problems of the experiment consists of suppressing this perturbing radiation.

Whereas the atmosphere produces essentially only line radiation above 30 km, continuum radiation is produced by the reflecting surfaces of the telescope optics and the Dewar window (see 4.2.5). Its flux density per unit surface area of emission is also given by (4.5). The emissivity of the mirrors is $\varepsilon \approx 0.01$ in the most favorable case, and its temperature is specified by the surrounding temperature for the first flights, i.e., we will have $T = 230°$ K at an altitude of 35 km. For five mirrors (this number is usually required), we then have:

$$i_{Sp} = 2{,}5 \cdot 10^{-4} \text{ W/cm}^2\text{sr} .$$

If we assume the same temperature for the Dewar window as for the telescope optics, we obtain, for a polyethylene window with a thickness of 100 μ, an emissivity of about 0.05 (

$$(\varepsilon = 1 - e^{-\varepsilon_0 d} \approx \varepsilon_0 d$$

for sufficiently small values of d, $\varepsilon_0 = 0.5 \text{ mm}^{-1}$). The window can, if necessary, be cooled so that its flux density is reduced according to

$$i_{Fe} = 2{,}5 \cdot 10^{-4} \, (T/230)^4 \text{ W/cm}^2\text{sr}$$

For the case where the window is not cooled below the surrounding temperature, the entire flux density is given by: /83

$$i = i_{Al} + i_{Sp} + i_{Fe} = 5{,}5 \cdot 10^{-4} \text{ W/cm}^2\text{sr}$$

It is possible that, from this, such large fluxes at the detector will result so that it becomes overcontrolled. In this case, measurements cannot be carried out and the detector has to be exchanged or the system solid angle range must be reduced. If the fluxes are within permissible values, then it is possible to eliminate them by differencing between two measured values (it is questionable what the accuracy of this will be). On the

other hand, the photon noise of this radiation cannot be eliminated. For black body radiation, the normalized noise power (see 2.4.3) is given by

$$NEP = \left\{ F\Omega \cdot \varepsilon \cdot \frac{4}{\pi} \cdot 2kT^5 \right\}^{1/2} = \left\{ 4F\Omega \cdot i \cdot kT \right\}^{1/2} \qquad (4.6)$$

If all radiators are at 230° K, we have:

$$NEP = \left\{ F\Omega \cdot \varepsilon \cdot 6{,}4 \cdot 10^{-23} W^2 s/cm^2 sr \right\}^{1/2} \qquad (4.7)$$

The magnitude of these fluxes and noise power levels at the detector depends on the telescope solid angle range which will be found from the developments given in the next section.

4.2. Optical System

4.2.1. The given variables

First of all, only the dimensions of the main mirror and the lamella grid are specified.

The main mirror has a diameter of 1 m and an aperture ratio of f/2. The mirror area was selected as large as possible in order to obtain the optimum radiation flux from interstellar sources. A larger mirror would have made the telescope too large and heavy, which would have had a detrimental influence on the aligning accuracy [1]. In order to make the length and, therefore, the moment of inertia of the telescope small, we selected the short focal length of 2 m. Originally the aperture ratio was to have been f/1.5, but because of the aberrations which occur in conjunction with the rocking mirror, this led to distortions of the wave fronts which were too large after the secondary mirror (see below). Also, the correction of

the field of view becomes too involved. Since the rocking mirror will image various regions of the sky on the detector, the main mirror must be corrected for a larger field of view than would correspond to the vision angle of the detector. The main mirror is corrected over a field of 10', whereas the range imaged onto the detector has a diameter of 1' (this approximately corresponds to a refraction limitation at 200 μ of $1.22 \cdot \lambda_M/D = 2.44 \cdot 10^{-4}$ rad = 0.84'). /84

The dimensioning of the lamella grid is justified in Section 3.5. Here again we should mention the fact that the edge length of the optically active area is 10 cm and the beam divergence at the grid should not exceed 10' by much.

The remaining optical elements of the instrument must now be defined. Two solutions can be considered for the balloon experiment: a Gregory and a Cassegrain system.

4.2.2. The Gregory system

Figure 23 shows one possible configuration for the Gregory system. The parabolic secondary mirror is the rocking mirror and is arranged so that its focal point coincides with that of the main mirror. Therefore, there is an intermediate imaging between the main mirror and the secondary mirror, which makes it possible to adjust the optical components of the telescope relatively simply and this can be used for limiting the field of view. The latter is done using a slit diaphragm for which the width d corresponds to the diameter of the image. The length ℓ must be at least large enough so that it will pass an angular range of 10' on the sky, which is being scanned by the motion of the mirror. For a field of view diameter of 2θ = 1', we have:

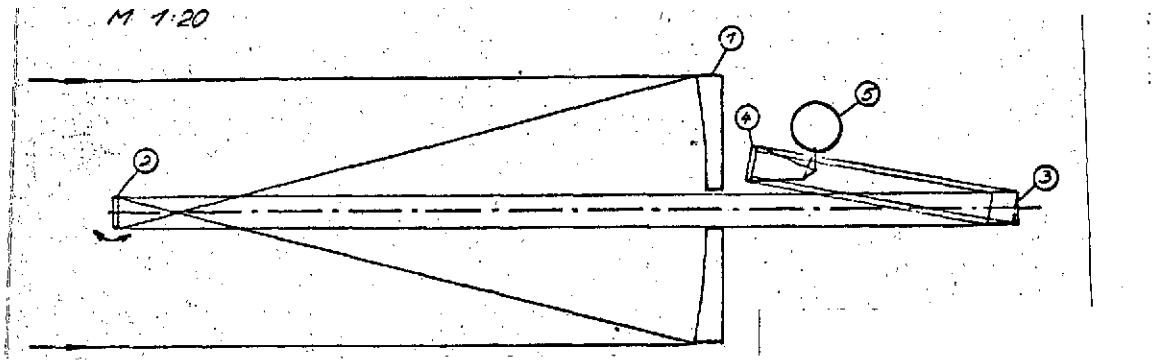

Figure 23. Gregory system for the IR experiment.

1- main mirror D_1 = 100 cm, f_1 = 200 cm; 2- secondary mirror D_2 = 10 cm, f_2 = 20 cm; 3- lamella grid; 4- collimator system; 5- detector.

$$d = 2\theta \cdot f_1 = 0{,}58\text{mm} \quad \text{and} \quad l \gtrsim 5{,}8\text{mm} .$$

The actual dimensions should be somewhat larger so that the edge of the diaphragm is not imaged onto the detector. The slit diaphragm is installed so that it is perpendicular to the lamella structure of the grid. Its purpose is to prevent the spectra of higher order from sky regions lying outside of the desired field of view from being imaged onto the detector as this would disturb the modulation. (This is only important when the sources are larger than the field of view.) Therefore, we obtain the following picture in the detector plane (Figure 24).

Because of the motion of the rocking mirror, the strips wander up and down by a maximum of ±5'; so that the various areas of the sky are imaged on the detector.

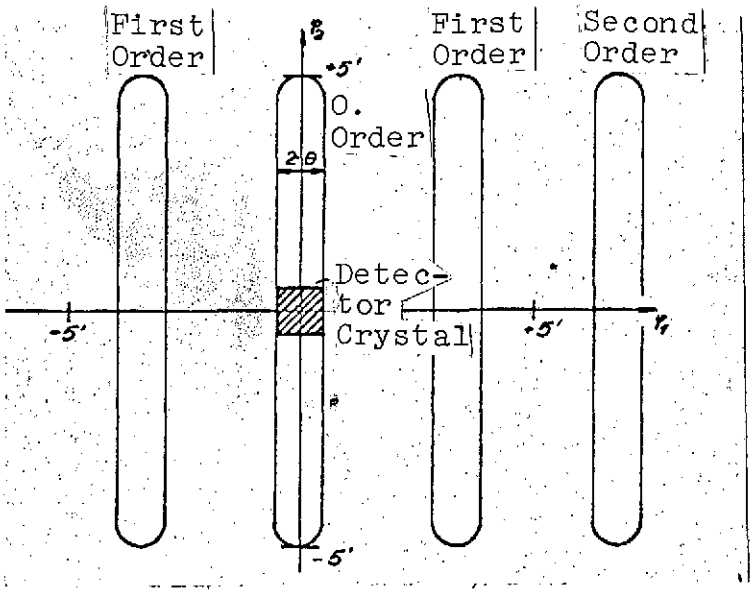

Figure 24. Image of the slit diaphragm in the detector plane for $\lambda = 48.2\ \mu$.

φ_1 - direction of grid structure. The coordinates refer to the points of the intermediate image, as seen from the main mirror.

The instrument operates optimally as long as the ray divergence at the grid corresponding to the image diameter does not exceed the limits given in Section 3.2 by much, that is, when the given grid dimensions do not become greater than 10'. This requirement can be satisfied if, for an image diameter of 1', the angle amplification is not greater than 10. In the case of the Gregory system, this is given by:

$$\frac{2\varphi_G}{2\Theta} = f_1/f_2 = 10 \ .$$

For $f_1 = 200$ cm, it follows that $f_2 = 20$ cm. On the other hand, the diameter of the secondary mirror equals the edge length of the grid:

$$D_2 = D_G = 10\text{cm} \ .$$

The aperture ratio, therefore, is f/2 for the secondary mirror.

Now the rocking mirror should not be moved around the focal point, as will be required for exact optical imaging, but instead, it should perform rotational oscillations around an axis which is close to its center of gravity. (The motions around an axis very far removed from the center of gravity can only be performed with great difficulty, especially at high frequencies.) The aberrations caused by simple rotation should not produce any phase differences greater than $\lambda_M/10 = 2\ \mu$ in order to not disturb the coherence of the incoming radiation. According to a communication of Zeiss, the aperture ratio must remain smaller than f/2. Therefore, the maximum aperture ratio for the telescope optics is specified. The 10 cm mirror with f/2 can be built.

The deflection of the rocking mirror is a maximum of ±25' = ±0.36 mm linear deflection at the edge of the mirror. If this motion is to occur with an accuracy of ±10% of the field of view, that is, with ±0.5', then the final position of the mirror must be defined to within ±7 μ at its edge. /87

After reflection at the lamella grid, the frontal surface of which is located about 80 cm behind the main mirror, the radiation is focused onto the detector crystal by a collimator system. As already mentioned, the noise power of the detector becomes smaller as its area is decreased. For this reason, the image should be made as small as possible. The linear image diameter is given by:

$$D_{Det} = 2\Theta \cdot f_1 f_3 / f_2 \qquad (4.8)$$

One problem occurs because of the size of the Dewar, which makes it necessary to take the focal point of the collimator out of the incoming ray bundle. This requirement is difficult to reconcile with the requirement for a small image and, therefore, a small f_3. Since these difficulties also occur for the Cassegrain system, we will discuss them in more detail later on (Figure 23 shows a Newton telescope as the collimator system).

4.2.3. The Cassegrain system

An alternate solution is the Cassegrain system (Figure 25). Here again, the secondary mirror is hyperbolic and is the rocking mirror and one of its focal points again coincides with that of the main mirror. The secondary mirror, this time, is located in front of the focal point of the main mirror and produces a convergent light bundle which is focused onto the second focal plane. The effective focal length of the system is: /88

$$f_e = f_2 \cdot D_1/D_2 \,. \qquad (4.9)$$

The selection of f_2 and D_2 is not as restrictive as for the Gregory system. D_2 = 10 cm is again a favorable solution because, on the one hand, the shadowing of the main mirror is not yet very great (1%) and, on the other hand, the distance of 1.8 m from the main mirror represents a relatively small construction length for the telescope. If we select f_2 = 1.6 m, in order to not make the overall length of the balloon gondola excessively large, which is determined by $2f_2$ (distance between secondary mirror 2 — collimator mirror 3 in Figure 25), then the image will still lie within the telescope, 20 cm ahead of

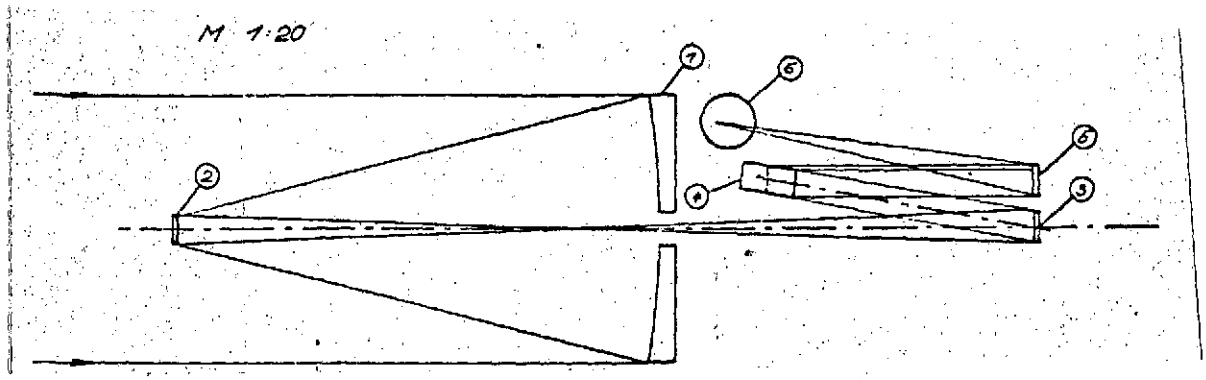

Figure 25. Cassegrain system for the IR experiment.
1- main mirror, D_1 = 100 cm, f_1 = 200 cm; 2- secondary mirror, D_2 = 10 cm, f_2 = 160 cm; 3- collimator mirror, D_3 = 10 cm, f_3 = 160 cm, 5° off-axis; 4- lamella grid; 5- collimator, D_5 = 12 cm, f_5 = 120 cm; 6- detector.

the main mirror. At this point, it is possible to install a diaphragm which reflects on the back side. The imaging with mirrors leads to low emissivity. Or one can install a diaphragm made of dichroic material, which lets visible light pass through, but which absorbs the IR radiation (in the case of a dichroic mirror, which is located just ahead of the detector crystal, the visible light can be separated from the IR radiation and can be used for adjusting the instrument). In both cases, the diaphragm would be arranged in a tube and would separate the chamber located behind the main mirror from the space.

No slit diaphragm is required for this system, because the rocking mirror is located in front of the intermediate image. The main purpose of the diaphragm is to prevent the imaging of spectra of higher order onto the detector for areas in the sky which are outside of the field of view. With the assumed data, the effective focal length of the telescope is 10 m, so that the /89 image size for a field of view of 2θ = 1' is given by

$$D_1 = f_e \cdot 2\theta = 4{,}6\text{mm} \qquad (4.10)$$

The diaphragm again should have a somewhat larger diameter so that its edges are not imaged onto the detector.

The motion of the rocking mirror has the same amplitude and tolerances as in the case of the Gregory system.

Since the secondary mirror, as well as the grid, has a diameter of 10 cm, a parabolic mirror with the same diameter with f/16 must be arranged symmetrically with respect to the diaphragm which illuminates the grid. Since the grid must be installed behind the ray beam, which illuminates this mirror, an off-axis mirror must be used. The off-axis angle for a distance of 90 cm between the frontal surface of the mirror and the grid must be at least $2\beta = \arctan(10\text{cm}/90\text{cm}) = 6.34°$. Because of the oblique grinding of the lamella, we select $2\beta = 10°$. For these parameters (f/16, 10°), the phase difference caused by aberration still is below the tolerance level and, therefore, does not disturb the coherence of the radiation impinging on the grid.

The ray divergence at the grid is given by

$$2\vartheta_e = B_1/f_3 = 2\theta \cdot f_2/f_3 = 10'$$

for $2\theta = 1!$ and, therefore, is in the range which corresponds to a very good modulation for the grid.

The image diameter at the detector, in this case, is:

$$D_{Det} = 2\theta\, D_1 f_4/D_2 , \qquad (4.11)$$

if f_4 is the focal length of the collimator system.

4.2.4. Comparison of the two systems

The Gregory system has the advantage that it requires one less ground mirror surface than the Cassegrain system. The /90
intermediate image after the main mirror somewhat facilitates the adjustment of the optical components. Since it is very small (0.5 mm Ø), a chopper system in the form of [tuning] fork could be used for absolute flux measurements (atmospheric measurement).

The main advantage of the Cassegrain system is the favorable moment of inertia of the telescope (for about the same length of both systems, the weight distribution of it is more favorable). The larger intermediate image allows a simpler adjustment of the diaphragm. It separates the telescope from the "instrument chamber" located behind the main mirror, which would make it possible to cool the chamber with nitrogen and down to a temperature of about 70° K. The small diaphragm aperture of about 5 mm prevents, to a significant extent, the convective heat exchange and the diffusion of gases from the atmosphere (for example, H_2O). If the thermal radiation of the [Dewar] window can be ignored, which is the case for the 4 μ polyethylene foil used by Low, then the photon noise is reduced by about 30% by doing this. The method would, therefore, not be advantageous if one were to consider the difficulties for the motion of the lamella grid caused by the low temperature (lubrication, thermal insulation of the motor). If the [Dewar] window is relatively thick ($d \approx 0.1$ mm, $\varepsilon \approx 0.05$), then the photon noise would be reduced by more than 60%, which means that the cooling looks favorable. However, we did not consider the fact that one part of the thermal radiation of the instrument chamber, for example, from the holders and from the edges of the mirrors and of the lamella grid, also reaches the

detector. If this radiation makes a major contribution to the total flux, then cooling will certainly be appropriate. Another advantage of the Cassegrain system is that the ray diameter can be relatively easily varied at the dispersion element by exchanging the collimator mirror. Therefore, it can be adapted to various instruments. In the case of the Gregory system, it would be necessary to exchange the rocking mirror. Since this mirror /91
is corrected, together with the main mirror, this is not a trivial matter. For the Cassegrain system, there is also the advantage that the mechanical stability and the adjustability is somewhat better than for the Gregory system.

Overall, none of the advantages of either system are great enough to favor either one of them. Both are equally suited for the IR experiment.

4.2.5. The adjustment of the detector to the telescope optics

We already mentioned that the adaptation of the detector to the telescope presents some problems, independent of the selection of the telescope system. We will now discuss these.

The ray divergence at the grid amonts to the following for either the Gregory system or the Cassegrain system:

$$2\varphi = 10 \cdot 2\theta \ .$$

Therefore, the problem of adapting the detector to the instrument is the same for both systems. The diameter of the collimator mirror is 12 cm, according to Section 3.5. It is difficult to select a suitable focal length f_4 which defines the image size, or for a given detector diameter, the field of view, in terms of the following relationship:

$$D_{Det} = 2\theta \cdot 10 \, f_4 \ . \qquad (4.12)$$

This is only correct for

$$2\theta \gtrsim 1{,}22 \cdot \lambda_M / D_1 = 2{,}44 \cdot 10^{-4} \text{rad} \cong 0{,}84'.$$

For smaller fields of view, the image size is determined by the diameter of the refraction disc. For optimum operation, the image size should equal the detector size and both should have the same diameter, just like the refraction disc at the maximum wavelength. /92

The focal length f_4 and the field of view diameter 2θ can be varied within certain limits. The diameter of the detector is fixed, first of all, because the first detectors have been bought. (As soon as a few detectors are available, their size can be adapted to the requirements.)

The detector required for the experiment must absorb radiation from the wavelength range between 20 and 200 μ with a good effectiveness, and must be able to detect it. The eigen noise should be 10^{-13} to 10^{-14} $W/\sqrt{Hz}$ at the most. In addition, the interferogram point should be obtainable in 100 msec in order to make possible the recording of an interferogram containing about 10^4 points in a reasonable amount of time. These requirements can only be satisfied at the present time with bolometers cooled with helium. The best available instruments of this type are made by F. Low. One of his bolometers will be used in the first experiments. The following table gives its data:

Area A (cm^2)	0.001	0.01	0.1
Working temperature T_D (°K)	1.5	2.0	4.2
Heat conduction value G (W/°K)	$1 \cdot 10^{-7}$	$1 \cdot 10^{-6}$	$5 \cdot 10^{-4}$
Resistance R_0 (Ω)	$7 \cdot 10^{6}$	$5 \cdot 10^{5}$	$1 \cdot 10^{5}$
Sensitivity S_{max} (V/W)	$4 \cdot 10^{6}$	$3.5 \cdot 10^{5}$	$5 \cdot 10^{3}$
Time constant (s)	$8 \cdot 10^{-3}$	$1.5 \cdot 10^{-2}$	$1.5 \cdot 10^{-3}$
Modulation frequency f_0 (Hz)	20	10	100
Noise ($nV/\sqrt{Hz}$)	30	10	7
NEP ($W/\sqrt{Hz}$)	$7 \cdot 10^{-15}$	$3 \cdot 10^{-14}$	$1.4 \cdot 10^{-12}$

First of all, we are only interested in the crystal dimension. Its edge length (they are square) is as follows in the order of detectors given above:

0.32 1.0 3.2 mm.

The first of these detectors is not well suited for the IR experiment, because its dimensions are of the same order of magnitude as the maximum wavelength, which would lead to high losses based on refraction effects and to a low absorption capacity for the maximum wavelengths. In addition, the image diameter cannot be easily reduced to the detector diameter. (f_4 = 11 cm would be required for this, which would mean an aperture ratio of f/0.9 for a 12 cm mirror.) /93

The third detector can be eliminated because its noise power is too large. The measurement time for typical interstellar sources would become intolerably large, if a reasonable s/n ratio is to be produced.

Therefore, we only have the detector with an edge length of 1 mm. If we set the image diameter (that is, its edge length) equal to twice the half-width value of the small refraction disc

for $\lambda = 200\ \mu$, then for the longest useful focal length of the collimator system, we obtain:

$$f_{\text{ges}} = D_{\text{Det}}/2{,}44 \cdot 10^{-5} \approx 41\text{cm} . \qquad (4.13)$$

The system operates at the maximum wavelength with limited refraction and the field of view diameter is 0.84'.

The following points must be considered when selecting the collimator focal length:

i) The maximum focal length should not be exploited, because at this value, the refraction losses become large in the region of large wavelengths.

ii) The achievable stability in time and space of the telescope alignment means that a field of view diameter of less than 1' does not make sense.

iii) If the field of view diameter is made considerably larger than 1', then it is larger than the dimensions of most sources, and therefore, only the radiation load of the detector /94 is increased, but not the flux from the interstellar source.

iv) There is a vacuum in the Dewar of the detector and, therefore, the inlet opening is closed with a polyethylene window. This leads to various problems:

a) If the window is warm, then the detector should be as far away from it as possible, so that it is seen under small angles and the flux from thermal radiation of the window is small. The angle under which the window is seen from the detector should not exceed 20°, so that an aperture ratio of

f/2.8 or f_k = 34 cm and 2θ = 1.0' follows.

b) Since the window has an index of refraction different from 1, part of the incoming radiation is reflected, and to an increasing extent, when the incident angle increases. If the window consists of polyethylene, then n ≈ 1.5 and for an incidence angle of 10°, 3.8% of the radiation polarized parallel to the incident plane is reflected, and 4.2% of the radiation perpendicular to the incident plane. These losses are not especially large and could be accepted.

c) The radiation passed through experiences a phase displacement at the window which has an effect on the interference at the detector. The phase difference between two rays, one of which impinges on the detector perpendicular to it and the other which impinges at the angle φ, is greater by an amount

$$\Delta = d\left(\frac{n}{\cos\chi} - \frac{1}{\cos\varphi} - (n-1) + (\tan\varphi - \tan\chi)\cdot\sin\varphi\right)$$

than for propagation through a homogeneous medium with the index of refraction 1, for the case where the window has thickness d and index of refraction n along the ray path. (χ is determined by the refraction law sin φ = n · sinχ.) For n = 1.5 and φ = 10°, we find

$$\Delta = d\cdot 5{,}1\cdot 10^{-3},$$

that is, for d = 1 mm : Δ = 5.1 μ. This displacement can noticeably disturb the interference figure under some conditions. Therefore, d should be made as small as possible. This is possible by reducing the window thickness. Polyethylene foils 4/95 with a thickness of d = 0.1 mm can be produced without difficulty and can withstand the pressure difference of 1 atm. For

such cases, Δ is about 0.5 μ for an incidence angle of 10° and is, therefore, no longer critical.

v) The detector is in a Dewar with a diameter of about 17 cm. This vessel cannot be brought into the ray path of the radiation impinging on the collimator, as already mentioned. Therefore the focal point of the collimator must be taken out of the path of the incoming radiation either using a flat mirror (Newton telescope) or an off-axis mirror, or a combination of both.

The use of an off-axis mirror leads to aberrations for the largest aperture ratios, which can considerably disturb the phase relationships of the rays going to the detector and, therefore, can disturb the interference. According to a communication by Zeiss, for a f/4.5 system with 34° off-axis angle, 10 cm diameter, and 20' radiation divergence of the incoming radiation, the phase difference between edge rays having the maximum inclination with respect to the axis of the ray bundle amounts to 10 μ. For a wavelength of 20 μ, the phase relationships of the reflected beams would be disturbed to an intolerable extent. In addition, for the aperture ratio given, the focal length is already greater than allowed according to Equation (4.13). The aperture ratio would therefore have to be enlarged, which again would lead to greater aberrations. This solution can therefore not be used for the experiment.

A Newton system as collimator has a disadvantage that the deflection mirror will shield some of the incoming radiation. For a f/2 system, the shading amounts to 25% of the flux coming from the grid and it is 10% for a f/3 system, if the collimator mirror is 12 cm and the focal point is 4.5 cm outside of the incoming radiation bundle. Therefore, the Newton telescope is also not optimal. 2/96

Thus, we have arrived at the following situation: the size of the field of view and the geometry of the Dewar require that $f_4 \approx 35$ cm or f/2.9. For this aperture ratio, we are not able to use any off-axis systems as collimators, because the required off-axis angle would lead to large aberrations. It would still be possible to use a Newton telescope, but we have a light loss of at least 10%. One way out of this is to use the suggestion of F. Low. A small off-axis mirror with a diameter of 3.5 mm, f/2.4, and 8° off-axis angle is installed in the Dewar, which focuses the radiation from the collimator onto the detector. The system is designed so that down to 15 μ, it still has limited refraction. For a ray divergence at the grid of $2\psi_G = 10'$, this arrangement would result in a collimator focal length of

$$f_4 = 0{,}35\text{cm}/2\psi_G = 120\text{cm}$$

This corresponds to an aperture ratio of f/10 and makes it possible to use an off-axis mirror as a collimator system with an off-axis angle between 5 and 10°. Such an arrangement is given in Figure 25.

The data of this detector are the following:

Edge length	0.7 mm
Temperature	1.5° K
Heat conduction coefficient	$G = 1.0 \cdot 10^{-6}$ W/°K
Optimum modulation frequency	$f_0 = 40$ Hz
Normalized noise power	$NEP = 3 \cdot 10^{-14}$ W/$\sqrt{\text{Hz}}$
Maximum sensitivity	$S_{max} = 6 \cdot 10^5$ V/W.

For the optical structure of the experiment, the detector suggested by Low is better suited than the 1 mm detector. However, the load capacity and the modulation frequency are very /97 important here, as well as the sensitivity of the detectors.

4.3. Detector

4.3.1. Radiation and noise powers in the detector

Since the field of view of the telescope and the expected radiation intensities are approximately known, it is possible to determine the fluxes and noise powers in the detector.

For $2\theta = 1'$, the solid angle range of the system is:

$$E = (D_1 \cdot \theta \cdot \pi/2)^2 = 5{,}2 \cdot 10^{-4}\,\mathrm{cm}^2\,\mathrm{sr}\ .$$

The source intensities estimated in 4.1 lie within the range of 10^{-10} to 10^{-11} W/cm^2 sr from one line. If the source diameter is at least equal to 2θ, then the fluxes from one line (which reach the detector for the transmission 1 of the total system) equal:

$$\mathcal{B}_Q \approx 5 \cdot 10^{-14} \text{ bis } 5 \cdot 10^{-15}\,\mathrm{W}\ .$$

The atmosphere produces the following per line

$$\mathcal{B}_{A,\nu} \approx 2{,}5 \cdot 10^{-10}\,\mathrm{W}$$

or, on an integral basis,

$$\mathcal{B}_A \approx 2{,}5 \cdot 10^{-8}\,\mathrm{W}\ .$$

The flux from the five reflecting surfaces of the telescope is the following for T = 230° K and $\varepsilon \approx 0.01$:

$$\mathcal{B}_{Sp} \approx 1{,}3 \cdot 10^{-7}\,W .$$

The window at the Dewar produces the same amount. Therefore, we have the following for the photon noise of the total flux:

$$NEP_{At+Sp+Fe} = 6{,}1 \cdot 10^{-14}\,W/\sqrt{Hz}$$

without using optical filters. If a filter is used which absorbs radiation $\lambda \lesssim 20\ \mu$, then we have

$$NEP_{At+Sp+Fe} = 3{,}1 \cdot 10^{-14}\,W/\sqrt{Hz} .$$

The smallest signal which can be detected is 10^4 to 10^5 times weaker than the perturbation radiation of an atmospheric line and is 10^6 to 10^7 times smaller than the total radiation flux from the atmosphere. It is 10^7 to 10^8 times smaller than the flux from all perturbation radiation sources. This ratio can be changed within narrow limits only. One way of reducing the flux would be to reduce the field of view, which would make no sense because of the refraction effect. The radiation from the telescope optics can be considerably reduced by cooling the instrument to 70° K. The radiation from the atmosphere can only be reduced by large flight altitudes, but for balloons, this altitude cannot exceed 50 km. We have gained a factor of 10 compared to the values used here (the values used up to the present apply for an altitude of 35 km). The detector would therefore have to process the fluxes just estimated. Therefore, we must ask ourselves how this detector must be structured. /98

4.3.2. Characteristic dimensions of the detector

The properties of the bolometer are determined by volume, temperature, and material of the detector crystal. Low gives the following empirical relationships for his detectors [24]:

Optimum modulation frequency

$$f_o = 1{,}6 \cdot 10^6 \cdot G/(AT_D^3) \quad [\mathrm{Hz}] \tag{4.14}$$

Maximum sensitivity

$$S_{max} = 0{,}7 \cdot (R/T_D G)^{1/2} \quad [\mathrm{V/W}] \tag{4.15}$$

Normalized noise power

$$NEP_D = 1{,}5 \cdot 10^{-11} \cdot T_D \cdot G^{1/2} \quad [\mathrm{W}/\sqrt{\mathrm{Hz}}]. \tag{4.16}$$

In order for the detector to be able to process the maximum flux $\mathcal{B}_{st}$ of the perturbation radiation, we must also have [24]:

$$G \gtrsim 10 \cdot \mathcal{B}_{st}/T_D \,. \tag{4.17}$$

Here we have G — heat capcity [W/°K]; A — absorbing area of the detector [cm^2]; T_D — working temperature of the detector [°K]; R — resistance of the detector crystal [Ω]; $\mathcal{B}_{st}$ — flux of perturbation radiation [W].

Only the area A and the resistance R are determined by the detector crystal. The temperature is defined by the cooling bath and the heat conductivity through the suspension of the crystal. G and T_D can, therefore, be relatively easily changed.

From (4.14) to (4.17), we can derive two other relationships /99 which will be interesting for specifying the detector. One of these follows from (4.17) and the relationship between the radiation flux and the photon noise. The latter relationship is as follows in the case where a body with frequency-dependent emissivity produces the flux $\mathcal{B}_{st}$ at the temperature T:

$$NEP_{St} = (4k \cdot T_{st} \cdot \mathcal{B}_{st})^{1/2}.$$

This relationship is solved for $\mathcal{B}_{st}$ and is substituted in the inequality (4.17)

$$G = 10 \cdot NEP_{st}^2 / (4k \cdot T_{st} \cdot T_D \cdot c) \quad \text{with } 0 \leq c \leq 1.$$

By substituting in (4.16), we find

$$NEP_D = 6{,}4 \cdot \sqrt{\frac{T_0}{c \cdot T_{st}}} \cdot NEP_{st} \,. \tag{4.18}$$

In an optimum design of the detector, G will be made as small as possible in order to hold the noise level as low as possible. On the other hand, (4.17) must also be satisfied which results in a lower limit for G. By selecting c = 1, i.e., by going from the inequality to an equation, we therefore find the optimum solution. In this case, there is a definite relationship between the normalized noise power level of the detector and the radiation source, because the arbitrarily selectable constant (4.18) is specified. For T_D = 2° K and T = 230° K, and with c = 1, we find:

$$NEP_D \approx 0{,}6 \cdot NEP_{st} = 3{,}6 \cdot 10^{-14} \ W/\sqrt{Hz} \,,$$

where

$$NEP_{st} = 6{,}1 \ 10^{-14} \ W/\sqrt{Hz}$$

(for T_D = 1.5° K, we have

$$NEP_D \approx 3{,}1 \ 10^{-14} \ W/\sqrt{Hz} \,.)$$

If the NEP of the detector is equal to this value, or is greater than this value, then the inequality is also satisfied and the detector is not overcontrolled by the perturbation radiation. This is no longer satisfied for the 1 mm detector at T_D = 2° K. For the 0.7 mm detector with T_D = 1.5° K, the inequality is only satisfied if a filter is installed ahead of the detector, which absorbs the radiation with $\lambda \lesssim 20\mu$.

From the fact that G must be adapted to the radiation load and it is related to the photon noise, in the present case, it follows that for the given detector temperature, the noise power /100 levels of the background radiation and the detector are approximately the same.

By eliminating G from (4.14) and (4.16), we find the second important relationship:

$$NEP_D^2/f_o = 1{,}4\cdot10^{-28}\ A\cdot T_D^5\ [W^2/Hz^2]. \qquad (4.19)$$

For fixed temperature and given detector crystal, this value is constant. By changing the heat conductivity coefficient G, that is, by modifying the suspension of the crystal, we can therefore vary NEP and f_0 within certain limits without having to carry out changes on the detector crystal itself.

This fact is important because of the following: The data of the 0.7 mm detector show that its NEP, which is $3\cdot10^{-14}\ W/\sqrt{Hz}$, is very good, whereas the time constant of $\tau = 4$ msec is relatively large and the modulation frequency of $f_0 = 40$ Hz is relatively low, which leads to long transient times (it is assumed that the preamplifier has the same time constant as the detector). A shorter transient time would be advantageous here as well as a larger NEP [the radiation load of the detector could be made larger, which seems desirable considering the fact that inequality (4.17) is not satisfied].

The transient time can be determined as follows: the detector operates in conjunction with an alternating voltage amplifier so that only the change in the radiation flux is recorded. The sensitivity is greatest when this change is carried out with the optimum modulation frequency f_0. If the

lamella grid is adjusted to the phase difference z, and if the rocking mirror oscillates at the frequency f_0, then the change in the flux during this motion is recorded, that is, the signal /101
of the source is recorded. If the phase difference is changed at the lamella grid, then the flux at the background and source radiation will also vary at the detector. Since the former is much greater than the latter, this displacement brings about a much greater flux change than by modulation with the motion of the rocking mirror. The detector must then adjust to a new value of the constant flux. The measurement must be interrupted until the signal change related to this transient process is smaller at the amplifier output than the one produced by the direction modulation (motion of the rocking mirror). This transient time is determined by the detector time constant and the ratio of source flux and background flux.

For a certain grid position, let us assume that the flux absorbed by the detector is given by

$$\mathcal{B}_{sz} + \mathcal{B}_a \cdot (\cos(2\pi f_0 t) + 1)/2$$

(if the rocking mirror carries out harmonic oscillations, which is assumed here for simplicity). The signal at the preamplifier output is then proportional to

$$\mathcal{B}_a \cdot (\cos(2\pi f_0 t) + 1)/2 .$$

Now, let us assume that the phase difference and, therefore, the fluxes are changed, and they are not equal to $\mathcal{B}_{sz}'$ and $\mathcal{B}_a'$, respectively. The signal is then approximately proportional to

$$(\mathcal{B}_{sz}' - \mathcal{B}_{sz}) \cdot e^{-t/\tau} + \{ \cos(2\pi f_0 t) + 1 \} \cdot \mathcal{B}_a'/2.$$

The first term describes the transient behavior of the system consisting of detector and preamplifier. (The change of the source flux is not considered for the transient process, because it is much smaller than the change in the background flux.) After the above estimates, on the average, the radiation of the source is 10^6 times smaller than that of the entire background. Measurements only make sense if the first term changes relatively less than the second term during a mirror oscillation. The /102
second expression can change by $|B_a'|$ at the most. The first term during a mirror oscillation ($t = 1/f_0$) decreases by

$$|B_{st}' - B_{st}| \cdot (e^{-t_0/\tau} - e^{-(t_0 + 1/f_0)/\tau}) = |B_{st}' - B_{st}| \cdot e^{-t/\tau} (1 - e^{-1/f_0\tau})$$

Now if this change is not to be any smaller than $0.1 \cdot |B_a'|$, then we have

$$|B_{st}' - B_{st}| \cdot e^{-t/\tau} (1 - e^{-1/f_0\tau}) \approx 0.1 \cdot B_a'$$

For low detectors, we have $f_0\tau = 0.15$ and the term $(1 - e^{-1/f_0\tau})$ can be replaced by 1 to a good degree of approximation:

$$|B_{st}' - B_{st}| \cdot e^{-t/\tau} \approx 0.1 \cdot B_a'$$

The remainder of the calculation depends greatly on the difference $(B_{st}' - B_{st})$, which follows from the characteristic variation of an interferogram (Figure 26).

Such interferograms are obtained for black body radiation, such as is emitted by the dominating perturbation source, the telescope optics. Its main characteristic is a decrease in the modulation, according to $1/x^2$ [21]. Therefore, large changes in the radiation flux only occur for small phase differences.*

*That is, at the beginning of the interferogram.

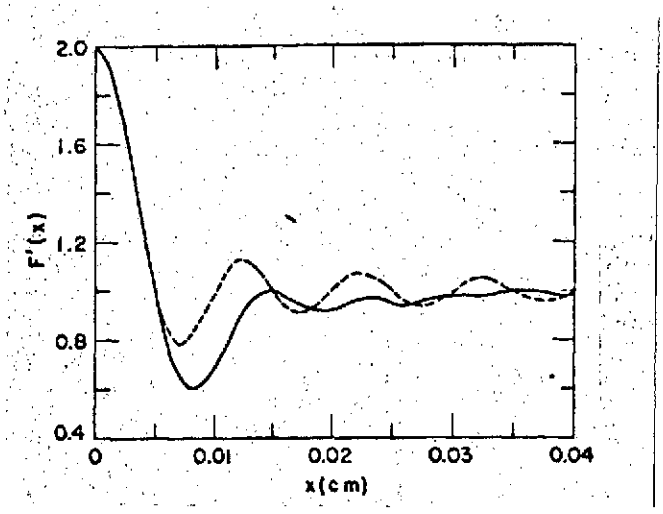

Figure 26.

For the spectral range to be processed in the IR experiment, the flux variations for the first hundred grid steps amount to approximately 10% of the maximum value of the interferogram and they will probably even be less than 1% for very large phase differences. Therefore, we must distinguish two cases: /103

i) In the vicinity of the maximum of the interferogram, that is, around x = 0, we have

$$|(\mathcal{B}_{sl}' - \mathcal{B}_{sl})| \approx 0{,}1\,\overline{\mathcal{B}_{sl}},$$

where $\overline{\mathcal{B}_{sl}}$ is the average flux of the background. With

$$\mathcal{B}_a = 10^{-6}\,\overline{\mathcal{B}_{sl}}$$

we then have

$$0{,}1\cdot\overline{\mathcal{B}_{sl}}\; e^{-t/\tau} \approx 10^{-6}\cdot 0{,}1\,\overline{\mathcal{B}_{sl}}$$

and, therefore, we find:

$$e^{-t/\tau} \approx 10^{-6} \Rightarrow t \approx 14\tau\,. \qquad (4.20)$$

ii) For large phase differences, we find

$$|(B'_{st} - B_{st})| \leq 0{,}01 \cdot \overline{B_{st}}$$

and, therefore,

$$0{,}01 \cdot \overline{B_{st}} \cdot e^{-t/\tau} \approx 10^{-6} \cdot 0{,}1\, \overline{B_{st}}$$

from which we find:

$$e^{-t/\tau} \approx 10^{-5} \Rightarrow t \approx 11{,}5\, \tau \,. \qquad (4.21)$$

For the 0.7 mm detector, we find 56 msec in the first case and 46 msec in the second case for the transient time. Now an interferogram should be obtainable in not more than 30 minutes, which means about 100 msec of measurement time per interferogram point (16,000 points). This would mean that half of the measurement time would be used as waiting time. Therefore, we must decide whether the optimum modulation frequency should not be increased at the expense of the NEP, which is possible, according to (4.19). For the 0.7 mm detector, this relationship is given by

$$NEP^2/f_0 = 2{,}25 \cdot 10^{-29}\ (W/Hz)^2 \,.$$

If we select f_0 = 100 Hz and, therefore, τ = 1.5 msec, then we find the following for the noise power of the detector:

$$NEP = 4{,}8 \cdot 10^{-14}\ W/\sqrt{Hz} \,.$$

This noise power is quite acceptable and, in this way, the transient time is reduced by a factor of 2.5 and, therefore, only 20% of the time is lost for the transient process. At the same time, the NEP becomes so large that the inequality (4.17) is then also satisfied when no filters are placed in the beam path.

One disadvantage of the high modulation frequency is that /104
the directional modulation of the flux can no longer occur using rectangular mirror oscillations, as was the case for 40 Hz. Instead, harmonic oscillations are required for which, again, part of the measurement time is lost for the motion process (see Section 5.1.2). Thus, the effectiveness, i.e., the ratio of the integration time per mirror oscillation to the duration of the mirror oscillation, is about 0.5 for rectangular oscillations (the reference measurement at the atmosphere is not included). For harmonic oscillations, this amounts to 0.3 in the most favorable case. Now for a measurement time of 100 msec per interferogram point, the useful time when using the 40 Hz detector is about 50 msec. If the effectiveness is set equal to 0.5, then 25 msec remains for pure integration time. For a modulation frequency of 100 Hz, 80 msec of useful time remains so that 24 msec of pure integration time remains for an effectiveness of 0.3.

By increasing the modulation frequency, it was possible to reduce the waiting time but the higher effectiveness of the rectangular oscillation of a rocking mirror with an oscillation frequency of 40 Hz equalizes this gain again. Only if the mirror could carry out 100 Hz rectangular oscillations could one bring about a better exploitation of the measurement time by increasing the modulation frequency.

4.3.3. The signals at the output of the preamplifier

The maximum sensitivity of a 0.7 mm detector is $4.3 \cdot 10^5$ V/W for f_0 = 40 Hz and $2.7 \cdot 10^5$ V/W for f_0 = 100 Hz. The amplification factor of the preamplifier is 10^3. For a typical flux per line of an interstellar source, the signal at the output of the preamplifier (for S = $4.3 \cdot 10^5$ V/W) amounts to:

$$s = 10^{-14}\,W \cdot 4{,}3 \cdot 10^{5}\,V/W \cdot 10^{3} = 4{,}3 \cdot 10^{-6}\ V\ .$$

Voltages of this order of magnitude must at least be detectable if the radiation of the interstellar sources is to be determined. /105 In contrast to this, the average flux of the background (atmosphere plus telescope optics) amounts to 10^{-7} W, which results in the following average signal if one uses a direct voltage amplifier

$$s = 10^{-7} \cdot 4{,}3 \cdot 10^{5} \cdot 10^{3}\ V = 4{,}3V$$

This means that the detector and the preamplifier must operate linearly in a range of at least ten powers of six, and the voltages must be measured to an accuracy of more than six decimals, if the signal of the source is to be separated from the background. Even the best digital voltmeters produce accuracies of a maximum of 100 ppm (for a 50 msec integration time). In addition, their dynamic range does not suffice by far. Therefore, an alternating voltage amplifier is used with which the constant background signal can be suppressed to a significant degree (for a fixed phase difference). Right after carrying out the grid step, voltages of the order of 0.1 V occur, at least in the vicinity of the central maximum of the interferogram. As long as the signals are present, it is not possible to make measurements.

In spite of the fact that an alternating voltage amplifier is used, the measurement cannot be directly carried out with a digital voltmeter, because the measurement frequency is too great for the required accuracy. Instead, a lock-in amplifier is used which, at the same time, forms the average value over several mirror oscillations. Its output signal can then be digitalized with sufficient accuracy.

4.3.4. The s/n ratio for dominating detector noise

For the case where the detector is the dominating noise source, we can give some information on the s/n ratio in the calculated spectrum.

According to 2.4.4, we have the following for a spectral element which has the flux $\mathcal{B}$:

$$s/n = \frac{\mathcal{B}}{NEP} \cdot \sqrt{\frac{\eta t}{1s \cdot \Delta f}} \; .$$

If we set $\mathcal{B} = 10^{-14}$ W, NEP = $3 \cdot 10^{-14}$ W/$\sqrt{\text{Hz}}$, and Δf = 10 Hz (the reciprocal of the measurement time of 100 msec per interferogram point), we find

$$s/n = \frac{1}{3}\sqrt{\eta t/10} \; .$$

The measurement time required to achieve a certain s/n ratio is

$$t = 1s \cdot \Delta f/\eta \cdot \left(\frac{s/n \cdot NEP}{\mathcal{B}}\right)^2 .$$

In order to obtain results which are statistically significant, s/n should be at least 3. For the detector with f_0 = 40 Hz and NEP = $3 \cdot 10^{-14}$ W/$\sqrt{\text{Hz}}$ and for the assumed source flux and maximum effectiveness of 0.5, a measurement time of 405 seconds is required. For the detector with f_0 = 100 Hz and NEP = $4.8 \cdot 10^{-14}$ W/$\sqrt{\text{Hz}}$, the requirement measurement time is about 10^3 seconds, in order to achieve s/n = 3. The flux for which the s/n ratio just reaches this value after a measurement time of 10^3 seconds and η = 0.5 is $1.27 \cdot 10^{-14}$W in the first case and $2 \cdot 10^{-14}$ W in the second case. Therefore, for a specified measurement time and effectiveness, a slower detector can detect lines which are weaker by about a factor of 2 than if the faster one is used.

If the very fast but insensitive detector with NEP = $1.4 \cdot 10^{-12}$ W/$\sqrt{\text{Hz}}$ is used, then for the same flux and maximum effectiveness, as well as for the amplification bandwidth of $\Delta f = 1$ Hz, the total measurement time would have to amount to $t = 24.5$ hours in order to achieve $s/n = 3$. This detector can, therefore, not be used for the balloon experiment.

5. Execution of the Experiments /107

The previous discussion was restricted to the dimensions of the individual components of the IR telescope and of the interferometer. Now we must determine the mode of operation and operational frequency of the rocking mirror and the lamella grid. The decisions to be made influence the processing of the measurement data and, therefore, it is important to consider the information flow of the experiment. In principle, it looks like the following (Figure 27).

The interstellar source and the atmosphere radiate into the telscope. Using a suitable method (see below), the source and background fluxes as well as the background flux alone are measured and compared with each other either simultaneously (two-beam system) or in sequence (rocking mirror) for a definite position of the grid. The difference between two such measured values or an average value from several of these differences produces a point in the interferogram of the source, and the second coordinate is determined by the phase difference of interfering rays and, therefore, by the grid shift. If necessary, the grid shift can be measured as well as the deviation from the nominal value, in order to perform regulation or for correcting the measurement values. The measured data must be digitalized and then communicated via telemetry. They are stored on the ground for later processing in a large computer. However, we wish to have the capability of transforming part of the interferogram points during the measurement in order to have an overview of the operation of the instrument.

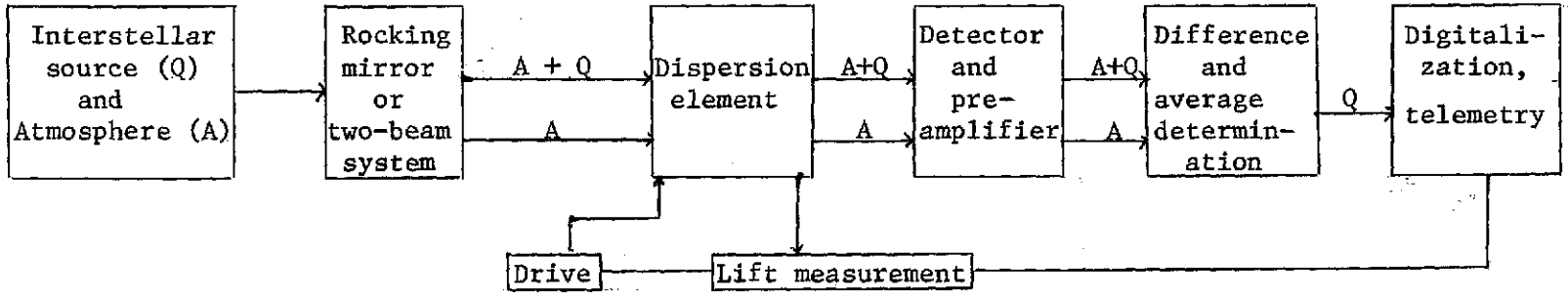
Interstellar source (Q) and Atmosphere (A)
Rocking mirror or two-beam system
A + Q
A
Dispersion element
A+Q
A
Detector and pre-amplifier
A+Q
A
Difference and average determin-ation
Q
Digitali-zation, telemetry
Drive
Lift measurement

Figure 27.

The time sequence for the experiment is given by the following time constants: /108

τ_1: time for recording an interferogram of one source

τ_2: effective measurement time (integration time) for an interferogram

τ_3: rocking mirror

τ_4: integration time for one measurement point

τ_5: optimum modulation period of detector = $1/f_0$

τ_6: time constant of detector ($\tau_6 = 0.15\ \tau_5$, empirical).

If η is the effectiveness of the total system, that is, the ratio of the integration time and measurement time per interferogram point, and if the interferogram consists of N points where each is defined as an average value over M differences of measured values, then we have the following relationships if M' oscillations of the rocking mirror are required per interferogram (M' > M, because a few oscillations are included in the transient time of the detector):

$$\tau_1 = NM' \cdot \tau_3; \quad \tau_2 = NM \cdot \tau_4; \quad \tau_2 = \eta \tau_1. \tag{5.1}$$

In order for the radiation to be modulated by the frequency f_0, we must also have:

$$\tau_3 = \tau_5 \tag{5.2}$$

τ_5 and τ_6 and therefore τ_3 are specified by the detector selection. N is therefore determined by the required resolution, as well as by the spectral range being investigated. M can be arbitrarily selected and should be large enough so that τ_1 does not exceed 0.5 hours considerably. In this case, about 10 spectra could be obtained per flight. Considerably longer measurement times would reduce the data yield per flight and, therefore, the ratio of gain to expense would be reduced.

The quantity η depends on the motion of the rocking mirror, as well as on the motion of the lamella grid and time constant of the detector. The exact relationship will be discussed in the following.

5.1. Difference Formation among Measured Fluxes /109

5.1.1. Possibilities for compensation for atmospheric radiation

The estimations in 4.3 have shown that the atmospheric radiation produces fluxes per line which are about four powers of ten higher than those of the interstellar sources. This means that a method must be found in order to suppress the atmospheric radiation with an accuracy of better than 10^{-4}. Two possibilities exist: the two-beam method and the directional modulation with a rocking mirror.

The two-beam method uses two separate optical channels which only have the main beam and a secondary beam in common. Therefore, two dispersion elements and two detectors are required. Since the same sky regions are always imaged onto the detectors, the effectiveness can be made greater than 0.5 if the modulation of the signal at the detector is produced by the motion of the interferometer (rapid scan) [1]. The two detectors can be installed in a bridge circuit, so that the measured signal is proportional to the flux difference and is, therefore, proportional to the flux of the interstellar source.

The disadvantage of the method is the fact that the two optical channels will not behave the same with respect to the incoming radiation with the required accuracy. The main difficulty is related to the detectors, and their properties probably will not remain the same over long time periods. In order to make the boundary conditions for their operation as identical as possible, they would both have to be arranged in a Dewar and, if possible, on the same substrate. If it is then possible to electronically balance the bridge between the recording of two interferograms (or at short intervals), then we should be able to bring about the same behavior with respect to radiation load and with sufficient accuracy. For the time being, such detectors are not available and, therefore, we must /110 use a rocking mirror in this experiment. It has the advantage that the same optical elements are used for all measurements and only one detector is needed. Since the time separation between two measured values used to form the difference is 50 msec at the most, we should not expect that the properties of the system would change in this time enough to influence the measurement result. The measurement of the source and the background is done in sequence so that the effectiveness of the entire measurement installation is smaller than 0.5, and at least half of the measurement time is lost.

In the following, we only discuss the rocking mirror system just as in the previous discussion, as long as we do not explicitly mention the two-beam system. However, we should always keep in mind the fact that the two-beam method is the better solution.

5.1.2. Rocking mirror

There are two possibilities for moving the rocking mirror: either it carries out rectangular tipping motions or harmonic oscillations. According to 4.2, the maximum deflection of the mirror is 25' or 0.36 mm at its edge. The oscillation frequency is between 10 and 100 Hz, depending on the modulation frequency of the detector.

The oscillation mode of the mirror has a decisive influence on the effectiveness of the system. If all other components of the instrument were to operate in an ideal fashion, it could be very close to the theoretical maximum value of 0.5 for the tipping motion because the motion phase can be made very small compared with the rest phase. This is also an advantage of this type of motion.* However, the mirror cannot be moved at an arbitrary rate, because otherwise, strong shaking will occur when it is braked, which would be transferred to the rigid frame of the telescope and then to the detector. The detector is very /111 sensitive to oscillations. In this case, the beginning of the measurement would have to be delayed long enough until these oscillations had decayed, which gives an upper limit for the frequency of the mirror oscillations. However, these effects should not be very noticeable at small amplitudes. Greater difficulties could occur if the mirror is induced to perform eigen oscillations because of the wide frequency spectrum of the rectangular oscillations. This would then deform its surface more than could be allowed. These problems must be investigated in experiments. Tipping oscillations with frequencies above 50 Hz are probably out of the question because of the problems mentioned.

*The oscillation problems discussed have been investigated by J. Stoecker.

In this range, the mirror must carry out harmonic oscillations. Since its velocity will then also be harmonic, no pulses occur when it reverses the direction of motion; instead the momentum is continuously transferred to the telescope frame. By installing a second mass oscillating the opposite way, the momentum transfer to the telescope frame can be significantly reduced [1], so that barely any oscillation will reach the detector. In addition, with this type of motion, there is only one single well-defined frequency, and the transmission of this frequency to the detector can be considerably reduced by suitably selecting its suspension. In addition, the excitation of the eigen oscillations of the rocking mirror is prevented as long as the oscillation frequency is not close to the eigen frequency. The motion can also be maintained with almost no energy supply, if its frequency is somewhat below the resonant frequency of the oscillating system, which is again an advantage, compared with the tipping oscillations.

When tipping oscillations are used, the measurements can begin when the mirror is at rest and, therefore, the field of view is uniquely defined. If the mirror carries out harmonic oscillations, we must consider the variation of the field of view during the measurement. It is advantageous for the mirror /112
to remain relatively long in the range of maximum deflection, so that we can bring about a usable effectiveness. Its value depends greatly on the relationship between the source diameter, field of view diameter, and deflection of the mirror. For point sources, it can even become 0.5 (for sufficiently small wavelengths). In Appendix C, we give the determination of η for various source diameters.

Since the rectangular tipping oscillations usually bring about a better exploitation of the measurement time than do the harmonic oscillations, they are to be preferred, as soon as the side effects which occur (mirror deformation and mechanical excitation of the detector) are controlled and this does not disturb the measurement sequence.

Independent of the oscillation mode, the amplitude of the mirror oscillation should be held as small as possible so that the optical path will pass through atmospheric regions close to each other and equal column depths. Then the radiation flux will change by more than 10^{-5} of its value based on the image rotation or spatial inhomogeneities of the atmosphere and this change has the same order of magnitude as the flux from an interstellar source. Since both changes occur at the same frequency (that of the rocking mirror), they cannot be separated and the measurement of the source without additional information is not possible. The strongest atmospheric radiator is hydrogen with a scale height between 7 and 10 km [19]. When the field of view is displaced by 10', the sideways deflection of the line of vision amounts to about 20 m, after a distance of 7 km. The atmosphere would have to be homogeneous with an accuracy of better than 10^{-5} if it is not to have any detrimental effects on the measurement. Since successful measurements have already been carried out with the rocking mirror,* we can assume that the atmosphere is sufficiently homogeneous.

Now when the direction of the optical path is changed, the /113
length of the atmospheric layer traversed also changes, as well as its emission. We have the following relationship for the intensity of those lines for which the medium is optically thick:

*Fourier spectroscopy of astronomical bodies has been performed by Witteborn [28], Aumann (NASA Flugzeug C141) and Jennings [31] using rocking mirrors and by P. Connes [3], Bussoletti [23], Smyth [32], and Kneubuehl (with lamella grids) without rocking mirrors.

$$i = \frac{2hc^2}{\lambda^3} \cdot \frac{1}{e^{hc/kT\lambda} - 1} \cdot \Delta\sigma_{1/2} \left[\frac{W}{cm^2 sr}\right]$$

where $\Delta\sigma_{1/2}$ is the half-width of these lines. It is proportional to the square root of the layer thickness traversed* and for the flat atmosphere model (which is sufficiently accurate here), it is proportional to $1/\sqrt{\sin\tilde{\varepsilon}}$. The quantity $\tilde{\varepsilon}$ is the elevation (Figure 28a) of the observed object in the sky. If we now vary the elevation by $d\tilde{\varepsilon}$, then the corresponding change in the half-width of the line is given by

$$\frac{d\Delta\sigma_{1/2}}{\Delta\sigma_{1/2}} = -\frac{1}{2} \cdot \cot\tilde{\varepsilon} \cdot d\tilde{\varepsilon}$$

From this, we find the following for the intensity change:

$$|\Delta i| = \frac{1}{2} i \cdot \cot\tilde{\varepsilon} \cdot \Delta\tilde{\varepsilon}$$

Since the intensity is proportional to the detector flux, we have the same relationship for this flux.

The quantity ε will be greater than 30° for the measurements, because otherwise, the atmospheric radiation is too strong and the transmission is too low. For $d\tilde{\varepsilon}$, we find

$$d\tilde{\varepsilon} \leq \delta \leq 9' \triangleq 2{,}5 \cdot 10^{-3}\,\text{rad}$$

where δ is the direction change of the optical path based on the motion of the rocking mirror. For the worst case, i.e., 30° elevation and mirror motion in the elevation direction, we have the following for the flux change at the detector:

$$\Delta\Phi = 0{,}5 \cdot \Phi \cdot 1{,}7 \cdot 2{,}5 \cdot 10^{-3} \approx 2 \cdot 10^{-3}\Phi$$

*See Appendix E.

On the other hand, we have

$$B_Q \approx 10^{-6} B_{AL},$$

and the atmosphere produces greater flux changes than the source and the measurement cannot be performed. Therefore, the motion of the rocking mirror has to be perpendicular to the elevation direction. Then we have $d\varepsilon = 0$ and the atmosphere produces no flux fluctuations at the detector.

We intend to have the telescope track the source so that it sees fixed points on the sky for the two positions of the rocking mirror (Figure 28). This means that the elevation for these two positions will change in time. For circumpolar sources, we have, for example (if we observe from the Equator), and for mirror motions which are started with constant elevation: /114

$$\Delta\tilde{\varepsilon} = \vartheta \cdot \sin\frac{\pi}{12}(t - t_0); \quad t[h].$$

If $t - t_0 = 0.5$ hours, then we find

$$\Delta\tilde{\varepsilon} = \vartheta \cdot \sin\frac{\pi}{24} \approx 2\vartheta \cdot 0{,}13.$$

$\Delta\vartheta$ is about $2 \cdot 10^{-3}$ rad and so we have, for $\tilde{\varepsilon} = 30°$:

$$\Delta\tilde{\varepsilon} = 2{,}6 \cdot 10^{-4}, \quad \Delta B = 2{,}2 \cdot 10^{-4} B.$$

This effect is big enough to have to be corrected (or the telescope is tracked so that the image field rotation at the detector is not compensated for). For sources near the sky Equator, $\tilde{\varepsilon}$ will practically not change at all during the measurement time and no correction is necessary.

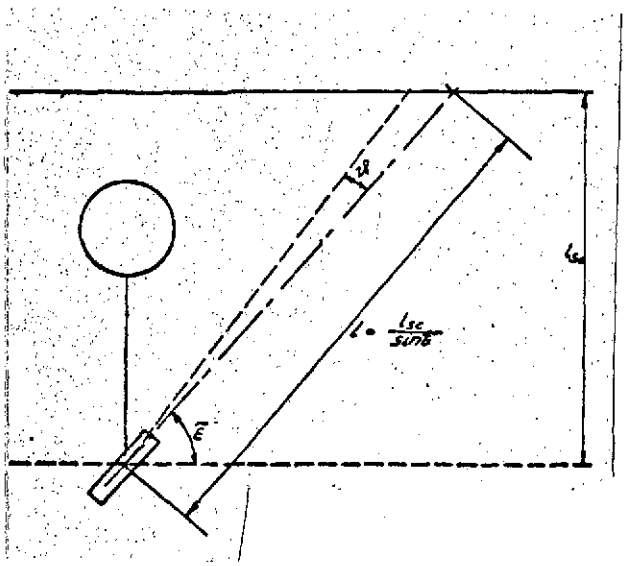

Figure 28a. Path of the ray of vision within one scale unit as a function of elevation.

L_{sc}- scale height; $\tilde{\varepsilon}$- elevation; $|\vec{s}|$ - change in elevation by motion of the rocking mirror.

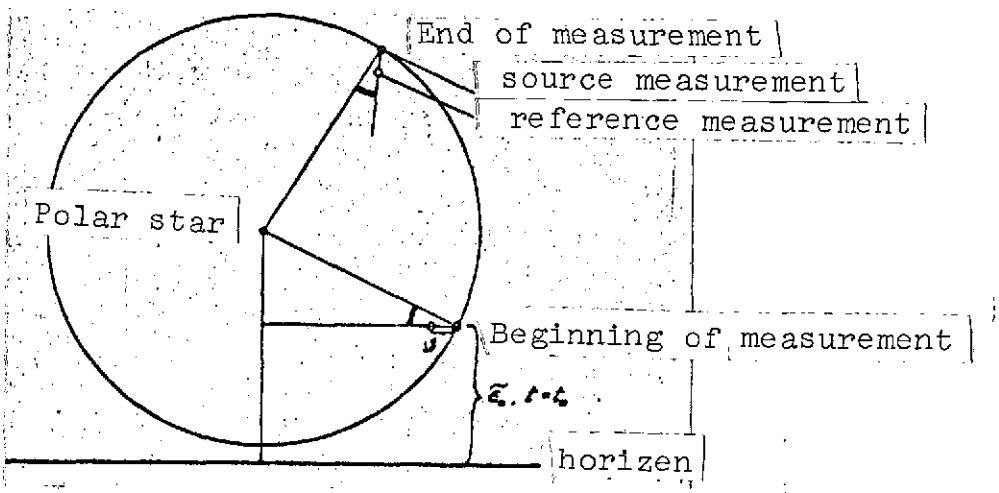

Figure 28b. Change in elevation of the ray of vision between the source and the reference measurements during the measurement period.

5.2. Continuous Operation of the Lamella Grid /115

We will now investigate the optimum type of motion for the grid as far as the experiment is concerned. First, we must consider the fact that we must have a good compensation for the atmospheric radiation and that the synchronization for the grid motion, motion of the rocking mirror, and beginning of the measurement processes must exist (it must be measured for a specified mirror position and grid position). In addition, the advance rate of the grid must be variable so that it can be adapted to various measurement durations. The mechanics must satisfy the tolerances given in 3.5 and the least possible amount of shaking must occur during the motion. The last requirement seems to indicate that a continuous advance of the grid would be the best type of drive. In this method, we must discuss whether the compensation for the atmosphere can be done with sufficient accuracy.

5.2.1. Measurement method

The processes involved in the determination of the source interferogram using a continuously moving grid can be summarized with the following example:

The atmospheric spectrum is assumed to consist of a line in the form of a delta function at the wave number δ_0, which produces the maximum flux $\mathcal{B}_A$ at the detector. For the source spectrum, we assume the same function with an amplitude which is smaller by a factor of 10^3. The flux from this source is therefore 10^{-3} times that from the atmosphere (which approximately corresponds to the situation for the fluxes per line). For the two interferograms, we then have:

$$F_A(x) \sim \mathcal{B}_A \cos(2\pi\sigma_0 x)$$
$$F_Q(x) \sim \mathcal{B}_Q \cos(2\pi\sigma_0 x) .$$

If the grid is moved continuously at a velocity v, then we have $x = 2vt$ and, therefore:

$$F_A(t) \sim \mathcal{B}_A \cos(2\pi\sigma_0 2vt); \quad F_Q(t) \sim \mathcal{B}_Q \cos(2\pi\sigma_0 2vt) .$$ /116

However, we did not measure these values but $F_A(t)$ and $F_{A+Q}(t + \Delta t)$ where $F_{A+Q} = F_A + F_Q$. The measurements were carried out separated by one-half of an oscillation period of the rocking mirror. This means that, in the meantime, the phase difference has changed by the amount $\Delta x = 2v \cdot \Delta t = v\tau_3$. The measured values are, therefore, given by:

$$F_A(t) \sim \mathcal{B}_A \cos(2\pi\sigma_0 2vt) \text{ and } F_{A+Q}(t+\Delta t) \sim (\mathcal{B}_A + \mathcal{B}_Q)\cos(2\pi\sigma_0 2v(t+\Delta t)).$$

Here we are looking for the interferogram of the interstellar source, that is, F_Q. The direct difference between these measured values would produce a result which would deviate considerably from F_Q, because the measured values change more because of the change in the phase difference between measurements than because of the modulation of the flux by the mirror motion. In the following, we will discuss how an interferogram of the source can be determined from these measured values.

5.2.2. The influence of the grid motion on the measured value during integration time

First, we will investigate the influence of the change in the flux on the measured value during the integration time. For this, we will again consider the interferogram of a single and

very narrow line. It is given by:

$$F(x) \sim \cos(2\pi\sigma 2vt) .$$

For an integration time of τ_4 seconds, the measured value is given by:

$$s(x,\Delta x) \sim \frac{1}{\tau_4} \int_{t_0-\tau_4/2}^{t_0+\tau_4/2} dt \cdot \cos(2\pi\sigma 2vt)$$

or

$$s(x,\Delta x) \sim \cos(2\pi\sigma x_0) \operatorname{sinc}[\sigma\Delta x],$$

where $\Delta x = 2v\tau_4$ and $x_0 = 2vt_0$. By changing the phase difference during the integration time by Δx, the measured value is reduced by a factor of $\operatorname{sinc}[\sigma\cdot\Delta x]$, compared to what would be obtained for a constant phase difference. For $\sigma = 500\ cm^{-1}$ and $v = 5 \cdot 10^{-3}$ cm/sec, as well as $\tau_4 = 12.5$ msec (half modulation period of the 0.7 mm detector), we find /117

$$[\sigma\cdot\Delta x] = 0{,}9935\ldots$$

This reduction in the signal by less than 1% does not represent a restriction, even for the maximum wave number. As long as the velocity of the grid advance and the period τ_4 do not change noticeably, the effect has this order of magnitude and can, therefore, be ignored.

5.2.3. Determination of the interferogram of the interstellar source

Now we will investigate how we can determine the interferogram of an interstellar source from measurement data taken with a continuously moving interferometer.

For this purpose, we will consider an idealized measurement for which the following applies:

i) During the measurement time for one point of the interferogram, we assume that the flux in front of the dispersion element is constant. Therefore, no orientation fluctuations or other disturbances occur which would produce signal fluctuation. The rocking mirror is at rest during the measurement.

ii) The atmospheric radiation is represented by a single monochromatic line with wave number σ_A, which produces the flux B_A in front of the interferometer.

iii) The source is also assumed to only radiate at a monochromatic line with the wave number σ_a and its flux is assumed to be B_a.

iv) The degree of modulation is assumed to be constant and equal to its maximum value, and can be set equal to 1 for the following discussion. The transmission of the dispersion element is also assumed to be 1.

Then the two interferograms are given by:

$$F_A(t) \sim B_A \cos(2\pi\sigma_A \cdot 2vt); \quad F_{A+Q}(t) \sim B_A \cos(2\pi\sigma_A \cdot 2vt) + B_Q \cos(2\pi\sigma_Q \cdot 2vt).$$

The measured values are determined as the integrals of these/118 functions over the measurement time and, according to 5.2.2, they can be described as the value of the interferogram at the center of the measurement interval:

$$F_A(t_1) \sim B_A \cos(2\pi\sigma_A 2vt_1);$$

$$F_{A+Q}(t_2) \sim B_A \cos(2\pi\sigma_A 2vt_2) + B_Q \cos(2\pi\sigma_Q 2vt_2), \quad t_2 = t_1 + \tau_s/2.$$

As already mentioned, the recording of an interferogram should not take much more than 30 minutes for reasons of economy. If the total measurement time is set equal to 10^3, then for 10^4 interferogram points, it is possible to carry out ten measurements per second. According to 3.5, the change in the grid shift between measurement points equals 5 μ. Therefore, we find an advance velocity of:

$$v_M = 5\ 10^{-3}\,\mathrm{cm/s} = \frac{\lambda_m}{4M'\tau_3}.$$

Here m' is the number of mirror oscillations per interferogram point and $\lambda_m/4 = 5$ μ is the step of the grid.

In order to see how the compensation of the atmospheric radiation depends on the wave number in the spectrum and on the advance velocity of the grid, we will now vary these quantities, and we will assume:

$$v = \chi v_M = \frac{1}{4\sigma_M M'\tau_3} = \frac{\chi}{4\sigma_M M'\tau_3}$$

where $0 < \chi \leq 1$. The time constants are fixed but the number of mirror oscillations per interferogram point is changed, which leads to an extension of the total measurement time by a factor of $1/\chi$ compared with the 10^3 seconds assumed above. In addition, we set

$$\sigma_A/\sigma_M = a, \quad \sigma_a/\sigma_M = q,$$

where σ_M is the maximum wave number (= 500 cm^{-1}) and $0 \leq a,q \leq 1$. In this way, the expression for the measured interferograms is given by:

$$F_A(t) \sim B_A \cdot \cos\left(\pi \frac{a\chi}{M_0} \cdot \frac{t_1}{\tau_3}\right),$$

$$F_{A+a}(t_1 + \tau_3/2) \sim B_A \cos\left(\pi \frac{a\chi}{M_0}\left(\frac{t_1}{\tau_3} + 0{,}5\right)\right) + B_a \cdot \cos\left(\pi \frac{q\chi}{M_0}\left(\frac{t_1}{\tau_3} + 0{,}5\right)\right).$$

/119

Now there are various possibilities of determining the points of the spectrum of the source from these measured values.

i) Both values are stored and we obtain two interferograms. Using an interpolation formula, the functional values at the support points of one functional value are calculated for the other one. Then both curves are subtracted from each other and the difference is transformed.

ii) The spectra are calculated from the stored interferograms and, after this, they are subtracted from each other, and one of them has to be interpolated.

If we consider the accuracy required in order to resolve the source spectrum, which has an amplitude which is at least 10^5 times smaller, from the background spectrum, then it seems very doubtful that this can be done with any kind of interpolation method. In addition, absolute flux measurements are required for these methods. Therefore, a direct voltage amplifier would have to be connected behind the bolometer which would lead to dynamic problems. The method of direct differencing remains, which first appears rather advantageous.

iii) Both measured values are subtracted from each other and the resulting function is transformed. This only makes sense when the non-compensated part of the atmospheric radiation is smaller than the flux from the interstellar source. We obtain the following values for the interferogram points:

$$F_{A+Q}(t_4 + \tau_3/2) - F_A(t_4) \sim$$

$$B_Q \cdot \cos\left\{\pi \frac{a\chi}{M_0}(t_4/\tau_3 + 0{,}5)\right\} - 2B_A \cdot \sin\left\{\pi \frac{a\chi}{M_0}(t_4/\tau_3 + 0{,}25)\right\} \cdot \sin\left(\pi \frac{a\chi}{4M_0}\right)$$

The first term is the signal to be measured and the second /120
is the flux of the atmospheric radiation based on the grid motion which is noncompensated. In order for the measurement to make sense, the latter must be greater than the former. If we set $t_1 = 0$, then we find the following from this condition:

$$\frac{B_a}{B_A} \cdot \left| \cos \frac{\pi q \chi}{2M_0} \right| \geq 2 \cdot \sin^2\left(\frac{\pi a \chi}{4M'}\right)$$

If we set the cosine on the left side of this inequality equal to 1, and $B_a = \varepsilon B_A$, we find:

$$\varepsilon \geq 2 \cdot \sin^2\left(\frac{\pi a \chi}{4M}\right)$$

Since $\varepsilon \ll 1$, we find from this:

$$\varepsilon \geq 2 \cdot \left(\frac{\pi a \chi}{4M'}\right)^2 \Longrightarrow a\chi \leq \frac{4M'}{\pi}\sqrt{\frac{\varepsilon}{2}}$$

If the definitions of a and χ are substituted, we find:

$$\sigma_A^2 V \leq \sigma_M V_M \cdot \frac{4M'}{\pi}\sqrt{\frac{\varepsilon}{2}} \approx 0{,}9\, M' \cdot \sqrt{\varepsilon}$$

Since the atmospheric radiation radiates down to the smallest wavelengths of the spectral range, the inequality also has to be satisfied for $\sigma_A^2 = \sigma_M^2$:

$$V \leq V_M \cdot 0{,}9 M' \cdot \sqrt{\varepsilon}$$

The flux from an interstellar source is smaller than that of the perturbing radiation by about 5 powers of 10; therefore, we have $\varepsilon \approx 10^{-5}$ and finally we find:

$$v \approx 0{,}03 \cdot v_M = 1{,}5 \cdot 10^{-4}\,\text{cm/s} = 1{,}5\,\mu/\text{s}$$

The grid could, at most, be moved at this velocity if, for a 100 Hz modulation frequency and a maximum wavelength of 500 cm^{-1}, the non-compensated part of the atmospheric radiation is not to exceed the flux from the source being investigated. In addition to the fact that such small velocities cannot be realized in practice, this would result in a total measurement time of 10^3 sec/0.03 = $3.3 \cdot 10^4$ sec, which amounts to more than nine hours. This time is much too long for the balloon measurements.

Continuous operation of the lamella grid is not possible in conjunction with a rocking mirror. However, we must consider /121 the fact that this type of grid motion might be advantageous if we use a two-beam system, because the advance velocity and, therefore, the grid shift can be well controlled and because no shaking will occur, which would be the case during stepped operation. Since the reference measurement of the atmosphere occurs simultaneously with the measurement of the source for the two-beam method, the problem just discussed is eliminated.

5.3. Stepped Operation of the Grid

5.3.1. The measurement method

As shown above, it is only possible to use a rocking mirror in conjunction with stepped operation of a grid. The measurement is performed by having the grid carry out a defined step, so that the phase difference of interfering ray bundles is changed by the specified amount. Then one must wait until the mechanical oscillations of the system have decayed. During this time, the detector and the preamplifier can adjust to the new flux at the detector crystal. As soon as the signal change at the output of the preamplifier caused by the transient process becomes smaller than the signal produced by the motion

of the rocking mirror, the measurement of the signal can be performed. Since the phase difference does not change during the measurement, the measured values for the case analogous to 5.2.3 are given by:

$$F_A(t_1) \approx \mathcal{B}_A \cos(2\pi\sigma_A x(t_1)) \cdot$$
$$F_{A+Q}(t_2) \sim \mathcal{B}_A \cos(2\pi\sigma_A x(t_1)) + \mathcal{B}_Q \cos(2\pi\sigma_Q x(t_1)) \cdot$$

Therefore, the difference of these measured values, taken at different times, directly produces (in the ideal case) one point of the interferogram of the interstellar source. In general, an interferogram point will be determined as an average over several measured values.

5.3.2. The time variation of the motions /122

In stepped operation, the difficulty is not in obtaining reliable data, but in the mechanics of the grid motion. In the ideal case, the rest phase would be considerably longer than the motion phase of the grid and then the motion, as a function of time, could be represented as a step function. Unfortunately, the stepping motor does not carry out such motions. Instead, in the unloaded state, it reaches its final position very fast but exceeds it and then gradually comes to rest. In the loaded state, the motion is slower and the overshoot is smaller. If the time available is too short or if the inertia or friction of the moving mass is too large, then it becomes possible that the required displacement is not reached, but this can be avoided by appropriate dimensioning of the motor if the distance between steps is not too small. Since the mass of the moving lamella unit is about 1.5 kg and must be compensated by a counterweight of the same size so that the motor has equal loading independent of the position of the grid in space, it

seems that the stepping frequency which can be obtained with a reasonable amount of effort amounts to 10 Hz. However, even for optimum motion, i.e., small overshoot and aperiodic approximation to the nominal value, it seems that between 20 and 30 msec will be lost for the transient process.

This is quite compatible with the data of the 0.7 mm detector (4 msec time constant and 40 Hz optimum modulation frequency). In order to reach the new value with sufficient accuracy and for a small grid shift, it requires about 55 msec. If the grid shift is large, it requires 45 msec after each grid step (see 5.3.2). The waiting time is then no longer determined by the mechanics of the grid but by the time variation of the detector. The times indicated mean that it is not possible to carry out measurements for two mirror oscillations, and for an advance frequency of 10 Hz, at least one-half of the measurement /123 time is lost. However, it is possible that in the wings of the interferogram, a transient time of 25 msec will be sufficient (this applies for the selected detector, if the signal per grid step changes by less than $2.5 \cdot 10^{-3}$ of its average). In this case, the measurement would have to be interrupted for only one mirror oscillation. In order to hold the waiting time as small as possible, an electronic device should be provided which determines the signal change just after the grid step is executed and then calculates the required transient time.

If the number of mirror oscillations per grid step equals M' and if measurements are carried out during M of these oscillations, and if ε is the ratio of the rest phase of the rocking mirror and one-half of the oscillation period, then we have the following relationship for the effectiveness of the system:

$$\eta = \frac{1}{2} \cdot \frac{M}{M'} \cdot \varepsilon \qquad (5.10)$$

Depending on the intensity of the signal change per grid step, we will have M = M' - 1 or M = M' - 2. One should expect that, for almost all interferogram points, the following will hold: M = M' - 1, so that the following applies for the effectiveness:

$$\varrho = \frac{1}{2}\left(1 - \frac{1}{M'}\right) \cdot \varepsilon \qquad (5.11)$$

In order to make 1/M' small, M' should be as large as possible. Because of the limited measuring time per interferogram, at the present time M' cannot be made substantially greater than 4. Smaller values can also not be used because, otherwise, the ratio of measurement time and waiting time becomes too unfavorable. With M' = 4 and ε = 0.9, which should be achievable with rectangular oscillations, we find the following effectiveness:

$$\varrho = 0{,}34$$

A similar development can be made for a rocking mirror which carries out harmonic oscillations. In this case, $\varepsilon/2$ is to be replaced by the effectivenesses η determined in Appendix D.

6. The Present State of the IR Experiment /124

6.1. The Optical Configuration

The telescope has a Cassegrain system, as discussed in Section 4.2.2 and as shown in Figure 25. We decided to use this because of the favorable moment of inertia and the possibility of being able to adjust the ray path to the other dispersion elements without a great deal of complexity (change in the ray diameter by displacing the collimator mirror 3 in Figure 25). In addition, the position and size of the intermediate image means that it is relatively simple to operate the diaphragm, which would have to be made very small for the Gregory system and which is difficult to adjust because of the small image diameter of about 0.5 mm. If it is made of glass, which is non-transparent for the IR radiation in the wavelength range of interest, then the field of view of the main mirror in the visible range can be imaged onto a star sensor rigidly attached to the bolometer (see below). The sensor consists of a field of 100 x 100 detectors, which react to visible radiation. The field of one of these detectors corresponds to the field of view of the bolometer which makes it possible to check the adjustment with visible light. In addition, a luminous diode can be installed in the glass diaphragm, the image of which is also assigned to a group of detectors when the instrument is exactly adjusted, so that the adjustment of the optical components behind the diaphragm is simplified and can be tested during the flight.

The main telescope mirror will be a f/2 light weight mirror with a diameter of 1 m made of glass ceramic material with a small expansion coefficient (CER - Vit C101). The blank is supplied by the firm Owens Illinois and the weight is reduced

to 95 kg by hollowing out the mirror. The central hole has a diameter of 15 cm (2.2% of the total surface area), so that the subsequent conversion to a tubing system is possible. The field /125 of view of the main mirror is corrected to within 10'.

The effective focal length of the telescope is 16 m, which results in an image size of 4.65 mm for a 1' source diameter. The image is 20 cm ahead of the surface of the main mirror. The adaptation to the lamella grid or to the detector is done as shown in Figure 25, using a 10 cm f/16 or a 12 cm f/10 off-axis mirror. The dimensions of the lamella grid were given in 3.5.

A Low bolometer with a 0.7 mm edge length of the sensitive surface is used as a detector, with a NEP of $3 \cdot 10^{-14}$ W/$\sqrt{\text{Hz}}$ and an optimum modulation frequency of 40 Hz. A spherical mirror is installed in the Dewar which focuses the IR radiation onto the detector. The data for it are given in 4.2.4. The field of view diameter amounts to one minute of arc for the optics discussed and the detector size. As Figure 29 shows, the Dewar has a dichroitic plane mirror which lets the visible light pass through to the detector field installed on the vessel, whereas the IR radiation is deflected towards the bolometer. The filter wheel installed between the plane mirror and the circle mirror at the present time contains three filters, which contain diamond dust for scattering the visible light. The filters will let radiation with wavelengths greater than 5 μ, 27 μ, and 50 μ pass through to the bolometer.

At the present time, we have not yet decided where we will install the pupils* of the system. One of them can be defined by the main mirror, the secondary mirror, or by a diaphragm in

*Pupils are the cross sections common to all ray bundles.

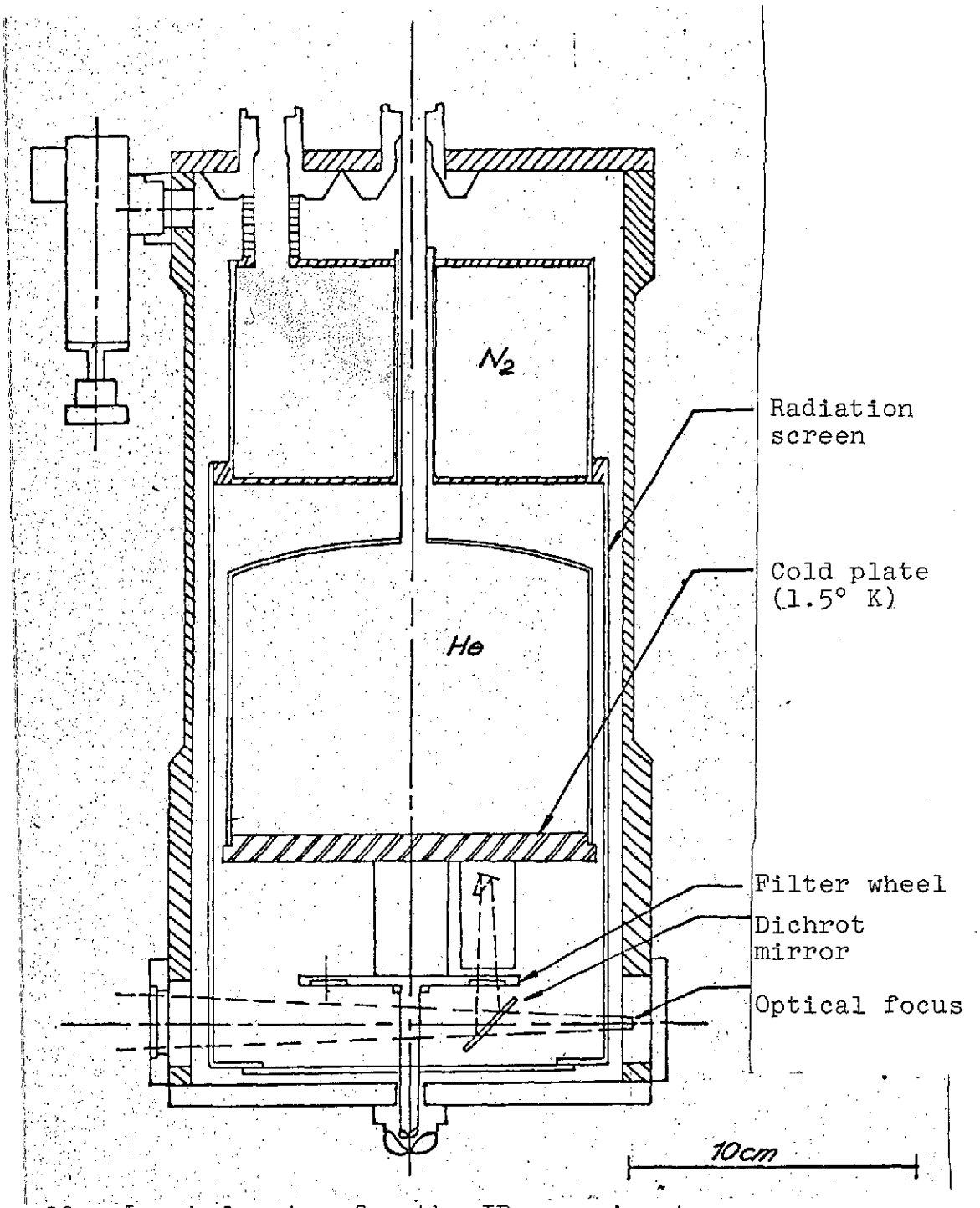

Figure 29. Low bolometer for the IR experiment.

the immediate vicinity of the detector, or by the detector itself [20]. The selection of the positions of the pupils is important because, among other things, they determine how much perturbation radiation from the telescope reaches the detector.

6.2. The Time Constants and the Data Flow /126

By selecting the detector, we have specified its time constant, the optimum modulation frequency, and, therefore, also the rocking mirror frequency.

We will select rectangular oscillations at 40 Hz as the form of motion for the rocking mirror. The effectiveness of the mirror motions should be about 0.9, i.e., the motion requires about 1/10 of the oscillation period [25].

The motion of the lamella grid is controlled by a stepping motor, which provides a rotation of 1.8° per control pulse with an accuracy of 3%. It is connected with the grid through a micrometer spindle with a step of 1 mm, so that per step, there is a lamella displacement of 5 μ + 0.15 μ.

If a total measurement time of 10^3 sec = 16.7 min = τ_1 is specified, then the grid must be moved at about 8 Hz, if 2^{13} = 8,192 interferogram points are to be recorded. This results in a measurement time of 125 msec per interferogram point. For small phase differences, the detector requires about 58 msec of transient time and 25 msec will suffice for larger phase differences. Therefore, it makes sense to use four mirror oscillations for the measurement and to move the grid slower for small phase differences (at 6.7 Hz). The number of mirror oscillations per grid step is, therefore, M' = 6 for a small grid shift and M' = 5 for a large grid shift. The number of

measured values per interferogram point is always equal to 4. The effectiveness of the system is, therefore, the following for almost all interferogram points:

$$Q = 0{,}5 \cdot (1 - 1/5) \cdot 0{,}9 = 0{,}36. \; *$$

The difference and the average are formed using a lock-in amplifier which produces points of the source interferogram at a rate of 8 sec^{-1} or 6.7 sec^{-1}, respectively (for small phase differences). If possible, a direct voltage amplifier should /127 be connected with the bolometer having a low sensitivity, which will measure the perturbation signal once per grid step. The data for it also arrives at 8 or 6.7 Hz. In addition, the grid step should be measured and should be relayed via telemetry together with the interferogram, so that we have the following data flux (Figure 30).

The time constants of the experiment are the following for the measurement discussed:

Time contant of the detector:	τ_6 = 4 msec
Optimum modulation period:	τ_5 = 25 msec
Oscillation period of rocking mirror:	τ_3 = 25 msec
Fraction of time per oscillation which cannot be used:	2.5 msec
Separation between two grid steps:	125 msec or 150 msec for small phase difference
Non-usable part:	20 to 50 msec (depending on signal change)

*This should be compared with the effectiveness of 0.025 which is achieved in an aircraft experiment with a Michelson interferometer [29].

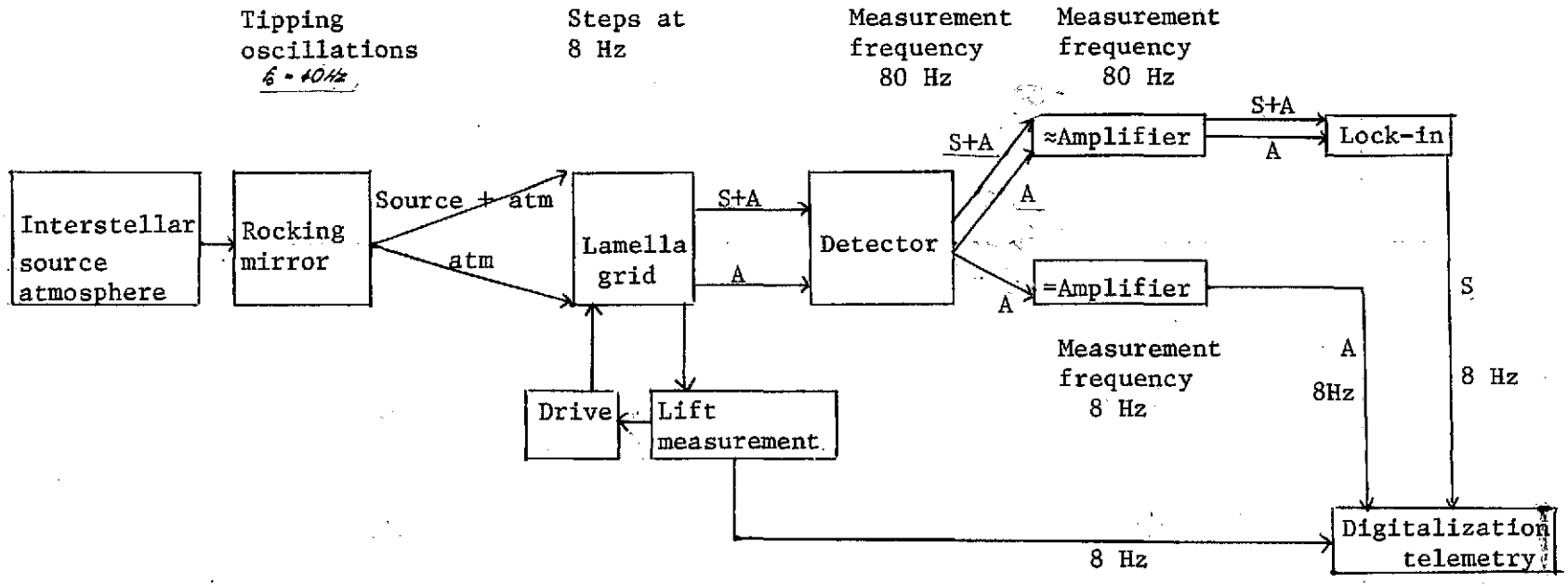
Tipping oscillations
6 - 10Hz
Steps at 8 Hz
Measurement frequency 80 Hz
Measurement frequency 80 Hz
Interstellar source atmosphere
Rocking mirror
Source + atm
atm
Lamella grid
S+A
A
Detector
S+A
A
≈Amplifier
S+A
A
Lock-in
=Amplifier
A
Measurement frequency 8 Hz
A
8Hz
S
8 Hz
Drive
Lift measurement
8 Hz
Digitalization telemetry

Figure 30.

Integration time per interferogram point:	45 msec
Total measurement time:	$\tau_1 = 10^3$ sec
Total integration time per interferogram:	$\tau_2 = 368.6$ sec = 6.14 min.

6.3. Typical Measurement Sequence

According to the present state of our knowledge, the production of a spectrum calculated from an interferogram from a typical interstellar source will be done approximately as follows:

About 1 sec after beginning of the measurement, the grid has/128 carried out 7 steps and produced a phase difference of 0.007 cm, which results in a resolution of 100 cm^{-1} for the calculated spectrum. With this resolution, it is possible to already demonstrate the continuum radiation of the dust which surrounds the source. According to 2.4, the s/n ratio for the resolved spectral elements is best at this time. Therefore, one can decide whether the telescope is indeed aligned with the source and whether it is advantageous to continue to observe the source. For execution of the experiment, it is important that this decision is reached after the measurement has begun with practically no time delay.

After a measurement time of about 10 sec, the grid has carried out 70 steps and has produced a phase difference of 0.07 cm, and therefore, a resolution of 10 cm^{-1}. In this way, it is possible to observe the structures in the dust continuum (absorption bands).

As the measurement continues, the resolved spectral elements become narrower and, finally, the lines of the gas from the continuous background appear. After a measurement time of 1000 sec, the phase difference is 8 cm, 8000 interferogram points have been recorded, and the spectral resolution is 0.085 cm^{-1}. For sufficient compensation of the atmosphere, it should be possible to determine the source spectrum from the transformed interferogram if the intensities are not too small. (Figure 31).

6.4. Outlook /129

One would expect that astronomical IR experiments with Fourier spectrometers will be flown on satellites or on a space shuttle in the foreseeable future.

The perturbation radiation of the Earth atmosphere is so small at satellite altitudes that the rocking mirror is not needed for cooled telescope optics. If the interferometer is operated so fast that no additional intensity modulation is required (rapid scan), then the effectiveness of the measurement can be increased substantially, compared to a balloon telescope with a rocking mirror (with a rocking mirror, we can achieve $\eta = 0.35$, without a rocking mirror we could achieve $\eta > 0.5$, and we could achieve almost 1 using a suitable measurement technique).

One stipulation for this is that the perturbation radiation of the telescope be so small that it does not have to be compensated for. For an emissivity of $\varepsilon = 0.01$ and 5 mirror surfaces, one obtains a radiation density of $i = 2 \cdot 10^{-6}$ W/cm^2sr for a telescope temperature of 70° K. On the other hand, the dust coupled to an interstellar cloud produces a radiation density of $i = 4.3 \cdot 10^{-6}$ W/cm^2sr at the same temperature of 70° K and the emissivity of 1. This perturbation radiation can

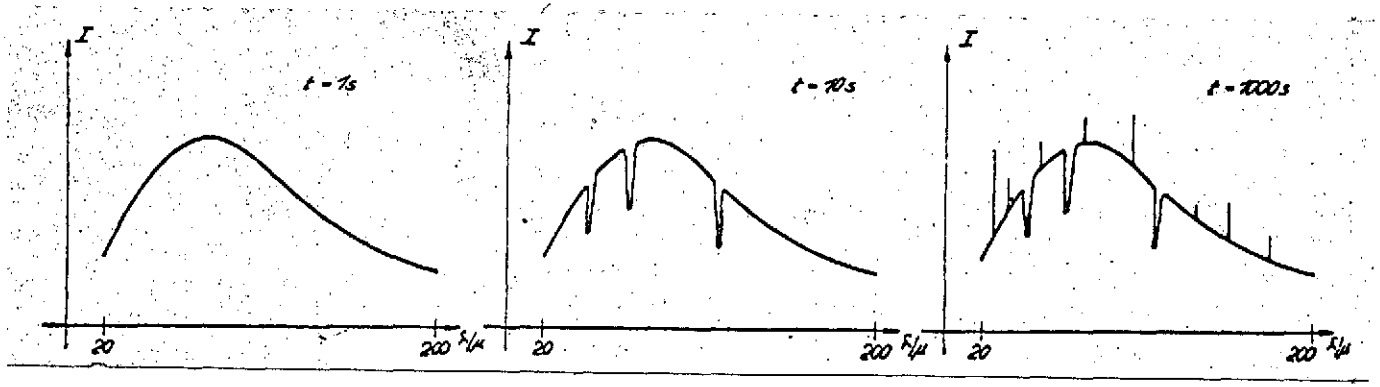

Figure 31. Time variation of a spectrum calculated from the interferogram points at a measurement frequency of 10 interferogram points per second.

not be eliminated in principle. Therefore, it is also not necessary to compensate for the mirror radiation which is one order of magnitude smaller, and therefore, no intensity modulation is required. Up to the present, there are no indications about the nature of interstellar dust at temperatures far below 70° K, because low thermal emission cannot yet be measured. If it is found that the dust temperatures never become smaller than 70° K, then this will have far-reaching consequences for Fourier spectroscopy of interstellar objects. In this case, the dust /130
will produce a radiation density which is similar to that of the Earth atmosphere at an altitude of 35 km. At T = 230° K and $\varepsilon \approx 0.01$, we have $i_{At}(35\ km) \approx 5.0 \cdot 10^{-5}$ W/cm^{2}sr. At an altitude of 45 km (at T = 250° K and $\varepsilon \approx 0.002$), we have $i_{At}(45$ $i_{At}(45\ km) \approx 1.4 \cdot 10^{-5}$ W/cm^{2}sr.

This means that no rocking mirror will be required for a balloon telescope operating at 45 km, if its optics are cooled to 70° K, because the perturbation radiation, which could be compensated for, amounts to only 30% of the non-compensatable dust radiation (in the case of the satellite, about 10% of the perturbation radition can be compensated for).

In order to not overtax the dynamics of the detector and the preamplifier, one should avoid the ray direction modulation using a rocking mirror in high altitude balloons (of course, in satellites as well), because only 1 to 10 ppm of the signal change produced by the mirror motion can be attributed to one line of the interstellar cloud. Most of it is produced by the dust (if its temperature is not substantially below 70° K). Of course, this makes it more difficult to determine the line spectrum of the gas cloud. In this case, the intensity modulation using the rapid scan method is more favorable because the modulation of the interferogram caused by a black body spectrum

decreases approximately with $1/x^2$ (x is the phase difference). The modulation caused by narrow lines is almost not attenuated at all. The dust radiation therefore produces only an approximately constant contribution to the interferogram, at least for a large phase difference (approximately for $x \gtrsim 0.1$ cm). Dynamic problems occur for very small phase differences.

An interferometer which operates outside of the Earth atmosphere will observe only continuum radiation (dust, telescope optics) in addition to the line radiation of a gas cloud. A balloon instrument will also see the lines of the atmospheric radiation. These lines must be discriminated from those of the interstellar source. This is possible if the atmospheric /131
spectrum is measured at the flight altitude of the balloon, which will lead to a decrease in the effectiveness. (The same effectiveness as obtained with an instrument outside of the Earth atmosphere could be brought about using the two-beam method.)

If we assume that the dust temperature is not substantially below 70° K, then the dust radiation will determine the perturbation radiation and, therefore, the achievable signal-noise ratio for high altitude balloons and satellites. This means that both instruments will reach the same s/n ratio for the same measurement time.

A balloon telescope which operates at an altitude of 45 km and has cooled mirrors (70° K) will, therefore, provide the same data as a telescope of equal size which is installed on a satellite or a space shuttle.

SUMMARY

/132

It was the purpose of this paper to discuss the experimental project "high resolution IR spectrophotometry with a balloon telescope" [1] so that construction of the telescope and the spectrometer could be begun. The central theme was the selection and optimization of a suitable dispersion element.

Simple developments showed that, in this experiment, the method of Fourier spectroscopy is more advantageous than conventional methods, because the processing of large spectral ranges becomes possible and a favorable signal-noise ratio is obtained in the spectrum.

The expressions for the signal-noise ratio in the spectrum were derived for various noise sources and we were able to show the following:

a) The multiplex gain is maintained for this experiment in contrast to most laboratory experiments, even when the atmosphere is the dominating disturbing radiation source.

b) The signal-noise ratio per resolved spectral element is inversely proportional to the square root of the measurement time for continuum radiation.

c) Insufficient alignment accuracy of the telescope and non-uniform interferometer advance produces sidebands in the spectrum, which must be interpreted as noise if errors are not known. If the errors are known, they can be eliminated by calculation.

Since interstellar sources are surrounded by dust which produces continuum radiation, b) can be applied in the planned measurements and immediately after the beginning of the measurement, one can decide whether the source is in the field of view of the telescope and whether it is useful to observe it for a long time.

An analytic estimation and the numerical determination /133
agreeing with it showed that the degree of modulation of a lamella grid is such that this instrument is superior to the Michelson interferometer for the planned measurement down to wavelengths smaller than 20 μ. The lamella grid was therefore selected as the standard instrument for the experiment and its dimensions and manufacturing tolerances were established so that it operates with optimum modulation in the spectral range between 20 and 200 μ. Fabry-Perot tipping filters will be used as additional instruments to determine fluxes from lines having known wave numbers.

The optical components required for the adaptation of the grid and the detector to the telescope could be defined using the data from the lamella grid and from the main mirror. This means that we have fixed the optical system of the experiment.

The data of the detector, a bolometer filled with helium, were investigated using semi-empirical formulas and we found the following:

a) a relationship between the normalized noise power of the detector and the perturbation radiation and

b) a relationship between the optimum modulation frequency and the noise power of the detector.

Using the second relationship, we investigated possibilities for changing the noise power and modulation frequency. We were able to show that small modulation frequencies and, therefore, small noise power levels of the detector are to be preferred, even though the measurement time is exploited more poorly because of the larger time constant of the detector and the resulting long transient time.

Finally, we discussed methods for compensating the perturbation radiation and the motion of the interferometer. We were able to show the following:

a) The ratio of the perturbation radiation to source radiation is on the order of 10^6. At the present time, the perturbation radiation can only be adequately compensated for by having the secondary mirror of the telescope in the form of a rocking mirror which carries out small amplitude oscillations and alternately images the source (together with the atmosphere) and a closely adjacent region of the sky (its elevation is equal to that of the source) without the source onto the detector (ray direction modulation). The difference in the signals measured is the signal of the source. A two-beam method (which would allow better exploitation of the measurement time) cannot be used because the required detectors do not yet exist. /134

b) The combination of the rocking mirror and the interferometer can only be used because of the great variation of the interferogram between adjacent measurement points and the required compensation for the perturbation radiation, if the interferometer shift is changed in steps. It is not possible to have continuous advance, which would be desirable because of the reduced mechanical problems (oscillations).

c) Because of economical reasons, it is desirable to make the waiting times between the measurements as small as possible. One measure for the time economy of the measurement arrangement is the effectiveness, which here is defined as the ratio of the integration time per interferogram and the measurement time per spectrum. It depends on the type of motion of the interferometer and of the rocking mirror, as well as the transient times of the detector and of the electronics. (The fact that the alternating voltage amplifier differentiates the signal is not considered.)

d) The maximum effectiveness is achieved when the time constants of the system are adjusted to each other and the rocking mirror carries out rectangular oscillations. It can reach the value 0.35, which comes quite close to the maximum value of 0.5 for the ideal rocking mirror operation.

e) When the temperature of the dust connected with the interstellar cloud is high enough so that its thermal radiation produces a flux at the detector which is higher by three or more orders of magnitude than that of the line radiation from the cloud (this is the case for $T \gtrsim 30°$ K), it becomes difficult to use the rocking mirror. This is because such great flux changes occur because of the ray direction modulation that the dynamics of the detection electronics connected to the detector become overstressed. One way out of this is to use the two-ray method or to measure from satellites. /135a

SYMBOL LIST

We only give symbols used many times.

A	area [cm^2]
a	grid constant [cm]
$\mathcal{B}$	radiation flux [W]
$B(\sigma)$	radiation flux per wave number [W/cm^{-1}]
b	radiation density [$W/cm^2 sr$]
D_i	diameter of imaging surfaces [cm]
E	solid angle range [$cm^2 sr$]
F(x)	interferogram
f_i	focal length [cm]
f_0	modulation frequency of detector [Hz]
G	heat conductivity [$W/^oK$]
$\tilde{G}$	amplification factor
i	radiation intensity [$W/cm^2 sr\ Hz$]
J	angular momentum quantum number
$\vec{k}$	wave vector
L	light yield
N	number of spectral elements
NEP	normalized noise power [$W/\sqrt{Hz}$]
NP	noise power [W]
R	spectral resolution
s/n	signal-noise ratio
S	sensitivity of bolometer [V/W]
T	Temperature
T_σ	Transmission
t	measurement time [sec]

v	v	velocity [cm/sec]
	x	phase difference [cm]
	z	interferometer shift [cm]
	α	incident direction on the dispersion element
	β	reflection direction
	$\delta\sigma$	spectral resolution [cm^{-1}]
	Δf	bandwidth of preamplifier [Hz] /136
	$\Delta\sigma$	width of spectral element [cm^{-1}]
	ε	emissivity
	η	effectiveness
	λ	wavelength [cm]
	σ	wave number [cm^{-1}]
	2θ	field of view diameter
	2ψ	ray divergence at dispersion element
	τ_i	time constant [sec]
	Ω	solid angle

REFERENCES

1. Naumann, F., and K. W. Michel. "High resolution IR spectral photometry with a balloon telescope." MPI-PAE/TB Extraterr. 9 Oct. 1973.

2. Chantry, G. W. Submillimetre spectroscopy (Submillimeter Spectroscopy), London, New York, Academic Press, 1967.

3. Connes, J., P. Connes, and J.-P. Maillard. J. Phys., Vol. 28C, 1967, p. 120.

4. Guelachivilli, G. Aspen International Conference on Fourier Spectroscopy. AFCRL-71-0019, 1970, p. 151.

5. Vanasse, G. A., and H. Sakai. Progress in Optics VI. Amsterdam, North-Holland Publishing Company, 1972, p. 261.

6. Connes, P. Rev. Opt., Vol. 35, 1956, p. 37.

7. Sakai, H. Aspen Internat. Conf. on Fourier Spectroscopy. AFCRL-71-0019, 1970, p. 19.

8. Jacquinot, P. J. Opt. Soc. Am., Vol. 44, 1954, p. 761.

9. Fellgett, P. B. Thesis, University of Cambridge, 1951.

10. Schnopper, H. W., and R. I. Thompson. Methods of Experimental Physics, Vol. 12A, New York, Academic Press, 1974.

11. Drew, H. D., and A. J. Sievers. Appl. Opt., Vol. 8, 1969, p. 2067.

12. Mertz, L. Transformations in Optics. New York, Wiley, 1965.

13. Richards, P. L. J. Opt. Soc. Am., Vol. 54, 1964,p. 1478.

14. Tescher, A. G. Aspen Internat. Conf. on Fourier Spectroscopy, AFCRL-71-0019, 1970, p. 225.

15. Pritchard, J., H. Sakai, and G. Vanasse. Two-Meter Path Difference Interferometer for Fourier Spectroscopy. AFCRL-TR-73-0223.

16. Strong, J., and G. A. Vanasse. J. Opt. Soc. Am., Vol. 50, 1960, p. 113.

17. Connes, J. Aspen Internat. Conf. on Fourier Spectroscopy, AFCRL-71-0019, 1970, p. 83.

18. Joder, M. J. J. Chem. Phys., Vol. 56, 1972, p. 3226. /138

19. Goldman, G., W. G. Murcray, F. H. Murcray, W. J. Williams, and J. N. Brooks. Appl. Opt., Vol. 12, 1972, p. 1045.

20. Low, F. J., and J. N. Rieke. Methods of Exp. Phys., Vol. 12A, New York, Academic Press, 1974, p. 415.

21. Dowling, J. M. Investigations in the Far-Infrared with a Lamellar Grating Interferometer. SSD-TR-67-30.

22. Parshin, P. F. Opt. Spectr., Vol. 16, 1964, p. 275.

23. Baluteau, J. P., and E. Bussoletti. Nature Phys. Sc., Vol. 241, 1973, p. 113.

24. Infrared Lab. Datenblatt fuer Low-Bolometer (Data for Low Bolometer). Tucson, Arizona.

25. Fahrback, U., K. Haussecker, and D. Lemke. Astron. & Astrophys., Vol. 33, 1974, p. 265.

26. Drapatz, S., and K. W. Michel. On the Intensity of Rotational Lines of H_2 and HD from Dense Interstellar Clouds,preprint in Astron. & Astrophys.

27. Petrosian, V. Astrophys. J., Vol. 159, 1970, p. 833.

28. Witteborn, F. C. Low Resolution Spectrum of the Orion Nebula in the 60 — 300 Micron Range. Unpublished, 1973.

29. Stair, A. T., Jr. Aspen Internat. Conf. on Fourier Spectroscopy, AFCRL-71-0019. 1970, p. 127.

30. Roesler, F. L. Methods of Exp. Phys. Vol. 12A, New York, Academic Press, 1974, p. 551.

31. Jennings, R. E. $8^{\underline{th}}$ ESLAB Symposium, HII Regions and the Galactic Center. Abstracts Franscati, 1974; Infrared Maps of the Galactic Center and W-51.

32. Smyth, M. V. Infrared Detection Techniques for Space Research. V. Manno and Ring, publishers. Dordrecht-Holland, Reidel Publishing Company, 1972, p. 284.

APPENDIX A

The Intensity Distribution Behind the Grid in the Fraunhofer Approximation

If $\hat{e}$ is the direction vector of the incident ray, $\hat{r}$ that of the reflected ray, and $\vec{x}$ the direction vector of the reflecting grid location, then the phase difference of a ray reflected at $\vec{x}$ compared with the ray reflected at the origin is given by:

$$\Delta = \vec{x}\cdot(\hat{e} - \hat{r})$$

and the angular phase difference is given by

$$\delta = k\cdot\vec{x}\cdot(\hat{e} - \hat{r}),$$

where $k = 2\pi\sigma$. In addition, we assume that $\varphi_i = e_i - r_i$. Then we have the following for the intensity distribution behind the grid:

$$I \sim \left| \int_{\text{grid surface}} db \cdot e^{i2\pi\sigma\vec{x}(\hat{e}-\hat{r})} \right|^2 =$$

$$= \left| \int_{-b/2}^{+b/2} dy \cdot e^{iky\cdot\varphi_y} \cdot \int_{-Na/2}^{+Na/2} dx \cdot e^{ik(x\varphi_x + z(x)\cdot\varphi_z)} \right|^2$$

The origin of the coordinate system was placed in the center of the grid surface. The second factor of the last expression is formally identical with the expression for the two-dimensional problem and, therefore, we have:

$$I \sim \Big| \int_{-b/2}^{+b/2} dy \cdot e^{ikyq_y} \cdot \frac{a}{2} \cdot \operatorname{sinc}[2\pi q_x a/2] \cdot \frac{\sin(\pi 2 q_x N a)}{\sin(\pi 2 q_x a)} \cdot 2\cos\{k(q_z z/2 + q_x a/4)\} \cdot e^{ikq_z z/2} \Big|^2 ;$$

$$\int_{-b/2}^{+b/2} dy\, e^{ikyq_y} = \frac{1}{ikq_y} \cdot (e^{ikq_y b/2} - e^{-ikq_y b/2}) = \frac{2i \cdot \sin(\pi 2 q_y b)}{2i\pi 2 q_y} = b \cdot \operatorname{sinc}[2q_y b];$$

$$I \sim 2F_i^2 \operatorname{sinc}^2[2q_x a/2] \cdot \operatorname{sinc}^2[2q_y b] \cdot \frac{\sin^2(\pi 2 q_x N a)}{\sin(\pi 2 q_x a)} \cdot \{1 + \cos(2\pi 2(q_x z + q_x a/2))\},$$

where $F_i = ab/2$ – area of a lamella.

For the configuration shown in the figure of the incident and reflected ray (direction vectors $\hat{e}$ and $\hat{r}$, respectively), we have: /140

$$e_x = \sin\varphi_e \cdot \cos 2\vartheta_e \; ; \quad e_y = -\sin\varphi_e \cdot \sin 2\vartheta_e \; ; \quad e_z = -\cos\varphi_e \; ;$$
$$r_x = \sin\varphi_r \cdot \cos 2\vartheta_r \; ; \quad r_y = \sin\varphi_r \cdot \sin 2\vartheta_r \; ; \quad r_z = \cos\varphi_r \; ;$$

It follows from this that:

$$q_x = e_x - r_x = \sin\varphi_e \cdot \cos 2\vartheta_e - \sin\varphi_r \cdot \cos 2\vartheta_r \; ;$$
$$q_y = e_y - r_y = -\sin\varphi_e \cdot \sin 2\vartheta_e - \sin\varphi_r \cdot \sin 2\vartheta_r \; ;$$
$$q_z = e_z - r_z = -\cos\varphi_e - \cos\varphi_r \; ;$$

Now if $2\vartheta_e = 2\vartheta_r = 0$, then we have

$$q_x = \sin\varphi_e - \sin\varphi_r \; ; \quad q_y = 0 \; ; \quad q_z = -\cos\varphi_e - \cos\varphi_r \; ;$$

These values correspond to the two-dimensional solution discussed in 3.2.

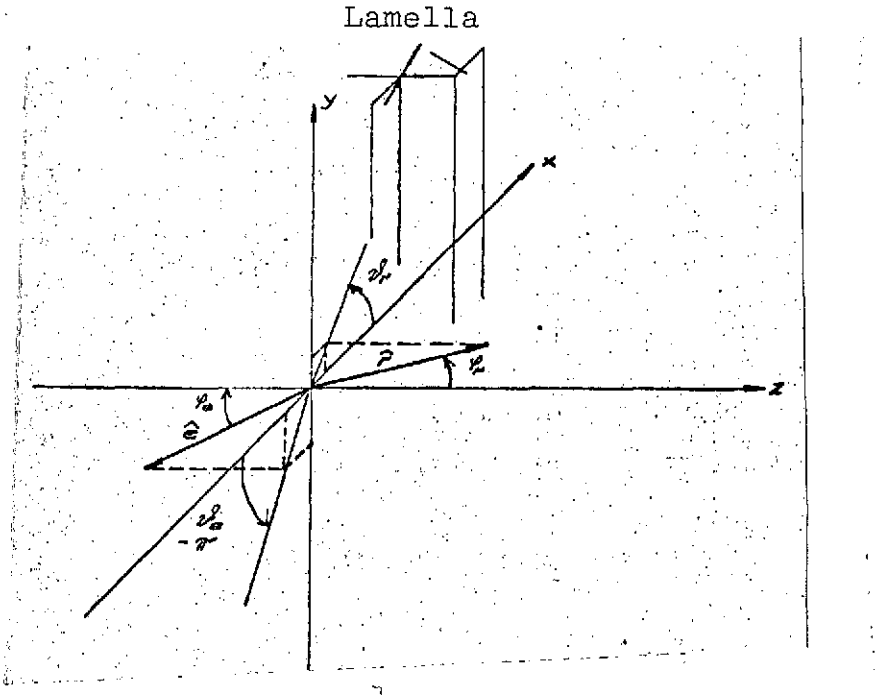

On the other hand, if we set $2\delta_e = -2\delta_r = \pm\pi/2$, we obtain

$$R_x = 0; \quad R_y = 0; \quad R_z = -\cos\varphi_e - \cos\varphi_r ;$$

which means that the intensity distribution in the y direction is the same as the distribution along one diameter of the Haidinger rings for the Michelson interferometer, because we have $\varphi_e = \varphi_r$. (Refraction effects are not important in this direction.)

APPENDIX B

/141

The Two-Dimensional Analytical Solution Considering Shading

For the following, we assume an ideal lamella grid in which all lamellae are exactly parallel to each other and all lamellae of one family have exactly the same grid shift.

For given incident and reflected angles, then the shading for all the lamellae pairs will be the same (if we disregard edge effects at the outer lamellae). Therefore, we have the following for the intensity distribution: $I \sim E \cdot E^*$.

$$E \sim \sum_{\text{lamella pairs}} \left\{ \int_{\text{fixed lamellae}} dx\, e^{ik\varphi_x x} + \int_{\text{movable lamellae}} dx\, e^{ik(\varphi_x x + \varphi_z z)} \right\}$$

$$= \frac{1}{ik\varphi_x} \cdot e^{ik\varphi_x a/2} \cdot \frac{\sin k\varphi_x N a/2}{\sin k\varphi_x a/2} \cdot \left\{ \left(e^{ik\varphi_x AU_1} - e^{ik\varphi_x AL_1}\right) + e^{ik\varphi_z z} \cdot \left(e^{ik\varphi_x AU_2} - e^{ik\varphi_x AL_2}\right) \right\}.$$

The z coordinate of the fixed lamellae is set equal to zero and AL_1, AU_1, AL_2, and AU_2 are defined by Figure 32.

For the intensity distribution, we therefore obtain: /142

$$I \sim \frac{2}{(k\varphi_x)^2} \cdot \left(\frac{\sin k\varphi_x N a/2}{\sin k\varphi_x a/2}\right)^2 \cdot \left\{ 2 - \cos\left[k\varphi_z (AU_1 - AL_1)\right] - \cos\left[k\varphi_z (AU_2 - AL_2)\right] + \cos\left[k\varphi_x (AU_2 - AU_1) + k\varphi_z z\right] + \cos\left[k\varphi_x (AL_2 - AL_1) + k\varphi_z \cdot z\right] - \cos\left[k\varphi_x (AU_2 - AL_1) + k\varphi_z \cdot z\right] - \cos\left[k\varphi_x (AL_2 - AU_1) + k\varphi_z \cdot z\right] \right\}.$$

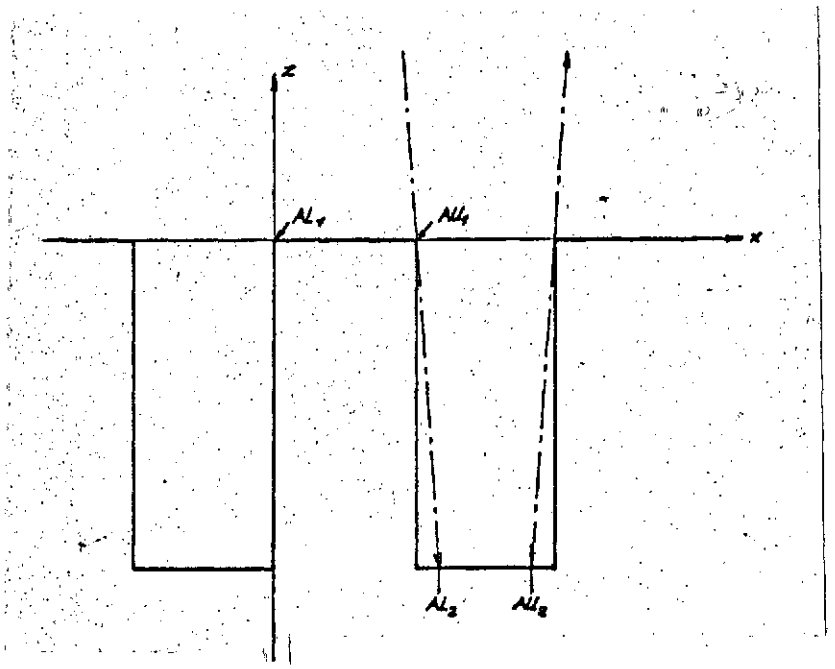

Figure 32. Definition of the integration limits for covering.

APPENDIX C

/143

The Effectiveness of a Rocking Mirror Carrying Out Harmonic Oscillations

Let us assume that the field of view diameter of the instrument is 2θ, the amplitude of the mirror oscillations is α_s and that the source diameter is 2ψ. The equation for the center of the field of view is then:

$$\alpha(t) = \alpha_s \cdot \cos(2\pi f_0 t)$$

f_0 is the frequency of the mirror oscillations. In a similar way, we have the following for the edges of the field of view:

$$\alpha_u(t) = \alpha_s \cdot \cos(2\pi f_0 t) - \theta$$
$$\alpha_o(t) = \alpha_s \cdot \cos(2\pi f_0 t) + \theta$$

Figure 33 shows the time variation of the mirror oscillation.

The effectiveness which can be obtained depends on the source size to be investigated. First of all, we consider a point source which is assumed to have an angular separation of α_Q from the zero position of the mirror.

In order for the source to remain in the field of view of /144
the detector in the vicinity of the maximum deflection of the mirror, we must have:

$$\alpha_a \geq \alpha_s - \theta$$

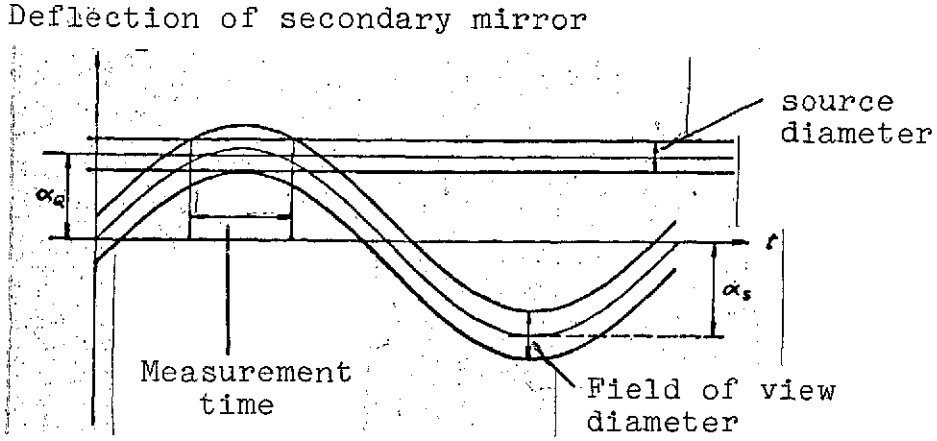

Figure 33.

The longest observation time is reached for $\alpha_Q = \alpha_s - \theta$; it is given by

$$\alpha_s - \theta = \alpha_s \cdot \cos \pi f_0 \tau + \theta \quad \rightarrow \quad 1 - 2\theta/\alpha_s = \cos \pi f_0 \tau$$

$$\tau = \frac{1}{\pi f_0} \cdot \arccos (1 - 2\theta/\alpha_s).$$

The observation duration must be smaller than one-half the oscillation duration of the mirror; therefore we must have $t \leq 1/2f_0$. From this, we find:

$$\frac{1}{\pi} \cdot \arccos (1 - 2\theta/\alpha_s) \leq 1/2,$$

$$1 - 2\theta/\alpha_s \geq 0.$$

The observation time is a maximum for minimum argument of the arccos, i.e., for $1 - 2 \cdot \theta/\alpha_s = 0$, and therefore,

$$\alpha_s = 2\theta, \qquad t = 1/2f_0$$

The optimum solution for a point source is therefore:

$$\alpha_s = 2\theta, \qquad \alpha_Q = \alpha_s - \theta = \theta$$

The observation time would be $1/2f_0$, that is, the theoretical maximum value and the effectiveness would be $\varrho_s = 0{,}5$.

Unfortunately, this case is not realistic, because even a point source will appear to have a finite diameter because of refraction effects and, therefore, $2\psi = 0$ does not occur in practice.

Now we will consider an extended source, whose diameter is smaller than the field of view diameter of the telescope. Therefore, we have $\psi < \theta$. If we now require that the source remain inside the field of view of the detector during the integration time, we must have:

$$\alpha_o(t) \geq \alpha_Q + \psi, \qquad \alpha_u(t) \leq \alpha_Q - \psi$$

α_Q is the position of the center of the source relative to the zero position of the mirror. From the inequalities we first find at $2\theta \geq 2\psi$, which is already satisfied, according to our assumption.

The longest observation time is achieved for

$$\alpha_u(0) = \alpha_s - \theta = \alpha_Q - \psi \quad \Rightarrow \quad \alpha_Q = \alpha_s - (\theta - \psi).$$

From this, we find:

$$\begin{aligned} \alpha_o(\tau/2) &= \alpha_s \cdot \cos \pi f_0 \tau + \theta = \alpha_Q + \psi \quad \Rightarrow \\ \alpha_s \cdot \cos \pi f_0 \tau &= \alpha_s - 2 \cdot (\theta - \psi) \end{aligned}$$

and the effectiveness is:

$$\varrho_s = \tau / f_0 = \frac{1}{\pi} \cdot \arccos\left(1 - 2\,\frac{\theta - \psi}{\alpha_s}\right).$$

However, we must now remember the fact that the source must remain completely outside of the field of view during half of the oscillation period of the rocking mirror. It will still be partially in view of the detector, as long as we have

$$\alpha_0(t) \geq \alpha_a - \psi.$$

and it will vanish from the field of view for

$$\alpha_0(t'/2) = \alpha_a - \psi \Rightarrow \alpha_s \cdot \cos \pi f_0 t' = \alpha_s - 2\theta;$$
$$t' = \frac{1}{\pi f_0} \cdot \arccos(1 - 2\theta/\alpha_s).$$

t' must be smaller than $1/2f_0$ and the optimum solution is $t = 1/2f_0$, from which we find

$$1 - 2\theta/\alpha_s = 0, \quad \alpha_s = 2\theta,$$

and, therefore,

$$\alpha_a = \theta + \psi$$

Finally we find the following for the effectiveness:

$$\eta_s = \frac{1}{\pi} \cdot \arccos(\psi/\theta).$$

As soon as the source diameter is equal to the field of view diameter, the effectiveness vanishes. One again obtains a finite value if we require that only a certain part of the source is to lie within the field of view during the integration time.

Finally, we will now investigate the case $\psi > \theta$. In this case, it is not possible to include the entire source and it is advantageous to select the integration time so long that the field of view of the detector is filled with the image of the source only during the measurement.

The edge of the source is assumed to have the angular separation β from the direction of viewing of the telescope at $\alpha_s = 0$. The source then is partially within the field of view for

$$\beta \leq \alpha(t) + \theta$$

From this, we find the possible observation time:

$$\tau = \frac{1}{\pi f_0} \cdot \arccos\left(\frac{\beta - \theta}{\alpha_s}\right)$$

τ must be smaller than $1/2f_0$, that is:

$$1 \geq \frac{\beta - \theta}{\alpha_s} \geq 0 \Rightarrow \beta \geq \theta, \; \alpha_s \geq \beta - \theta.$$

The time is a maximum for

$$\beta = \theta.$$

Now we will select the measurement time so that when it begins, a specified fraction χ of the field of view is filled with the source. If the source has a straight line boundary (source diameter very large compared with the field of view diameter), this means that the center of the field of view must have reached the angle deviation γ which is specified by the following relationship:

$$\chi = \frac{1}{\pi\theta^2} \cdot \left\{\gamma \cdot \sqrt{\theta^2 - \gamma^2} + \theta^2 \cdot \left(\arcsin\frac{\gamma}{\theta} + \frac{\pi}{2}\right)\right\}$$

$$\gamma/\theta = \varphi; \quad \chi = \frac{1}{\pi}\left\{\varphi\sqrt{1-\varphi^2} + \arcsin\varphi + \frac{\pi}{2}\right\}$$

From this, it is possible to determine φ for a specified χ and, therefore, the position of the field of view center at the beginning and end of the measurement.

$\varphi =$	-1	-0,75	-0,5	-0,25	0	0,25	0,5	0,75	1
$\chi =$	0	0,07	0,19	0,34	0,5	0,65	0,8	0,93	1,0

We have:

$$\alpha(\tau/2) = \alpha_s \cdot \cos \pi f_0 \tau = \varphi \cdot \theta + \beta .$$

and from this, the effectiveness:

$$\varrho_s = \frac{1}{\pi} \arccos\left(\frac{\varphi \cdot \theta + \beta}{\alpha_s}\right) \leq 0{,}5 .$$

In order for η_s to remain smaller than 0.5, we must have: /147

$$1 \geq \frac{\varphi \cdot \theta + \beta}{\alpha_s} \geq 0 \Longrightarrow \alpha_s \geq \theta \cdot \varphi + \beta \geq 0$$

The maximum effectiveness for a prescribed φ is reached for the greatest possible α_s.. For extended sources, α_s should be made as large as possible; however, only large enough so that the source will remain within the field of view during the measurement. If it has the diameter 2ψ, then we must have

$$\alpha_s + \theta \leq \beta + 2\psi$$

and, for the greatest achievable effectiveness, we have:

$$\alpha_s = \beta + 2\psi - \theta ,$$

$$\varrho_s = \frac{1}{\pi} \cdot \arccos\left(\frac{\varphi \cdot \theta + \beta}{\beta + 2\psi - \theta}\right) .$$

APPENDIX D

Numerical Calculation for the Determination of the Degree of Modulation of the Lamella Grid

The double integral

$$\int d\alpha \, d\beta \, I(\alpha, \beta, e^2, z)$$

was evaluated using a Gauss integration algorithm, after test calculations had shown that this method results in a greater accuracy than all other algorithms and with a relatively short computation time.

The integration routine used requires 32 support points in the integration interval and is performed using double accuracy. It has the name DQG32 in the Fortran program library.

In order to achieve sufficient accuracy, we divided the integration range into 40 to 160 intervals, depending on the functional value of the integrand. The variation of the integral calculated in this way as a function of the second integration variable is so smooth that the integration range only had to be divided once for the second integration. This means that a double integral is determined by a maximum of

$$(32 \cdot 160) \cdot (32 \cdot 2) = 3{,}28 \cdot 10^5$$

support points.

The calculation was carried out on the IBM-360/90 of the Max Planck Institute for Plasma Physics in Garching. The calculation time per double integral was between 10 and 30 seconds. At least two such integrals were calculated for each point of the curves determined. Substantially more values were determined in order to have a check on the dependence of the integrals on the grid shift.

APPENDIX E

The Halfwidth of Atmospheric Lines

The halfwidth of the atmospheric lines is determined by the pressure broadening at the altitudes of 35 to 40 km of interest here. Approximately, we have:

$$\Delta\omega_{1/2} = \frac{1}{c}\sqrt{\frac{\pi e^2}{mc^2}\cdot\frac{f\cdot l}{4\pi^2\ln 2}\cdot n_{J,K}\cdot\gamma}$$

Here we have f — oscillation intensity; $n_{J,K}$ — numerical density of particles in the corresponding rotational state capable of radiating, $n_{J,K} = \zeta_{JK}\bar{n}$; $\bar{n}$ — total density averaged over scale height; γ — collision damping constant $\gamma = \sigma_L\sqrt{\frac{8kT}{\pi\mu}}\cdot n$; σ_L — optical broadening cross section; l — scale length of light path, $l = l_{sc}/\sin\tilde{\varepsilon}$; l_{sc} — scale height of water density; and $\tilde{\varepsilon}$ — elevation of object observed.

Since the temperature is approximately constant over the scale length of the light path, we have $\zeta_{JK} = \text{const.}$, and, therefore:

$$\Delta\omega_{1/2} = \text{const.}\cdot\bar{n}/\sqrt{\sin\tilde{\varepsilon}}.$$

ACKNOWLEDGEMENTS /150

I wish to thank Professor Dr. Pinkau for letting me perform this work at his institute.

Special thanks goes to Dr. Michel for many discussions and support.

Professor F. Low should be thanked for his contribution about the overall design of the telescope and his suggestions for adapting the detector to the optical system.

I am grateful to Dr. Drapatz and Dr. Naumann for the many discussions on problems which occurred, suggestions, and review of the manuscript.

I would also like to thank Mr. Stoecker for his collaboration in the design of the lamella grid and the optical components of the telescope.

I thank Dr. Hornugg for his friendly support in the design of the computer program.

Translated for National Aeronautics and Space Administration under contract No. NASw 2483, by SCITRAN, P. O. Box 5456, Santa Barbara, California 93108